Jessica Ariana Madeira Machado

Bachelor of Science in Applied Chemistry

Synthesis of Smart Biocompatible Nanoparticles for Bio-Applications

Dissertation for the degree of Master of Science in Bioorganic Chemistry

Supervisor: Dr. Elisabete Oliveira, Post-Doc Researcher, FCT-UNL

Co-supervisor: Dr. Hugo Santos, IF Researcher, FCT-UNL

Examination Committee:

Chairperson: Prof. Dr. Paula Branco

Jury members: Prof. Dr. Maria Teresa Barros

FACULDADE DE CIÊNCIAS E TECNOLOGIA
UNIVERSIDADE NOVA DE LISBOA

January 2018

Jessica Ariana Madeira Machado

Bachelor of Science in Applied Chemistry

Synthesis of Smart Biocompatible Nanoparticles for Bio-Applications

Dissertation for the degree of Master of Science in Bioorganic Chemistry

Supervisor: Dr. Elisabete Oliveira, Post-Doc Researcher, FCT-UNL

Co-supervisor: Dr. Hugo Santos, IF Researcher, FCT-UNL

Synthesis of Smart Biocompatible Nanoparticles for Bio-Applications

"QUIEN no tiene tiempo para lo importante, no vive.

Vive por él el tiempo."

Pep Guerreiro

ACKNOWLEDGEMENTS

I would like to pay special thankfulness, warmth and appreciation to the people below who made my research successful and assisted me at every point to cherish my goal. Without them this dissertation would not be possible and an unforgettable experience for me.

First of all, I would like to express my deepest gratitude to my supervisor Dr. Elisabete Oliveira from FCT-UNL, who offered her continuous advice and encouragement throughout the course of this dissertation. The door to Dr. Elisabete's office was always open whenever I ran into a trouble spot or had a question about my research. She consistently allowed this work to be my own, yet steered me in the right direction whenever she thought I needed it. I thank her for the constant guidance and great effort she put into training me in this scientific field.

Second of all, I would like to thank to my co-supervisor Dr. Hugo Santos from FCT-UNL, without his support and assistance whenever I needed it, I would not be able to carry out my research.

I would also like to acknowledge Prof. Dr. Carlos Lodeiro Espiño and Prof. Dr. José Luis Capelo from FCT-UNL, for the opportunity to work in the Bioscope laboratory and research group, which has enabled me to work alongside excellent professionals. I want to leave a word of great appreciation to the Professors for their dedication, support and readiness to carry out this project.

I am thankful to my colleagues in the Bioscope group, for the help and support during my dissertation.

My gratitude also to my friends for the time with laughter, mutual encouragement during the course of this dissertation, and special for their care and precious friendship. And to my closest one for the patience, endurance, friendship and spiritual support whenever I needed it.

Finally, I must express my very profound gratitude from my deep heart to my beloved mother for providing me with unfailing support and continuous encouragement throughout my years of study and through the process of researching and writing this dissertation. This accomplishment would not have been possible without her. Thank you.

ABSTRACT

One of the backbones in nanomedicine is to deliver drugs specifically to unhealthy cells. Luminescent inorganic mesoporous silica nanoparticles (QDs@mSiO_2) are a new generation of nanocarriers acting as all-in-one diagnostic and therapeutic tools due to their excellent biocompatibility, biodegradability and high surface area.

Among all fluorescent agents, quantum dots have been widely used due to their high luminescence quantum yields and great optical properties. Based on such facts, herein we present a synthesis of Cadmium Telluride and Silicon quantum dots under mild conditions, in water and in open air conditions. These quantum dots were further functionalized with a layer of mesoporous silica nanoparticles.

In order to increase the solubility of these systems in water, a derivative of poly(ethylene glycol) (PEG) was added to their surface. Specifically, three types of PEG-derivatives were synthesized, having three different PEG-chain lengths with (i) MW 3000, (ii) MW 6000, and (iii) MW 8000. The nanoparticles were characterized by different techniques (TEM, SEM, DLS, FT-IR, absorption and emission spectroscopy), showing high surface area, an effective coating of the mesoporous silica nanoparticles with the PEG layer, and also improved monodisperse suspension in water in comparison with the unfunctionalized nanoparticles. The behavior of these nanoparticles was investigated at physiological pH (PBS, pH = 7.4) with single proteins exhibiting different sizes and pI, with the aim of gaining new insights regarding the encapsulation efficiency of these nanoparticles with proteins.

KEYWORDS: Quantum dots, Mesoporous silica nanoparticles, PEGylation, Proteins.

RESUMO

Uma das principais dificuldades em nanomedicina tem sido a administração de fármacos, especificamente em células não saudáveis. As nanopartículas inorgânicas luminescentes de sílica mesoporosa (QDs@mSiO_2) são uma nova geração de nano--transportadores que atuam como ferramentas de diagnóstico e terapia "tudo em um" devido à sua excelente biocompatibilidade, biodegradabilidade e elevada área de superfície.

Entre todos os agentes fluorescentes, os *quantum dots* têm sido amplamente utilizados devido aos seus altos rendimentos quânticos de luminescência e excelentes propriedades óticas. Tendo isso em conta, apresentam-se as sínteses de *quantum dots* de Cádmio Telúrio e Silício, realizadas em condições suaves, em água e em condições atmosféricas. Posteriormente, estes *quantum dots* foram funcionalizados com uma camada de nanopartículas de sílica mesoporosa.

De forma a aumentar a solubilidade destes sistemas em água, foi adicionado na sua superfície um derivado de poli(etilenoglicol) (PEG). Especificamente foram sintetizados três tipos de derivados de PEG, possuindo estes, cadeias com diferentes comprimentos (i) MM 3000, (ii) MM 6000 e (iii) MM 8000. As nanopartículas foram caracterizadas por diferentes técnicas (TEM, SEM, DLS, FT-IR, espectroscopia de absorção e emissão), apresentando elevada área de superfície, um revestimento eficaz das nanopartículas de sílica mesoporosa com a camada de PEG e uma melhoria na monodispersão da suspensão em água em relação às nanopartículas não funcionalizadas. O comportamento destas nanopartículas foi investigado em pH fisiológico (PBS, pH = 7.4) com proteínas de diferentes tamanhos e pI, com o objetivo de obter novos conhecimentos sobre a eficiência de encapsulamento destas nanopartículas com proteínas.

Palavras-chave: *Quantum dots*, Nanopartículas de sílica mesoporosa, PEGilação, Proteínas.

CONGRESS COMMUNICATIONS AND SCIENTIFIC PAPERS

Poster Communication

HC46 - Synthesis of Smart Biocompatible Nanoparticles for Bio-Applications. Jessica Ariana-Machado, Elisabete Oliveira, Hugo Miguel Santos, José Luis Capelo and Carlos Lodeiro. SPQ National Meeting (XXVEN-SPQ), Faculty of Pharmacy of Lisbon University, 16-17 July 2017.

Scientific paper

Authors: Nuno A. Morais, Luz Fernandes, Jessica Ariana-Machado, José Luis Capelo, Carlos Lodeiro*, Elisabete Oliveira*

Title: An unusual emissive and colorimetric copper(II) detection by a selective probe based on a pseudo-crown cysteine dye: solution and gas phase studies.

Journal: Inorganic Chemistry Communications, 2017, in press (https://doi.org/10.1016/j.inoche.2017.11.001)

TABLE OF CONTENTS

LIST OF FIGURES

LIST OF SCHEMES

LIST OF TABLES

LIST OF ACRONYMS AND ABBREVIATIONS

Φ_F	Fluorescence Quantum Yield
θ	Diffraction angle
λ	Wavelength
η	Solvent viscosity
AA	Ascorbic Acid
APTES	(3-Aminopropyl)triethoxysilane
APTMS	(3-Aminopropyl)trimethoxysilane
BSA	Bovine serum albumin
CA	Carbonic anhydrase
CCD	Charge-coupled device
CdTe	Cadmium Telluride
CENIMAT	Centro de Investigação de Materiais
CMC	Critical micelle concentration
CTAB	Cetyltrimethylammonium bromide
CYT	Cytochrome c
D_t	Diffusion coefficient
D_H	Hydrodynamic diameter of the particle
Da	Dalton
DLS	Dynamic Light Scattering
EE	Encapsulation efficiency
ES	Experimental Section
FT-IR	Fourier Transformed Infrared spectroscopy
Hb	Hemoglobin
in vitro	From Latin: "in glass", *i.e*. under simulated physiological conditions
in vivo	From Latin: "in living", *i.e*. under physiological conditions
IPTES	(3-Isocyanatopropyl)triethoxysilane
k	Boltzmann constant
LYS	Lysozyme
MCM-41	Mobil Crystalline Materials No 41

MSNs/$mSiO_2$	Mesoporous silica nanoparticles
MW	Molecular weight
Myb	Myoglobin
NCs	Semiconductor nanocrystals
NMR	Nuclear magnetic resonance
OVA	Ovalbumin
PBS	Phosphate-buffered saline
PDI	Polydispersity Index
PEG	Poly(ethylene glycol)
PEG1	PEG(3000)-Silane
PEG2	TsO-PEG(6000)-Silane
PEG3	TsO-PEG(8000)-Silane
PLGA	Poly(lactic-co-glycolic acid)
QDs	Quantum dots
SA	Sodium ascorbate
SEM	Scanning electron microscopy
Si	Silicon
T	Absolute temperature
TEM	Transmission electron microscopy
TEOS	Tetraethyl orthosilicate
THF	Tetrahydrofuran
TGA	Thioglycolic acid
TMOS	Tetramethyl orthosilicate
TMS	Tetramethylsilane
UV-Vis	Ultraviolet–visible
XRD/XRPD	X-ray powder diffraction

CHAPTER 1

INTRODUCTION

1.1. Luminescent Quantum Dots

1.1.1. Cadmium Telluride Quantum dots (CdTe QDs)

Quantum dots (QDs), also known as semiconductor nanocrystals (NCs) are a group of inorganic nanomaterials that present remarkable optical and electronic properties and possess distinct advantages over the traditional fluorescent organic dyes in terms of tunable broad excitation and narrow emission spectra, high fluorescence efficiency, large effective Stokes shift, long fluorescence lifetime and composition/size-tunability [1].

Cadmium is known to be one of the major components in the majority of quantum dots, which conjugated with telluride provides bright emission across the visible and near-infrared regions of the electromagnetic spectrum, Figure 1.1. However, CdTe QDs are known to be extremely toxic to cells and organisms [2,3]. Therefore a less toxic source for the quantum dots is needed, one that is less toxic and more biodegradable.

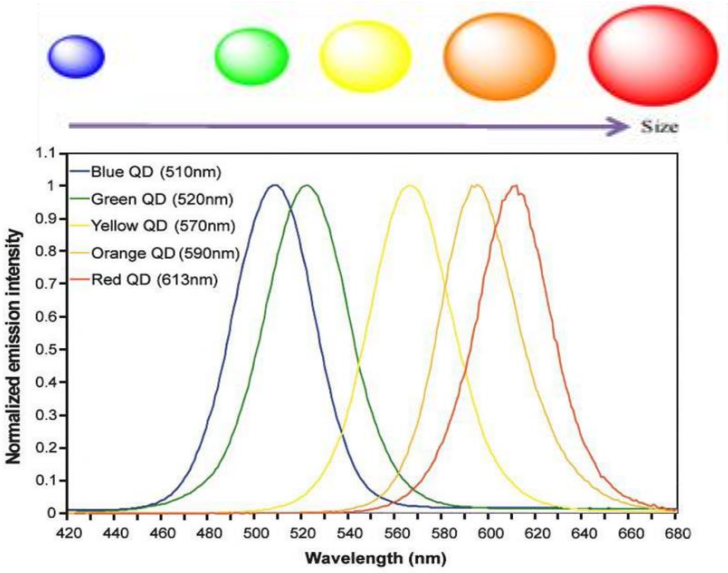

Figure 1.1 - Normalized emission spectra of CdTe QDs at different excitation wavelengths (adapted from ref. [4])

Concerning the synthesis of CdTe QDs, several methods have been developed, such as selective photochemical etching [5,6], ultrasonic irradiation [7] and microwave irradiation [8,9]. The aqueous synthetic approach, as a green alternative, compared with the others, is relatively simpler, cheaper, less toxic, and more environmentally friendly, end as a result has gained a lot of interest in research. Furthermore, the products often show improved water-stability and biological compatibility [10]. In addition, in most aqueous syntheses of CdTe QDs, an inert atmosphere was necessary during the synthesis due to the sensitivity of the tellurium precursor (H_2Te or NaHTe) [11]. However previous reported studies revealed that using thioglycolic acid (TGA) as ligand and K_2TeO_3 is possible to synthesize CdTe nanocrystals without the protection of nitrogen gas [11]. Subsequently, in this presented work, a simple and more friendly method was used to prepare highly luminescent water-soluble CdTe QDs using TGA as ligand without nitrogen gas atmosphere, when using Na_2TeO_3 as a stable Te source, and $NaBH_4$ as reducing agent.

1.1.2. Silicon Quantum Dots (Si QDs)

As previously said, the commonly used QDs are cadmium based, and their toxicity is still a problem in biological applications [12,13]. Silicon (Si) is a well-studied material in the semiconductor family, which have attracted great attention due to their intrinsic advantages, such as low cost, strong fluorescence, high stability, and photostability. In addition, Si QDs exhibit unique abilities such as low toxicity, favorable biocompatibility, and biodegradability, which make them widely accepted as promising alternatives to the toxic heavy-metal CdTe QDs. Therefore, Si QDs exhibit a significant potential in the biological field [14-16].

So far different methods of synthesis have been reported, including ultrasonic dispersion of electrochemically etched silicon [17], laser-driven pyrolysis of silane [18,19], gas phase synthesis [20], microemulsion synthesis [21], among others. However, in order to have application in biological systems, Si QDs have to be water-soluble. Recently, He *et al*. introduced an aqueous synthetic method to prepare fluorescent Si QDs under microwave irradiation at 160°C [22]. He *et al*. further developed a photochemical strategy capable of large-quantity synthesis of Si QDs under UV irradiation [23]. Li *et al*. reported the fabrication of ultrabright water-dispersible Si QDs through a designed chemical surface modification [24]. Wang *et al*. also reported a method for one-step synthesis of water-dispersible Si QDs for time-resolved imaging of living cells [25]. And more recently, Ma *et al*. developed a one-step synthesis of water-dispersible and biocompatible Si QDs for selective heparin sensing and cell imaging [26]. According to these previous studies, in this report, Si QDs were performed accordingly with ref. [25], and several optimizations were required to

create a simple one-step synthesis of water-dispersible Si QDs using (3-aminopropyl)trimethoxysilane (APTMS) and sodium ascorbate (SA) at 50°C for 2 h.

1.2. Luminescent Mesoporous Silica Nanoparticles

1.2.1. MCM-41

In 1992, researchers at Mobil Corporation discovered a new generation of materials with ordered mesoporous structure, which are aluminosilicates synthesized by surfactant micellar arrangements that originate pores of 30–100 Å diameter [27,28]. Within this family MCM-41 (Mobil Crystalline Materials No 41) is one of the most used materials as support [29,30]. Its structure is based essentially on a cylindrical tube aggregate on amorphous silica in a hexagonal arrangement of one-dimensional mesoporous with diameters ranging from 2 nm to 5 nm, having a high specific surface area (≈ 1000 m^2g^{-1}) and a meaning volume pore (≈ 1 cm^3g^{-1}) [28].

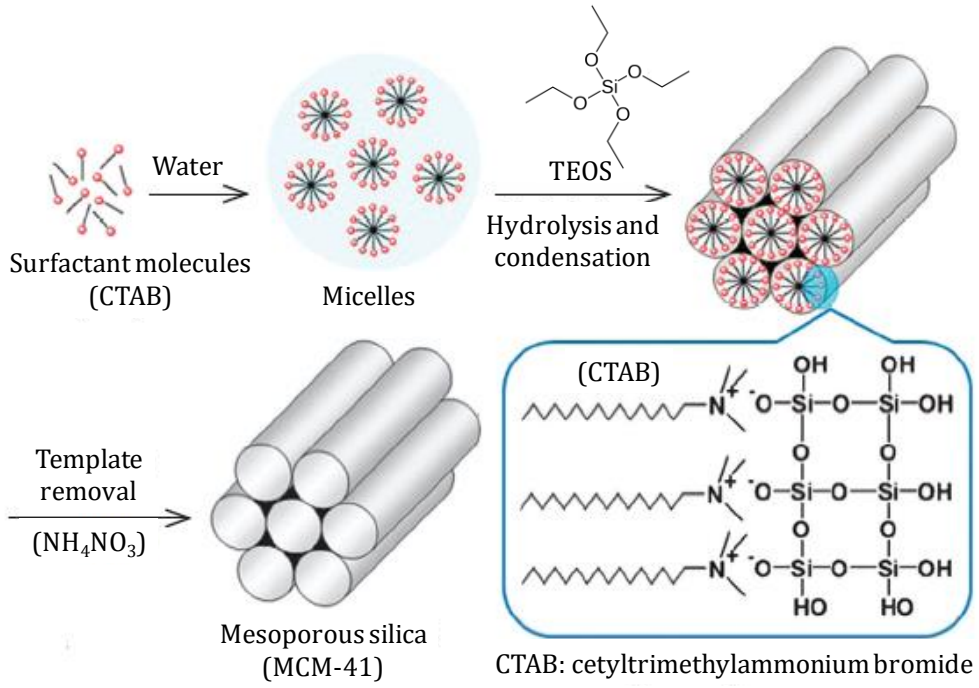

Scheme 1.1 – Synthetic procedure of MCM-41 (adapted from ref. [31]).

This material is thermally stable up to 650°C. The inner surface of the MCM-41 contains nucleophilic Si-OH groups that allow organometallic or inorganic compounds to be immobilized by various methods [29,30].

In the synthesis, cetyltrimethylammonium bromide (CTAB) is the cationic surfactant used as template, tetraethyl orthosilicate (TEOS) or sodium silicate (Na_2SiO_3) as

the silica precursor, and alkali as catalyst [27,32]. When the concentration is above the critical micelle concentration (CMC), the surfactant of CTAB would self-aggregate into micelles. Around the polar head region of the micelles, the silica precursors condensate at the surface of the surfactant and form a silica wall around the surface of the micelles. After removal of the surfactant, MCM-41 type mesoporous silica nanoparticles are obtained, Scheme 1.1.

1.2.2. QDs coated with mesoporous silica nanoparticles (MSNs/mSiO$_2$)

As previously discussed, inorganic QDs possess unique properties that make them suitable for several applications. However, its photoinstability is a disadvantage, and with time promotes their degradation and agglomeration. One key promising approach for this problem, is functionalization of QDs with MSNs, providing a better physical and chemical stability of the QDs [33], Scheme 1.2.

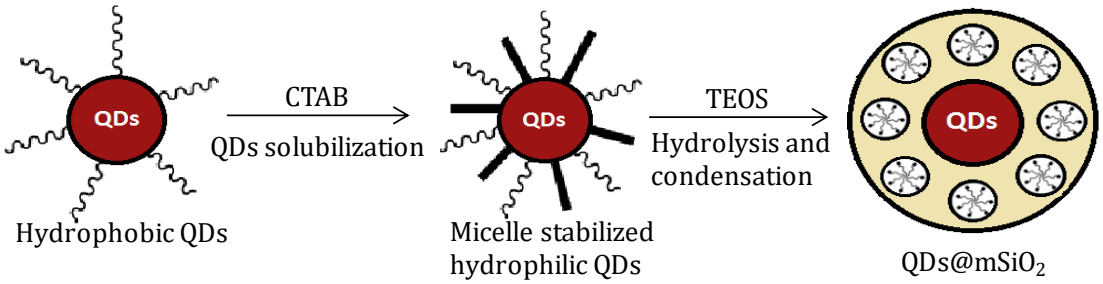

Scheme 1.2 – Synthetic procedure of QDs coated with MSNs.

The MSNs are considered to be one of the most powerful mesoporous structures as it generally possesses good bio-compatibility and ability to modify its surface, providing reservoirs for loading various functional molecules as a nanocarrier, and active sites for linking other targeted molecules by covalent associating [34]. As for the QDs, their luminescence provides an easy way to track the nanocarriers into the cells. Therefore, QDs functionalized with MSNs may not only prevent QDs agglomeration and resolve the instability problem, but also offer the quantum confinement effect to take advantage of the superior properties of both QDs and MSNs [35]. On the other hand, the drawback is the low solubility of these systems with a high polydispersity index (PDI) for *in vitro* and *in vivo* applications. Consequently, is needed a polymer functionalization of the MSNs surface in order to increase the water solubility.

The encapsulation of inorganic QDs with MSNs has been widely investigated, and the methods can be grouped into two general categories, by coating the inorganic QDs with MSNs or by introducing the QDs into the pores of the MSNs (dye-doping).

So far, a number of papers have reported the successful preparation of silica-coated QDs. Wolcott *et al.* exploited the grow of an amorphous silica shell onto as-synthesized water-soluble CdTe QDs functionalized with thiols for bioconjugation to immunoglobulin-G-type proteins [36]. Song *et al.* further demonstrated the fabrication of mesoporous CdTe/ZnO@SiO_2 core/shell nanostructures with tunable dual emission and ultrasensitive fluorescence response to metal ions [37]. Hu *et al.* also synthesized a new generation of silica encapsulated singles quantum dots [38]. And more recently, Zhou *et al.* fabricated mesoporous silica-coated CdTe QDs functionalized with folic acid for targeted lung cancer cell imaging [39].

Techniques such as electrostatic interactions, ligand exchanges, electrophoretic deposition, chemical vapor or bath deposition, have been developed for introducing QDs into the pores using mesoporous material as templates [40]. Wang *et al.* synthesized CdSe nanoparticles into the pores of mesoporous silica microspheres via direct reaction at low temperatures between selenosulfate and (noncomplexed) Cd ions bound to the Si-OH of the mesoporous silica microspheres [40]. Sha *et al.* further reported a method for fabricating CdTe functionalized MSNs loaded with conjugated polymers: a facile sensing platform for cupric (II) ion detection in water through fluorescence resonance energy transfer [41]. And more recently, Gao *et al.* focused on a simple approach to immobilize Ag NPs onto CdTe QDs embedded mesoporous silica nanospheres to prevent bacteria invasion for enhanced anticounterfeit applications [42], and Santos *et al.* created a successful aqueous route to grown stable CdTe nanocrystals *in situ* in thiol-modified MCM-41 mesoporous silica for electrochemical detection of Cu^{2+} [43].

Taking in consideration these previous studies, in this report, were performed the encapsulation of the inorganic QDs by coating the QDs with MSNs type MCM-41, performing the addition of the MSNs to the crude solution of inorganic QDs, in an aqueous synthesis.

1.3. Functionalization of MSNs with biocompatible and biodegradable polymers

1.3.1. PEG, PGLA

To increase water solubility and biocompatibility, and to reduce undesired interactions between the biological environment and the nanocarriers, the mesoporous nanoparticles can be functionalized with soft organic macromolecules such as dendrimers [44] or phospholipids [45-47]. In particular, the functionalization of the outer surface with poly(ethylene glycol) (PEG) and poly(lactic-*co*-glycolic acid) (PLGA) was developed

[48- 51]. For this purpose, these soft organic macromolecules also called polymers, must be non-toxic, biodegradable, and biocompatible.

PEG is a non-ionic hydrophilic polyether synthesized by polymerization of the monomer ethylene glycol and it can be obtained with a wide range of molecular weight from 300 Da to 100 000 Da, Figure 1.2. PEG is known to be commonly utilized in medicine such as an oral laxative, in drugs formulation as excipient, and in capsules preparation as coating agent [52]. Due to its hydrophilicity and ability to inhibit opsonization, PEG is considered to be profoundly attractive for biological applications such as drug delivery, as it can be used to stabilize nanoparticles in aqueous media and increase solubility. Moreover, as PEG is a non-ionic polymer, no problems occur when it enters in contact with charged biological molecules such as DNA [53,54].

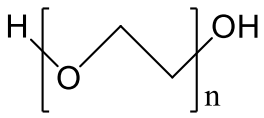

n = number of units of ethylene glycol

Figure 1.2 – Chemical structure of PEG.

PLGA is a synthetic copolymer obtained by random ring opening copolymerization of two cyclic dimers of lactic and glycolic acid, which are linked together by ester linkage in an occasional order during copolymerization, creating an aliphatic linear polyester [55], Figure 1.3.

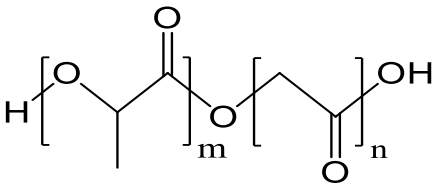

m = number of units of lactic acid
n = number of units of glycolic acid

Figure 1.3 – Chemical structure of PLGA.

Contrary to PEG, PLGA is known for its biodegradability in aqueous media, that occurs when the ester linkage presented in the polymer chain is subjected to hydrolytic degradation, and also for is extreme biocompatibility and mechanic strength [56,57].

1.3.2. Different methods of synthesis of PEG-derivatives

An increasing variety of mono-, homo- and heterobifunctional PEG reagents is commercially available, with different functional groups, molecular weights and multiple arms [58]. However, as described in previous studies, there are several methods to synthesize PEG-derivatives, being the major route by nucleophilic substitution on reactive, electrophilic PEGs, such as chloride, bromide, tosylate, mesylate or one of the active forms of PEG carboxylic acid [59]. Numerous functionalities can be introduced as end groups on PEG in this manner, including heterobifunctional products. For instance, Kataoka *et al*, synthesized a heterobifunctional PEG derivative containing aldehyde and thiol end groups [60]. Li and Kao, synthesized a library of 50 PEG-derivatives to expand the extent of conjugation with biologically active molecules and biomaterial substrates [61]. Hirsch *et al*, synthesized monofunctional PEG molecules, with a methoxy group at the free end [62].

Jayagopal *et al*, used bifunctional PEG molecules to introduce new functional groups on the surface, like with bifunctional crosslinkers in conjugation chemistry [63]. And more recently, Cauda *et al*, synthetized a well-known PEG-derivative, PEG-silane, commonly used in the functionalization of nanoparticles surface to increase water solubility [64]. Its synthesis generally consists in the formation of an intermediate leaving group, for example PEG tosylane, following the combination with (3-aminopropyl)triethoxysilane (APTES), creating the linear PEG-Silane [64].

1.4. Use of luminescent MSNs for drug/or proteins encapsulation

MSNs have particular properties which include large pore volume and high surface area, tunable particle size (10-1000 nm) and pore diameter (2-30 nm), uniform porosity, flexible morphology, easy surface functionalization, excellent biocompatibility and biodegradation. As a result, MSNs have been widely applied in the fields of separation and absorption [65], providing the possibility to load a high number of drugs or proteins within MSNs nanocarriers. In particular, the unique properties of these silica materials give them substantial potential for size exclusion separations of large molecules such as proteins [66,67]. On the other hand, these MSNs possess on their mesoporous channels surfaces and in the outer surfaces, several silanol groups, which facilitates the functionalization of the surface to allow a better control over the drug/protein diffusion kinetics, and also enhancing their selective absorption of several proteins with different molecular weights (MWs) or isoelectric points (pI), based on the exclusion mechanism [65]. In addition, functional materials, such as luminescent materials and polymers, can be combined with MSNs to form functional MSNs, which allow them to realize a targeted controlled drug/protein delivery and/or imaging. Therefore, MSNs have been considered to be excellent candidates as nanocarriers for drug/protein delivery [68-73].

Recently, many efforts have been made in the structural design and functional optimization to advance the development of drug/protein delivery systems based on MSNs, such as embedding functional materials in the mesoporous channels, and functionalizing the surface of the MSNs [74]. Because they cannot perform the targeted drug/protein delivery or track and evaluate the efficiency of the drug/protein release in diagnosis and therapy, it is necessary a combination of functional materials with the mesoporous channels, as a smart strategy to resolve these limitations, creating therefore luminescent MSNs. Luminescent labeling is a real-time, simple, and effective way to monitor the route of drug/protein delivery nanocarriers in a living system. Drug/protein delivery systems with

luminescent labels, such as QDs, can easily evaluate the efficiency of the drug/protein release and disease therapy, and also reduce the interference of the environment [31,75,76].

1.5. Characterization of nanoparticles

In this report was performed a combination of several techniques used to provide a detailed and precise structural information of the nanoparticles.

The standard characterization of MSNs included the use of electron microscopies (transmission electron microscopy, TEM, and scanning electron microscopy, SEM), X-ray powder diffraction (XRD/XRPD) and dynamic light scattering (DLS). The particle morphology was usually studied by SEM, while the ordered arrangement of the pores was detected by TEM. XRD was used to determine the ordered structure of the nanoparticles.

1.5.1. Electron microscopy

Electron microscopy is the best technique to study the size, shape and structure of nanoparticles. The electron microscope operates on the same basic principles as the light microscope however uses electrons instead of light, and because electrons have a much lower wavelength compared to photons, makes it possible to get a better resolution than with a light microscope [77].

The more commonly used are TEM and SEM [77].

1.5.1.1. Transmission electron microscopy (TEM)

Transmission electron microscopy is a microscopy technique in which a beam of electrons is transmitted through a specimen to form an image. TEM is composed by several elements, such as a vacuum system, where the electrons travel, an electron emission source to generate the electron stream, a series of electromagnetic lenses, as well as electrostatic plates [77-79].

A beam of electrons is generated by an electron gun and transmitted through the sample, interacting with the specimen as it passes through, creating an image from its interaction. Then the image is amplified and focused onto an imaging devise to be detected by a sensor, such as a charge-coupled device (CCD) camera. From these images, it is possible to obtain information about size and morphology, and also the distribution of the particles [77-79], Figure 1.4.

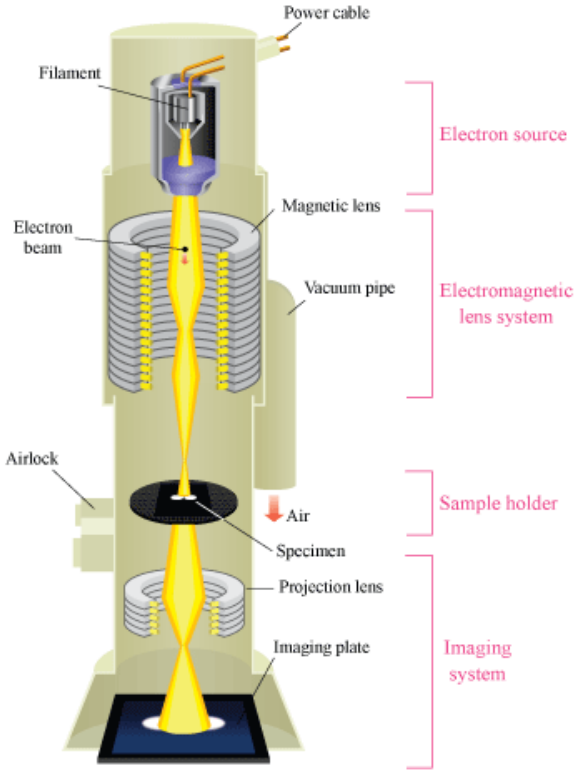

Figure 1.4 – Diagram outlining the internal components of a basic TEM system [80].

1.5.1.2. Scanning electron microscopy (SEM)

In scanning electron microscopy, an image of the specimen topography is formed when its surface is scanned with a focused beam of electrons [77-79].

Similar to TEM, a high voltage electron beam is created by an electron gun and focused to the sample by electrostatic and electromagnetic lenses. The primary electrons of the electron beam enter the sample and refract around one or several atomic nuclei, exciting the sample by nearly unchanged energy called backscattered electrons. When the beam scans a small area of the specimen surface, scattered secondary electrons are collected and an image of the specimen tomography is formed. Moreover, since the heavier nuclei refract more electrons, this method can be performed to determine the atomic composition of a sample [77-79], Figure 1.5.

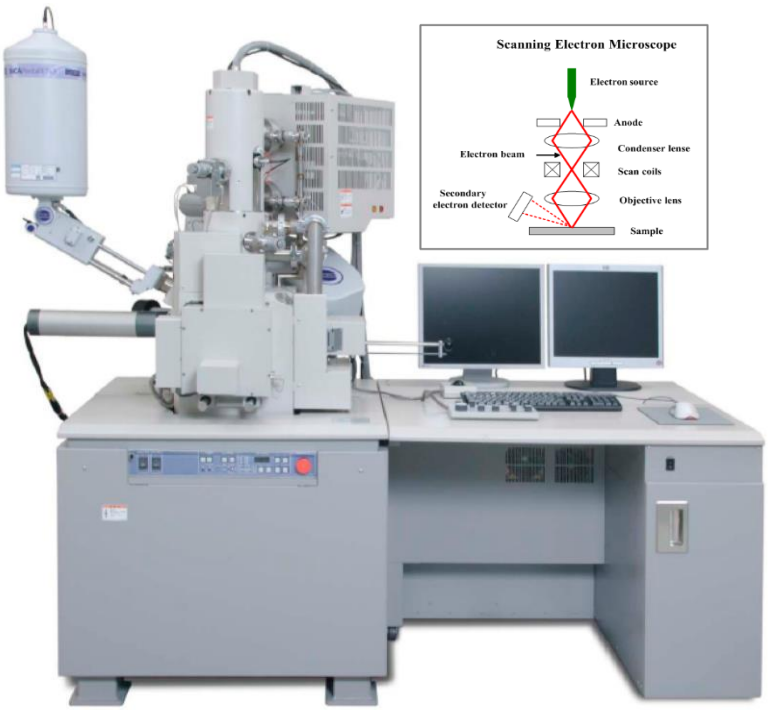

Figure 1.5 – Scanning electron microscope (Hitachi's SU6600 model) and schematic representation of the constituents' parts [81,82].

1.5.2. X-ray powder diffraction (XRD/XRPD)

X-ray powder diffraction is an analytical technique used for phase identification of a crystalline material by their diffraction pattern and it can provide information about unit cell dimensions [83].

In this technique, electrons are accelerated by an electrostatic potential in order to gain the desired energy to hit a target and generate the X-rays. These X-rays are collimated and directed onto the powder sample. Then a detector detects the X-ray signal to be processed, Figure 1.6 [83].

When the X-ray beam hits the sample and is diffracted, it is possible to measure the distance between the adjacent planes of the atoms (d-spacings) that constitute the sample by applying Bragg's Law:

$$(n\lambda = 2d \sin\theta) \qquad \text{(Equation 1.1)}$$

where n is the order of the diffracted beam, λ is the wavelength of the incident X-ray beam, d is the d-spacings, and θ is the diffraction angle of the incident X-ray beam. This law relates the wavelength of electromagnetic radiation with the diffraction angle and the lattice spacing in a crystalline sample. The characteristic set of d-spacings generated in the X-ray scan provides a unique "fingerprint" of the material present in the sample that when

properly interpreted, by comparison with standard reference patterns and measurements, allows the identification of the material [83].

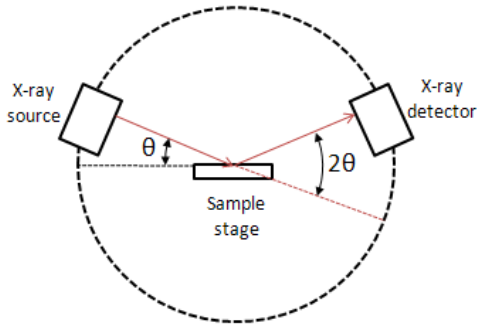

Figure 1.6 – Schematic representation of the XRD constituents' parts [84].

1.5.3. Dynamic Light Scattering (DLS)

Dynamic light scattering is used to determine the hydrodynamic size of a nanoparticle. It measures the Brownian motion of a particle at a certain speed, which is related to the size of the particles, defined by the Stokes-Einstein equation:

$$D_H = \frac{kT}{3\pi\eta D_t} \qquad \text{(Equation 1.2)}$$

where k is the Boltzmann constant, η is the solvent viscosity, T is the absolute temperature, D_t is the diffusion coefficient and D_H is the hydrodynamic diameter of the particle [85,86].

In the DLS instrument, Figure 1.7, when a sample is illuminated by a light source, such as laser, it scatters light in all directions. According to the Stokes-Einstein equation, Brownian motion of the particles is slower for bigger particles than for smaller particles, which leads to slower fluctuation of intensity-speckle change for bigger particles. In the case of a sample consisting of particles in two size classes equal in number, the bigger particles scatter more light resulting in a larger peak area by intensity. The size distribution of particles can also be determined by volume and by number. However, this data is normally generated from the raw data of the intensity [85,86].

Figure 1.7 – Dynamic light scattering instrument (Horiba SZ-100 Zetasizer Nano-Instrument model) [87].

1.5.4. Spectroscopic Techniques

In spectroscopic characterization, the techniques can be categorized into two groups:

- Vibrational spectroscopy (Fourier transformed infrared spectroscopy);
- Absorption and emission spectroscopy (absorption, photoluminescence).

1.5.4.1. Fourier Transformed Infrared spectroscopy (FT-IR)

This technique involves the interactions of photons with species in a sample which results in energy transfer to or from the sample, via vibrational excitation or de-excitation. Normally it is used to identify the type of bond between two or more atoms and consequently identify functional groups. In the FT-IR spectrometer, Figure 1.8, the infrared wavelengths range from 10 cm^{-1} to 14000 cm^{-1}, however in this report it has been mainly used in the middle infrared region that correspond to wavelengths between 400 cm^{-1} to 4000 cm^{-1}, and it is where the main vibrational models appear [88].

Figure 1.8 – FT-IR spectrometer (PerkinElmer Spectrum Two spectrometer model) [89].

1.5.4.2. Absorption spectroscopy

Absorption spectroscopy is an analytical technique, also called ultraviolet-visible (UV-Vis) spectrophotometry, based on the measurement of an amount of light absorbed by a sample at a given wavelength. The wavelength region is generally from 190 nm to 1000 nm, and the absorbing medium is at room temperature. However, in some cases, such as enzyme assays, it may be advantageous or necessary to perform measurements at temperatures above or below room temperature [90].

In UV-Vis spectrophotometry, the major energy levels are determined primarily by the possible spatial distributions of the electrons, and are called electronic energy levels. As for the lower extent, they are referred to as vibrational energy levels, which arise from various modes of molecule vibration (e.g. the stretching and bending of various covalent bonds). As a result, absorbance measurements allow the determination of a substance

concentration, the kinetic assay of certain chemical reactions and the identification of materials [90]. The UV-Vis spectrophotometer applied in this report is presented in Figure 1.9.

Figure 1.9 – UV-Vis spectrophotometer (JASCO V-630 model) [91].

1.5.4.3. Photoluminescence

Photoluminescence refers to the emission of light from a material after absorption of photons (electromagnetic radiation). This emitted luminescence is originated from photo excitation onto a sample, then collected by lens and passed through an optical spectrometer onto a photodetector [90].

This technique, provides information about the luminescence capabilities, structural and chemical changes, and emission lifetimes of different samples [90]. These measurements are carried out using a fluorescence spectrofluorometer, Figure 1.10.

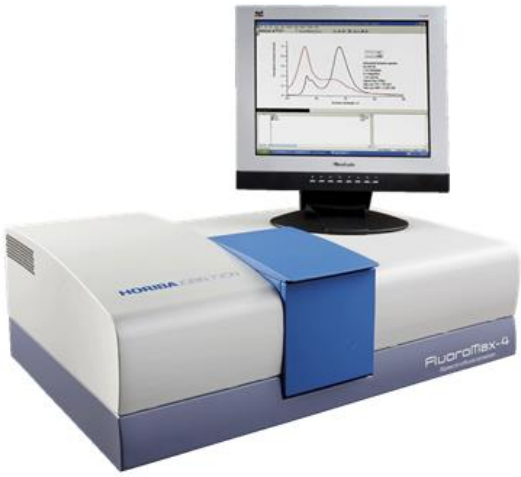

Figure 1.10 – Horiba JY Scientific Fluoromax 4 spectrofluorometer [92].

1.6. Aim of dissertation

As stated above, inorganic QDs have excellent optical properties; although, due to the use of heavy metal elements, they also are highly toxic and non-biodegradable. Therefore, Si QDs emerged as a new promising alternative to the toxic heavy-metal CdTe QDs, since they exhibit proper properties such as low toxicity and favorable biocompatibility and biodegradability. On the other hand, they are still chemically unstable, and as a result, they need to be incorporated into MSNs to provide better stability. However, MSNs have a drawback, which is low solubility and high PDI for *in vitro* and *in vivo* applications.

Considering all these aspects, the aim of this master dissertation is to synthesize and characterize MSNs doped with QDs (silicon and cadmium telluride) and functionalized with a PEG derivative to improve the water solubility, and their further application as protein loading/extraction system, Scheme 1.3.

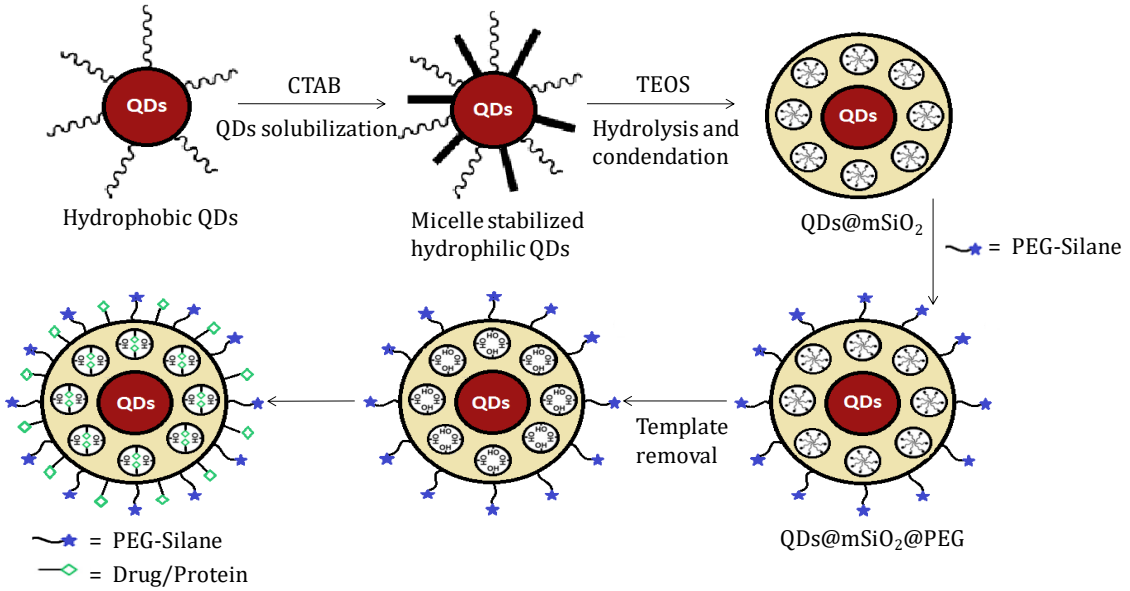

Scheme 1.3 – Synthetic procedure of luminescent MSNs functionalized with PEG-Silane and their application as protein loading/extraction system.

In Chapters 2 and 3 are summarized the synthesis and results concerning the formulation of the MSNs with CdTe QDs as a first approach (Chapter 2) and with Si QDs as the final approach and its optimization.

Chapter 4 summarized the synthesis and results of PEG-derivatives (PEG1 – PEG(3000)-Silane, PEG2 – TsO-PEG(6000)-Silane, PEG3 – TsO-PEG(8000)-Silane), which were functionalized in the surface of the luminescent MSNs, Figure 1.11.

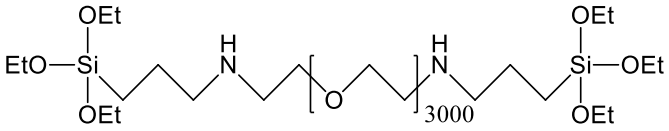

PEG(3000)-Silane (PEG1)

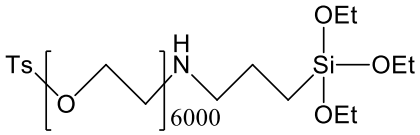

TsO-PEG(6000)-Silane (PEG2)

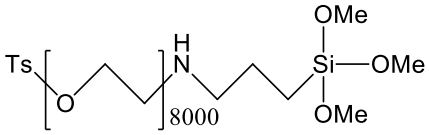

TsO-PEG(8000)-Silane (PEG3)

Figure 1.11 – PEG-derivatives discussed in Chapter 4.

Finally, some final remarks about the work present were covered in Chapter 5.

CHAPTER 2

SYNTHESIS OF CdTe QDs COATED WITH MESOPOROUS SILICA NANOPARTICLES

ABSTRACT

Herein we will focus on the synthesis and characterization of CdTe QDs coated with MSNs and their further application as protein loading/extraction systems. CdTe QDs with green and orange emission were synthetized in aqueous solutions, and further mixed with CTAB and TEOS, resulting in the luminescent mesoporous silica nanoparticles. To increase the solubility of these systems in water, PEG1 was functionalized on their surface.

KEYWORDS: Cadmium Telluride Quantum Dots, Mesoporous silica nanoparticles, PEG-Silane, Proteins.

2.1. EXPERIMENTAL SECTION

2.1.1. Reagents and Chemicals:

Thioglycolic acid (TGA, $C_2H_4O_2S$, ≥99%), cadmium acetate dihydrate ($Cd(CH_3COO)_2{\cdot}2H_2O$, 99.5%), tetraethyl orthosilicate (TEOS, $SiC_8H_{20}O_4$, 98%), cetyltrimethylammonium bromide (CTAB, $C_{19}H_{42}BrN$, ≥98%), bovine serum albumin (BSA), lysozyme (LYS), carbonic anhydrase (CA), ovalbumin (OVA), hemoglobin (Hb), myoglobin (Myb), cytochrome c (CYT) and phosphate buffered saline (PBS) were purchased from Sigma-Aldrich. Sodium borohydride ($NaBH_4$, 99%) and ethylene glycol ($C_2H_6O_2$, ≥99.5%) were produced by Fluka. Sodium tellurite (Na_2TeO_3, 99.5%) and ammonium nitrate (NH_4NO_3, 99.9%) were purchased from Alfa Aesar. Sodium hydroxide (NaOH) was produced by Panreac. Methanol (MeOH) was produced by Carlo Erba Reagents. All the reagents and solvents were of analytical reagent grade and were used as received.

2.1.2. Syntheses:

2.1.2.1. Synthesis of CdTe QDs

$Cd(CH_3COO)_2 \cdot 2H_2O$ (53 mg, 0.2 mmol) was dissolved into 50 mL of bi-distilled water in a stand-up flask (solution A). Then 18 μL TGA was added and the pH was adjusted to 10, adding dropwise a solution of 1 M NaOH (by adding TGA the solution becomes cloudy and then the NaOH must be added until it is transparent). After that, 8.86 mg (0.04 mmol) of Na_2TeO_3 which was dissolved in 50 mL bi-distilled water (solution B) was added into the previous solution (solution A). Then 80 mg of $NaBH_4$ was added to the final mixture and stirred at room temperature for 5 min. After this, the reaction mixture was divided in half and transferred into two twin-neck round-bottom flask which were attached to a condenser and refluxed at ~200°C under open-air conditions. The reaction time was controlled under UV light, giving green CdTe QDs at approximately 10 min and orange CdTe QDs at approximately 15 min [11].

2.1.2.2. Synthesis of CdTe QDs coated with MSNs (CdTeQDs@mSiO$_2$)

To the previous crude solution (2.1.2.1.) of CdTe QDs, was added 0.10 g of CTAB which was dissolved in 10 mL of bi-distilled water. This mixture was stirred for 30 min at 50°C. By this order, bi-distilled water (30 mL), ethylene glycol (10 mL) and NaOH 1M (165 μL) was added to the above mixture and stirred for further 30 min at 70°C. Then, 0.75 mL of TEOS was added dropwise to the mixture and left for 3 h at 70°C under stirring. The final product was washed three times with a solution of bi-distilled water and methanol. For template removal, a solution of 60 mg of NH_4NO_3 in 20 mL of methanol was added to the previous washed product and transferred to a round-bottom flask which was stirred for 30 min at 60°C. The last three steps were repeated twice.

2.1.2.3. Functionalization of green CdTeQDs@mSiO$_2$ with PEG1 (CdTeQDs@mSiO$_2$@PEG1)

A total of 200 mg of PEG1 was dissolved in 6.5 mL of bi-distilled water. Then, this solution was added to the green CdTeQDs@$mSiO_2$ suspension with template (50 mg in 6.5 mL of bi-distilled water), followed by 3 h of reflux at 100°C. The mixture was then stirred overnight at room temperature. The functionalized mesoporous nanoparticles were isolated by centrifugation (4000 rpm, 10 min), washed three times with bi-distilled water and twice with ethanol, and dried. The template was removed by the same procedure as mentioned in 2.1.2.2. After that, the final product was washed one time with bi-distilled water and twice with methanol, and dried [93].

2.1.3. Protein encapsulation studies

Protein stock solutions (0.5 mg/mL) of BSA, LYS, CA, OVA, Hb, Myb and CYT were prepared in phosphate buffer (0.01 M, pH 7.4). A suspension of luminescent MSNs (2 mg/mL) in 1 mL of PBS was sonicated for 10 min. After that 0.5 mL of proteins were mixed with 0.5 mL of luminescent MSNs. The final suspensions were stirred for 30 min. The samples were centrifuged and the supernatant quantified by absorption using the Bradford assay in a CLARIOstar® High Performance Monochromator Multimode Microplate Reader (BMG LABTECH). The encapsulation efficiency (EE) and the loading capacity were determined by the following equations ($t_{protein}$: the total amount of protein/molecule; $f_{protein}$: the amount of free protein/molecule) [72]:

$$EE\ (\%) = \frac{t_{protein} - f_{protein}}{t_{protein}} \times 100\% \qquad \text{(Equation 2.1)}$$

$$loading\ capacity\ (mg/g) = \frac{t_{protein\ (mg)} - f_{protein\ (mg)}}{amount\ of\ nanoparticles} \qquad \text{(Equation 2.2)}$$

This study was performed for **green CdTeQDs@mSiO$_2$** and **green CdTeQDs@mSiO$_2$@PEG1**, section 2.1.2.2. and 2.1.2.3., respectively.

2.1.4. Characterization:

2.1.4.1. Measurements

The UV-Vis absorption spectra were acquired on a *Jasco V-630* spectrophotometer. The fluorescence measurements were recorded using a *FluoroMax4* spectrometer (Horiba Yvon Jobin) at room temperature. The fluorescence quantum yield (Φ_F) of the CdTe QDs was estimated by comparison with acridine yellow in ethanol (Φ_F = 0.47)[94] for the green QDs, and with rhodamine B in ethanol (Φ_F = 0.70)[95] for the orange QDs. DLS to evaluate the particle size and zeta potential was carried out on a *SZ-100 Zetasizer Nano-Instrument* (Horiba). Morphology and size distribution were examined by SEM and TEM. SEM was performed in a *SEM-FIB – Zeiss Auriga CrossBeam*, workstation at Laboratory of Nanofabrication, CENIMAT, and TEM images was obtained in a *JEOL JEM 2010F* operating at 200 kV, and collected using a multi-scan camera and a Digital Micrograph software from Gatan. The XRD patterns were collected on a *Rigaku*, model *MiniFlex II*, diffractometer with a Cu Kα (λ = 1.5418 Å) radiation source (30 kV, 15 mA). Measurements were step-scanned in 0.02° 2θ steps in the 1-12° range, with a scan speed of 0.5°/min. Infrared spectra were recorded on a *PerkinElmer BX* or *PerkinElmer Spectrum Two* spectrometer.

2.2. RESULTS AND DISCUSSION

CdTe QDs were synthesized following the method reported by Wu and co-workers [11]. Briefly, CdTe QDs were obtained in one-pot method, in water and open-air conditions, using TGA as a ligand, without protection of nitrogen gas, and using Na_2TeO_3 as a stable Te source and $NaBH_4$ as reducing agent. The CdTe QDs were then further coated with a monolayer of MSNs and functionalized with the polymer PEG1 in order to increase water solubility.

2.2.1. CdTe QDs

In Figure 2.1 is represented the absorption (Figure 2.1 – A) and fluorescence emission (Figure 2.1 – B) spectra of the green and orange CdTe QDs in aqueous solution, which were taken at different refluxing times from the reaction mixture. Additional analysis concerning the size, PDI, zeta potential and Φ_F values of green and orange CdTe QDs are also presented in Figure 2.1 – C.

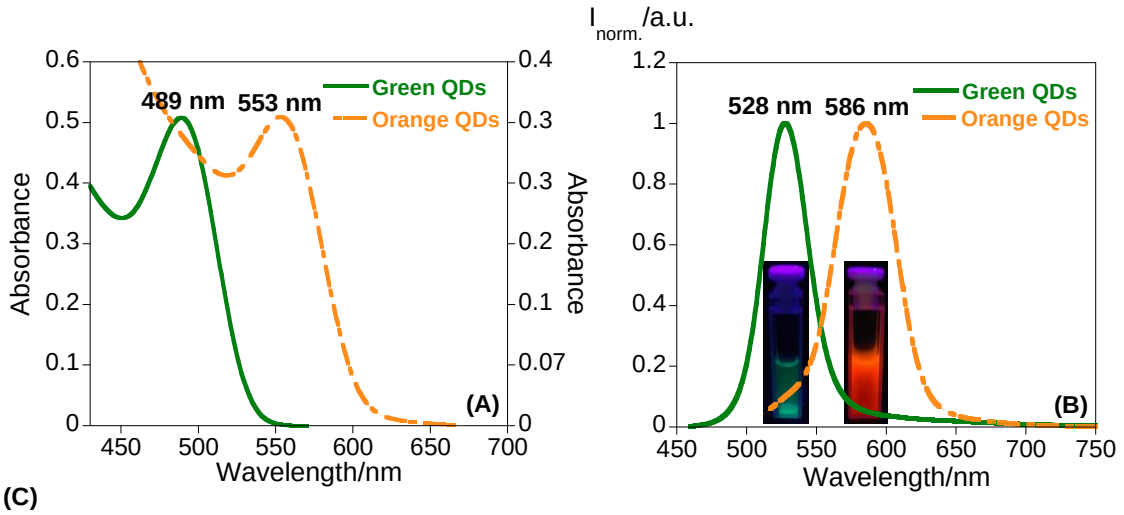

(C)

CdTe QDs	Size (nm) / PDI	Zeta Potential (mV)	Φ_F (%)
Green	4.56 / 0.38	-16.47	31.46
Orange	9.48 / 0.66	-32.43	11.54

Figure 2.1 – (A) Absorption spectra of green CdTe QDs and orange CdTe QDs; (B) Fluorescence emission spectra of green CdTe QDs (λ_{exc} = 450 nm) and orange CdTe QDs (λ_{exc} = 500 nm) and images of the QDs under UV irradiation (λ_{exc} = 365 nm). (C) Size, PDI, zeta potential and Φ_F values of green and orange CdTe QDs.

By prolonging the refluxing time, is shown that the absorption spectra of the CdTe QDs as well as the fluorescence emission spectra shifted to longer wavelengths with the increase of the particle size as a consequence of the quantum confinement. This behavior was possible to confirm by evaluating the particle size, zeta potential through DLS (Figure 2.1 – C) and color tunability (λ_{exc} = 365 nm, Figure 2.1 – B) from green to orange by

increasing the reaction time.

After 10 min and 15 min of reflux, a maximum absorption was obtained at 489 nm and 553 nm, and emission at 528 nm and 586 nm corresponding to the green and orange CdTe QDs, respectively.

As mentioned above, the size and zeta potential of the synthesized QDs were measured by DLS. Green QDs reached a size of ca. 4.6 nm and a zeta potential of ca. −16 mV, whereas for the orange QDs a size of ca. 9.5 nm and a zeta potential of ca. −32 mV was obtained. As expected, there is an increase in the size of the QDs, from green to orange QDs, and it was also observed that as the size increased the stability also increased, since the obtained values were shown to be negative with a value higher than −30 mV. Moreover, CdTe QDs presented Φ_F values of 31.46% and 11.54% for the green and orange QDs, respectively. The values herein obtained are in agreement to the ones obtained in literature in the same conditions (pH = 10.0, 528 nm (Φ_F = 30%) and 586 nm (Φ_F = 15%)) [11].

To overcome the issue of instability, the crude CdTe QDs were coated with a layer of MSNs.

2.2.2. CdTe QDs coated with MSNs (CdTeQDs@mSiO$_2$) and functionalization of green CdTeQDs@mSiO$_2$ with PEG1

This synthesis consisted in the creation of a protective layer around the CdTe QDs to prevent their oxidation and degradation. Also, this layer allows the functionalization of other molecules on its surface, making them useful for biological applications, such as drug delivery systems or protein loading/extraction [34].

As described in the experimental part (section 2.1.2.2.), in the synthesis of the MSNs, the cationic surfactant CTAB was used as a structural agent (template), TEOS as the silica source, ethylene glycol as the micelles stabilizer and sodium hydroxide as the morphological catalyst. Due to their poor solubility, the MSNs doped with CdTe QDs were characterized by solid-state emission spectroscopy to understand the effect of chemical binding on fluorescent properties (Figure 2.2 – A).

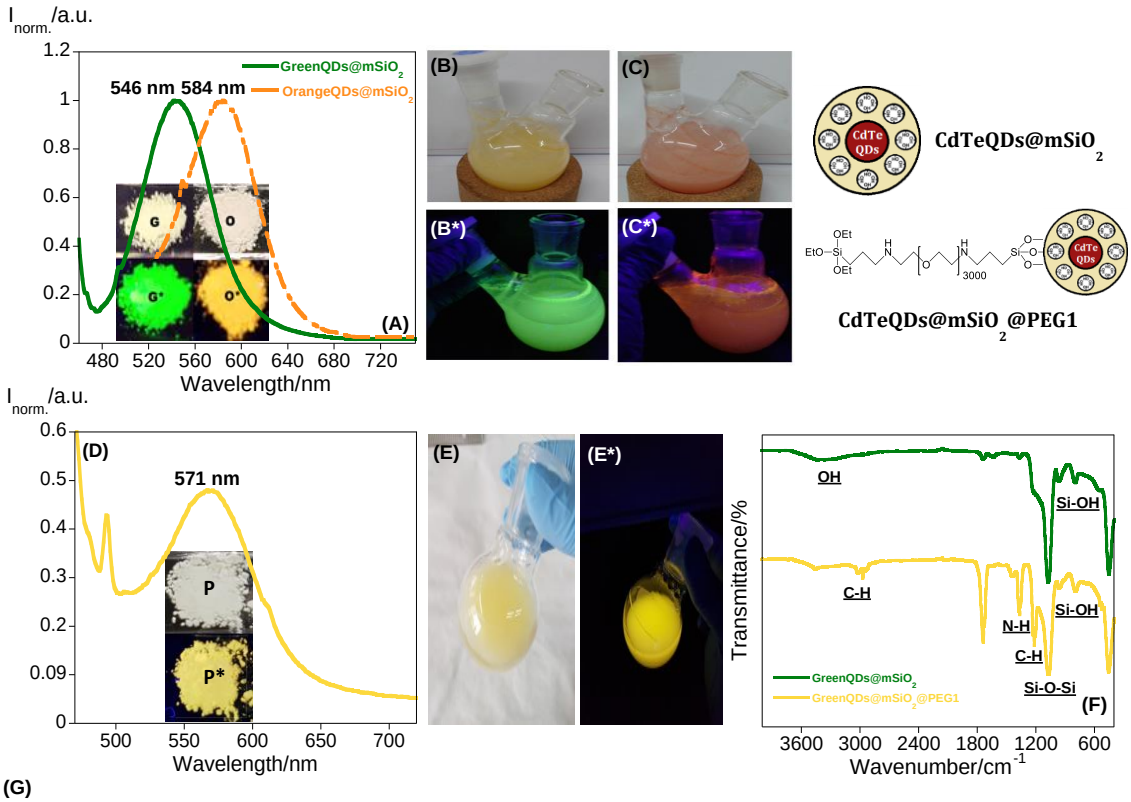

(G)

	Size (nm) / PDI	Zeta Potential (mV)
Green CdTeQDs@mSiO$_2$	1012 / 0.48	-13.43
Orange CdTeQDs@mSiO$_2$	1003 / 0.63	-14.17
Green CdTeQDs@mSiO$_2$@PEG1	1766 / 0.27	-34.27

Figure 2.2 – (A) Solid-state fluorescence emission spectra of (A) green (λ_{exc} = 450 nm) and orange (λ_{exc} = 500 nm) CdTeQDs@mSiO$_2$, and (D) green CdTeQDs@mSiO$_2$@PEG1 (λ_{exc} = 450 nm). Inset A, D: (G, O, P) Naked eye and (G*, O*, P*) under UV irradiation (λ_{exc} = 365 nm) of green CdTeQDs@mSiO$_2$, orange CdTeQDs@mSiO$_2$ and green CdTeQDs@mSiO$_2$@PEG1, respectively photographs. (B-C) Naked eye and (B*-C*) under UV irradiation (λ_{exc} = 365 nm) of green and orange CdTeQDs@mSiO$_2$ photographs. (E) Naked eye and (E*) under UV irradiation (λ_{exc} = 365 nm) of green CdTeQDs@mSiO$_2$@PEG1 photographs. (F) Infrared spectra of green and orange CdTeQDs@mSiO$_2$ and PEGylated green CdTeQDs@mSiO$_2$. (G) Size, PDI and zeta potential values of green and orange CdTeQDs@mSiO$_2$ and green CdTeQDs@mSiO$_2$ functionalized with PEG1. All these measurements were performed without template.

The solid-state emission spectra show a maximum of emission at 546 nm and 584 nm corresponding to the green and orange CdTeQDs@mSiO$_2$, respectively. It was possible to observe a slight shift in the maximum emission wavelength from CdTe QDs to CdTeQDs@mSiO$_2$, which can be explained by the change in ground-state and excited-state energies along with the change in the surrounding environments [42].

The images of CdTeQDs@mSiO$_2$ at naked eye (Figure 2.2 – B-C) and under an ultraviolet lamp (λ_{exc} = 365 nm, Figure 2.2 – B*-C*) are also presented, and they showed that no changes were detected in the color of the CdTeQDs@mSiO$_2$ compared with the CdTe QDs after the functionalization of the QDs with the MSNs.

This functionalization showed a great improvement on the photo-stability of the

QDs, however consequently was created a system with low water solubility for biological applications. Therefore, the functionalization of a polymer onto the mesoporous silica surface was needed.

This synthesis consisted of the increase of water solubility of the CdTeQDs@mSiO$_2$, by functionalizing the surface with the polymer PEG1. After removing the surfactant of the nanoparticles, the powder obtained was characterized by solid-state emission spectra, Figure 2.2 – D. It was possible to observe a maximum of emission at 571 nm corresponding to the green CdTeQDs@mSiO$_2$@PEG1 obtained. Any significant reduction in the fluorescence is observed. However a red shift of 25 nm (from 546 nm to 571 nm) is visualized in the maximum of emission band compared with green CdTeQDs@mSiO$_2$. As a result there was a change in color of the powder under UV irradiation from green to yellow, as can be seen in Figure 2.2 – E*.

Infrared spectra of the green CdTeQDs@mSiO$_2$ and CdTeQDs@mSiO$_2$@PEG1 nanoparticles (Figure 2.2 – F) was performed to confirm the chemical binding of the products. The typical peaks at 3387 cm^{-1}, 1072 cm^{-1}, 965 cm^{-1} corresponding to the vibrations O-H, Si-O-Si and Si-O-H are detected in CdTeQDs@mSiO$_2$ nanoparticles, confirming the pure nature of the mesoporous nanoparticles and the presence of silanol groups at its surface. The PEGylated nanoparticles show the characteristic peaks at 2980 cm^{-1} corresponded to C-H of methyl and methylene groups of the polymer chain. Additionally, peaks at 1736 cm^{-1}, 1366 cm^{-1} and 1206 cm^{-1} are characteristic of C=O, NH, and CH of the polymer backbone, respectively.

All these nanoparticles were also characterized by DLS (Figure 2.2 – G). DLS measurements were carried out in water, and the values of size suggest that by coating the CdTe QDs with mesoporous silica we were able to observe an increase in size compared with CdTe QDs. Moreover, it shows larger particle sizes for the sample containing the polymer PEG1 in comparison to the unfunctionalized green CdTeQDs@mSiO$_2$ nanoparticles. Despite the increase in the hydrodynamic diameter, the introduction of a PEG polymer, increases the stability of these nanoparticles leading to a more negative and stable zeta potential (changes from ca. −13 mV to −34 mV). In the same way, the aggregation state decreases as can be seen in the decrease of the PDI. In contrast, the unfunctionalized nanoparticles tend to aggregate in water, more in orange nanoparticles than in green nanoparticles, confirmed by a higher PDI.

The morphology of the nanoparticles was confirmed by TEM and SEM images of green CdTeQDs@mSiO$_2$@PEG1 (Figure 2.3). TEM and SEM images proved the spherical

shape of the nanoparticles, as well as their pore in Figure 2.3 – C, represented by the white dots. Through TEM and SEM images, was noticed that green CdTeQDs@mSiO$_2$@PEG1 nanoparticles have a size around 89 ± 7 nm. In general, the particle sizes obtained by DLS measurements are larger than those obtained from TEM and SEM measurements, since (i) the hydrodynamic diameter is measured and (ii) some degree of weak agglomeration can also increase the apparent particle size distribution [68].

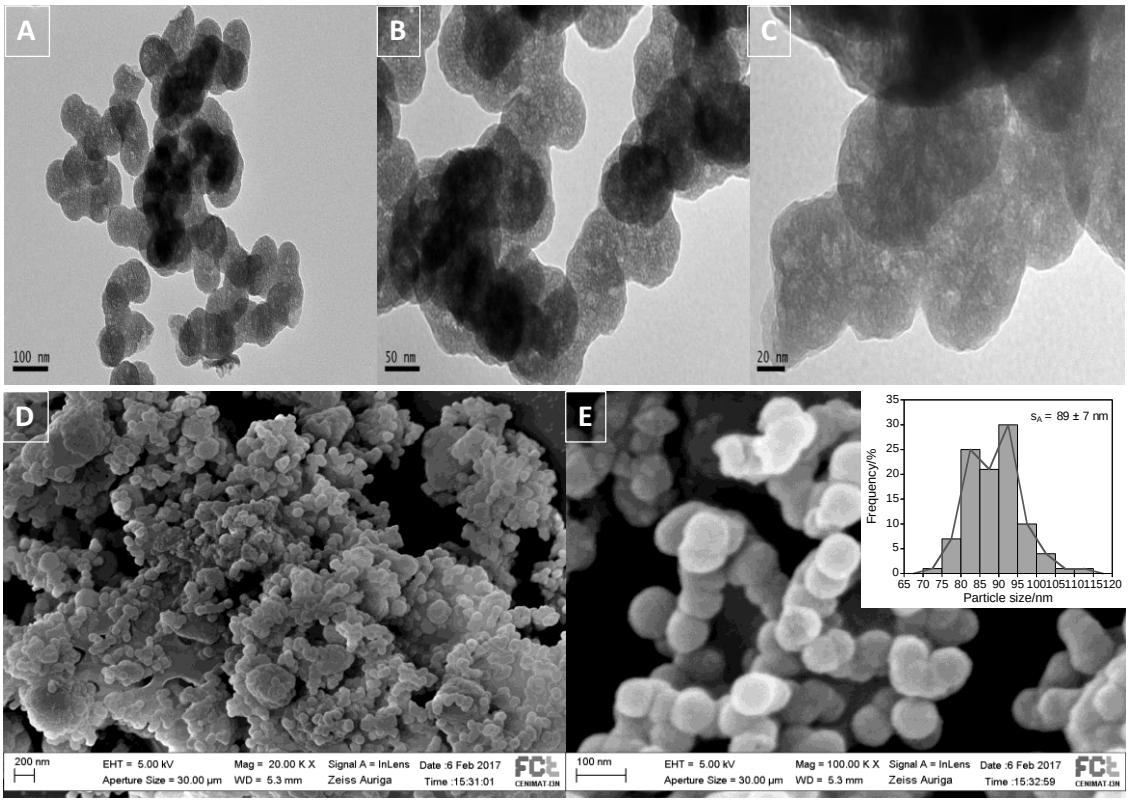

Figure 2.3 – (A-C) TEM images of green CdTeQDs@mSiO$_2$@PEG1. (D-E) SEM image of green CdTeQDs@mSiO$_2$@PEG1. The inset image shows the corresponding size distribution.

Powder XRD experiment also was performed to determine the specific structure of the obtained product. XRD pattern of the green and orange CdTe QDs MSNs without template, is shown in Figure 2.4.

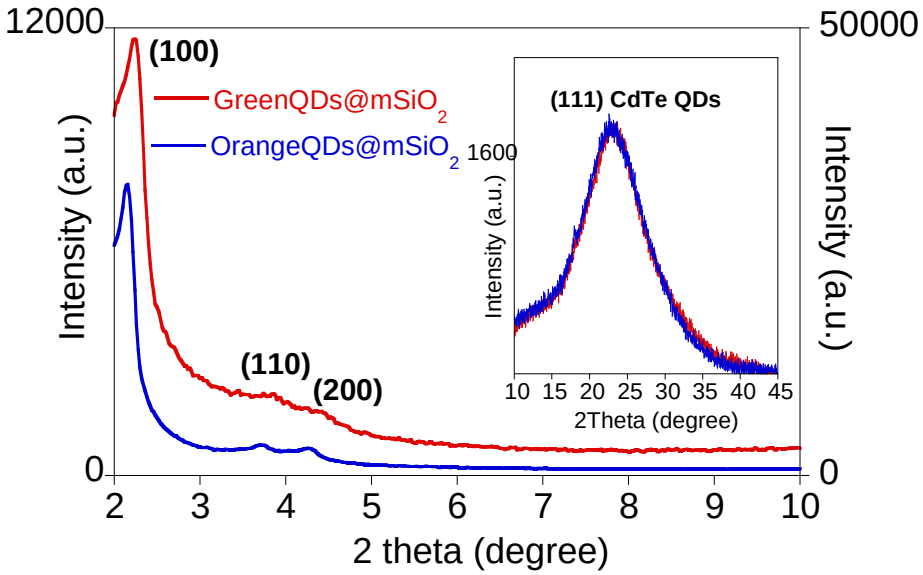

Figure 2.4 – Powder X-ray diffraction pattern of green and orange CdTeQDs@mSiO$_2$ without template.

In both cases, the XRD analysis shows the three-typical low-angle reflections of a hexagonal array, which can be numbered as (100), (110) and (200) Bragg peaks [28]. These results suggest well-ordered mesoporous nanoparticles. The broad peak located in the range of 15-35° indicate the presence of amorphous silicon dioxide. The maximum peak at 24.5° corresponds to the plane (111) of the cubic zinc blende structure of CdTe crystal [42].

2.2.3. Encapsulation studies on green CdTeQDs@mSiO$_2$ and PEGylated green CdTeQDs@mSiO$_2$

Encapsulation studies of the green CdTeQDs@mSiO$_2$ and PEGylated green CdTeQDs@mSiO$_2$ in physiological pH (PBS, pH = 7.4) with single proteins exhibiting different sizes and pI, such as BSA, LYS, CYT, Myb, Hb, CA and OVA were accomplished. These proteins were selected due to the wide variety of physical properties they collectively presented (Table 2.1 and Table A.1 - Appendix).

The proteins were incubated with the nanoparticles in PBS, with a weight ratio of 1:4 (protein:MSNs) for incubation times of 30 min. EE and the amount adsorbed were determined accordingly with section 2.1.3. in the experimental part, and the obtained results are gathered in Figure 2.5.

Table 2.1 – List of encapsulated proteins and their properties. [a]Geometric dimensions given by published literature [96,97]. [b]The residue count of these proteins come from the Protein Data Bank. PDB codes: BSA, 3V03; LYS, 1DPX; CYT, 1HRC; Myb, 1WLA; Hb, 1A3N; CA, 1V9E; OVA, 1OVA.

Protein	MW (Da)	Size (nm)	pI	Negatively charged residues (%)	Positively charged residues (%)
Bovine Serum Albumin (BSA)	69293	5 x 5 x 9	4.9	6.6	22.7
Lysozyme (LYS)	16239	3 x 3 x 4.5	10–10.5	4.8	28.6
Cytochrome C (CYT)	11833	2.6 x 3.2 x 3.3	11.35	2.9	23.8
Myoglobin (Myb)	17083	ca. 17.6	6.8-7.2	5.2	16.2
Hemoglobin (Hb)	15998	5.3 x 5.4 x 6.5	6.8	4.8	13.6
Carbonic Anhydrase (CA)	28822	3.9 x 4.2 x 5.5	5.9	5.7	16.1
Ovalbumin (OVA)	42881	4 x 5 x 7	4.9	3.6	16.8

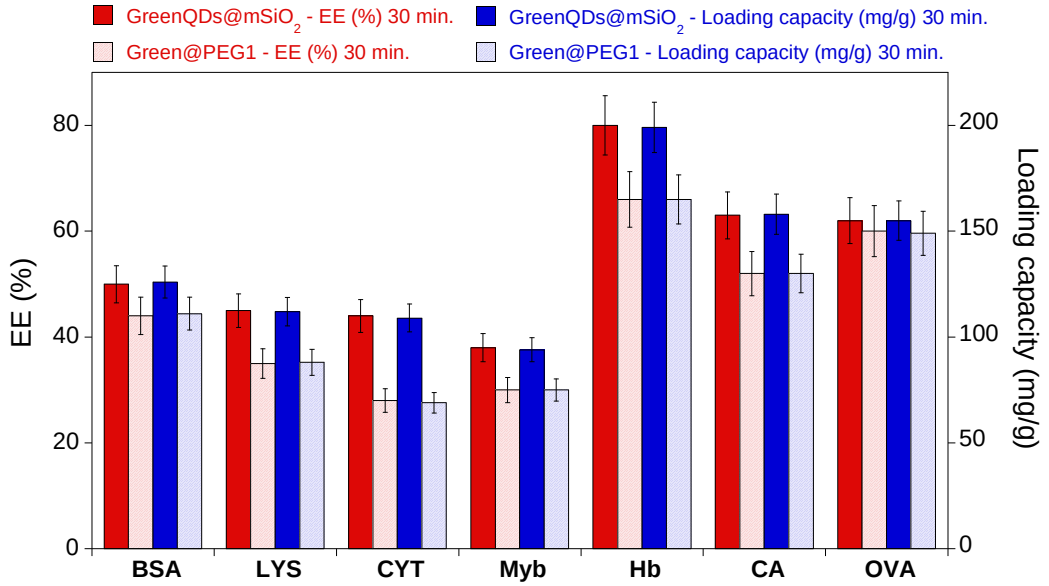

Figure 2.5 – Encapsulation efficiency and corresponding loading capacity of several proteins in green CdTeQDs@mSiO$_2$ and PEGylated green CdTeQDs@mSiO$_2$, weight ratio of 1:4 (protein:MSNs) in PBS pH = 7.4.

Zeta potential analysis (Figure 2.2 – G) revealed a negative surface charge for green CdTeQDs@mSiO$_2$ and PEGylated green CdTeQDs@mSiO$_2$ (−13.43 mV and −34.27 mV, respectively). Consequently, it should be expected an effect of the charge in the extent of the protein encapsulation, being a more efficient encapsulation for proteins with a positive surface charge, such as LYS and CYT. However, no significant changes were observed, as a matter of fact, the encapsulation with the negative/neutral charged proteins Hb, CA, OVA was more efficient, with EE around 70% and a loading capacity of ca. 150-200 mg/g, indicating that electrostatic interactions were not the main driving force for protein encapsulation. Moreover, the addition of PEG1 resulted in a slight decrease in the affinity of the nanoparticles to the proteins.

2.3. CONCLUSIONS

In summary, fluorescent CdTe QDs coated with MSNs have been successfully obtained and good dispersions in water were obtained through the introduction of PEG derivatives. Different techniques were applied to characterize CdTeQDs@mSiO_2 and PEGylated nanoparticles. Experiments prove that QDs coated with MSNs can induce a great improvement on the photo-stability of the QDs. Moreover, the functionalization of a polymer PEG1 onto the mesoporous silica surface also improved the problem of poor water solubility caused by the introduction of the protective layer of MSNs. The morphology of these nanoparticles with a size around 89 ± 7 nm for PEGylated nanoparticles, was also confirmed by TEM and SEM images, which proved to be of spherical shape. In addition, green CdTeQDs@mSiO_2 and CdTeQDs@mSiO_2@PEG1 have demonstrated a large affinity for several negative/neutral charged proteins, such as Hb, CA and OVA. Moreover, the addition of PEG1 resulted in a slight decrease in the affinity of the nanoparticles to the proteins. Due to these results, it is possible to conclude that there was created a system with possible biological applications.

CHAPTER 3

SYNTHESIS OF Si QDs COATED WITH MESOPOROUS SILICA NANOPARTICLES

ABSTRACT

Herein we will focus on the synthesis and characterization of Si QDs coated with MSNs and their further application as protein loading/extraction systems. Si QDs were synthesized in aqueous solutions, optimized and coated with MSNs, resulting in the luminescent mesoporous silica nanoparticles. To increase the solubility of these systems in water, PEG-Silane derivatives were functionalized on their surface.

KEYWORDS: Silicon Quantum Dots, Mesoporous silica nanoparticles, PEG-Silane, Proteins.

3.1. EXPERIMENTAL SECTION

3.1.1. Reagents and Chemicals:

(3-Aminopropyl)trimethoxysilane (APTMS, $H_2N(CH_2)_3Si(OCH_3)_3$, 97%), (3-aminopropyl)triethoxysilane (APTES, $H_2N(CH_2)_3Si(OC_2H_5)_3$, 99%), (+)-sodium L-ascorbate (SA, $C_6H_7NaO_6$, ≥98%), tetraethyl orthosilicate (TEOS, $SiC_8H_{20}O_4$, 98%), tetramethyl orthosilicate (TMOS, $SiC_4H_{12}O_4$, 98%), ammonia (NH_3, ≥99.9%), cetyltrimethylammonium bromide (CTAB, $C_{19}H_{42}BrN$, ≥98%), %), bovine serum albumin (BSA), lysozyme (LYS), carbonic anhydrase (CA), ovalbumin (OVA), hemoglobin (Hb), myoglobin (Myb), cytochrome c (CYT) and phosphate buffered saline (PBS) were purchased from Sigma-Aldrich. Ascorbic Acid (AA, $C_6H_8O_6$, 99%) and sodium hydroxide (NaOH, ≥98%) were produced by Panreac. Ammonium nitrate (NH_4NO_3, 99.9%) was purchased from Alfa Aesar. Ethylene glycol ($C_2H_6O_2$, ≥99.5%) and (3-isocyanatopropyl)triethoxysilane (IPTES, $(C_2H_5O)_3Si(CH_2)_3NCO$, 95%) were produced by Fluka. Methanol (MeOH) and ethanol (EtOH) were produced by Carlo Erba Reagents. All the reagents and solvents were of analytical reagent grade and were used as received.

3.1.2. Syntheses:

3.1.2.1. Assay A (proof-of-concept)

3.1.2.1.1. Synthesis of Si QDs (Si QDs I and II)

The Si QDs were prepared by adding 1 mL of APTMS in the synthesis I and APTES in the synthesis II to 4 mL of bi-distilled water while stirring. Then, 1.25 mL of 0.1 M SA was added to the above mixture and stirred for 30 min at room temperature [25].

3.1.2.1.2. Synthesis of Si QDs coated with MSNs (SiQDs@$mSiO_2$ I and II)

To the previous crude solution (3.1.2.1.1.) of Si QDs was added 10 mL of an aqueous solution of 0.1 M CTAB. This mixture was stirred for 30 min at room temperature. 500 µL of ammonia was added to the mixture and stirred for further 30 min. Then, 500 µL of TEOS was added dropwise to the mixture and left for 2 h at 80°C under stirring. The final product was washed with ethanol and filtered. For template removal, a solution of 60 mg of NH_4NO_3 in 20 mL of methanol was added to the previous washed product and transferred to a round-bottom flask which was stirred for 30 min at 60°C. The last three steps were repeated twice. The reaction mixture was washed three times with bi-distilled water and methanol, and dried.

3.1.2.1.3. Functionalization of SiQDs@$mSiO_2$ with PEG1 (SiQDs@$mSiO_2$@PEG1 I and II)

200 mg of PEG1 were previously dissolved in 6.5 mL of bi-distilled water. Then, this solution was added to the SiQDs@$mSiO_2$ (with template) suspension I and II (50 mg in 6.5 mL of bi-distilled water), followed by 3 h of reflux at 100°C. The functionalized mesoporous nanoparticles were isolated by centrifugation, washed three times with bi-distilled water and twice with ethanol, and dried. For template removal it was followed the same procedure reported in 3.1.2.1.2. [93].

3.1.2.2. Si QDs Optimizations

3.1.2.2.1. Varying the ratio of reducing agent and water

The Si QDs were prepared by adding 1 mL of APTMS to different amounts of bi-distilled water and 0.1 M of SA and AA, accordingly with Table 3.1. Then the mixtures were stirred for 1 h at 40°C [26].

Table 3.1 – Parameters used in the synthesis.

	Reducing agent - AA			Reducing agent - SA		
	APTMS (mL)	H_20 (mL)	AA (mL)	APTMS (mL)	H_20 (mL)	SA (mL)
E0)	1	5.25	-	1	5.25	-
E1)	1	4	1.25	1	4	1.25
E2)	1	3	2.25	1	3	2.25
E3)	1	2	3.25	1	2	3.25
E4)	1	1	4.25	1	1	4.25
E5)	1	-	5.25	1	-	5.25

3.1.2.2.2. Varying the concentration of the reducing agent

The Si QDs were prepared by the same procedure reported in 3.1.2.2.1., which to 1 mL of APTMS and 4 mL of bi-distilled water were added different concentrations of SA and AA (see Table 3.2).

Table 3.2 – Parameters used in the synthesis.

	Reducing agent - AA			Reducing agent - SA		
	APTMS (mL)	H_20 (mL)	AA (mL)	APTMS (mL)	H_20 (mL)	SA (mL)
R1)	1	4	1.25 (0.05 M)	1	4	1.25 (0.05 M)
R2)	1	4	1.25 (0.10 M)	1	4	1.25 (0.10 M)
R3)	1	4	1.25 (0.15 M)	1	4	1.25 (0.15 M)
R4)	1	4	1.25 (0.20 M)	1	4	1.25 (0.20 M)

3.1.2.2.3. Varying the silane source and reducing agent volumes

The Si QDs were prepared by adding 2 mL of APTMS to 4 mL of bi-distilled water while stirring. Then, 4 mL of 0.1 M SA were added to the above mixture and stirred for 2 h at 50°C.

3.1.2.3. Assay B

3.1.2.3.1. Synthesis of Si QDs functionalized with IPTES (SiQDs@Isoc)

After optimization of the reaction described in 3.1.2.2., the procedure 3.1.2.2.2. R2) was selected, and the Si QDs were prepared following this procedure with AA. After 30 min under stirring, the temperature was removed and 2 mL of IPTES were added to the mixture and stirred for 2 h at room temperature (a white precipitate was form after the addition of IPTES. The mixture was centrifuged, washed 3 times with bi-distilled water and dried.

3.1.2.3.2. Synthesis of SiQDs@Isoc coated with MSNs (SiQDs@Isoc@mSiO$_2$)

3.1.2.3.2.1. Via i (T1 and T2)

To the previous SiQDs@Isoc (200 mg), 0.10 g of CTAB were added which was dissolved in 10 mL of bi-distilled water. This mixture was stirred for 30 min at 50°C. By this order, bi-distilled water (30 mL), ethylene glycol (10 mL) and NaOH 1 M (165 µL) were added to the mixture above and stirred for further 30 min at 70°C. Then, 0.75 mL of TEOS (T1) or TMOS (T2) were added dropwise to the mixture and left for 3 h at 70°C under stirring. The final product was washed three times with methanol. For the removal of the template it was followed the same procedure reported in 3.1.2.1.2.

3.1.2.3.2.2. Via ii (T3 and T4)

To the previous SiQDs@Isoc (200 mg), 10 mL of an aqueous solution of 0.1 M CTAB was added. This mixture was stirred for 30 min at room temperature. 500 µL of ammonia were added to the mixture above and stirred for further 30 min at 50°C. Then, 500 µL of TEOS (T3) or TMOS (T4) were added dropwise to the mixture and left for 2 h at 80°C under stirring. The final product was centrifuged and washed 3 times with ethanol. For the removal of the template it was followed the same procedure reported in 3.1.2.1.2.

3.1.2.3.3. Functionalization of SiQDs@Isoc@mSiO$_2$ (T3) with PEG3 (T3@PEG3)

A total of 200 mg of PEG3 was dissolved in 13 mL of bi-distilled water. Then, this solution was added to the SiQDs@Isoc@mSiO$_2$ (T3) suspension without template (50 mg in 13 mL of bi-distilled water), followed by 3 h of reflux at 100°C. The functionalized mesoporous nanoparticles were isolated by centrifugation, washed five times with bi-distilled water in eppendorf-tubes, and dried [93].

3.1.2.4. Assay C

3.1.2.4.1. Synthesis of Si QDs coated with MSNs (SiQDs@mSiO$_2$)

To the crude Si QDs solution in 3.1.2.2.3. was added 10 mL of an aqueous solution of 0.1 M CTAB. This mixture was stirred for 30 min at 50°C. 500 µL of ammonia were added to the mixture above and stirred for further 5-10 min. Then, 1 mL of TEOS was added dropwise to the mixture and left for 2 h at 70°C under stirring. After that, the mixture was stirred overnight at room temperature. The mixture was centrifuged, washed 3 times with

methanol and dried. This method was performed using 240/500/750/1000 µL of TEOS, however only by adding 1000 µL of TEOS the pellet was formed. For template removal it was followed the same procedure reported in 3.1.2.1.2.

3.1.2.4.2. Functionalization of SiQDs@mSiO$_2$ with TsO-PEG-Silane (SiQDs@mSiO$_2$@PEG)

3.1.2.4.2.1. Synthesis of SiQDs@mSiO$_2$@PEG2 (C1)

A total of 400 mg of PEG2 was dissolved in 13 mL of bi-distilled water. Then, this solution was added to the SiQDs@mSiO$_2$ (with template) suspension (100 mg in 13 mL of bi-distilled water), followed by 3 h of reflux at 100°C. The functionalized mesoporous nanoparticles were isolated by centrifugation, washed two times with methanol and three times with bi-distilled water, and dried. For the removal of the template it was followed the same procedure reported in 3.1.2.1.2. [93].

3.1.2.4.2.2. Synthesis of SiQDs@mSiO$_2$@PEG3 (C2)

Same procedure performed in section 3.1.2.4.2.1., however applying 240 mg of PEG3 into 60 mg of SiQDs@mSiO$_2$ suspension.

3.1.2.5. Assay D

3.1.2.5.1. Synthesis of Si QDs functionalized with IPTES (SiQDs@Isoc)

To the crude Si QDs solution in 3.1.2.2.3., 2 mL of IPTES were added to the mixture and stirred for 2 h at room temperature.

3.1.2.5.2. Synthesis of SiQDs@Isoc coated with MSNs (SiQDs@Isoc@mSiO$_2$, D1)

To the previous SiQDs@Isoc (250 mg), was performed the same procedure described in section 3.1.2.4.1., however by adding 240 µL of TEOS.

3.1.2.5.3. Functionalization of SiQDs@Isoc@mSiO$_2$ with PEG3 (D1@PEG3)

Same procedure performed in section 3.1.2.4.2.1., however applying 400 mg of PEG3 into 100 mg of D1 suspension.

3.1.3. Protein encapsulation studies

Protein stock solutions (0.5 mg/mL) of BSA, LYS, CA, OVA, Hb, Myb and CYT were prepared in phosphate buffer (0.01 M, pH 7.4). A suspension of blue luminescent MSNs (2 mg/mL) in 1 mL of PBS was sonicated for 10 min. After that 0.5 mL of proteins were mixed with 0.5 mL of blue luminescent MSNs. The final suspensions were stirred for 30 min. The samples were centrifuged and the supernatant quantified by absorption using the Bradford assay in a CLARIOstar® High Performance Monochromator Multimode Microplate Reader (BMG LABTECH). The encapsulation efficiency (EE) and the loading capacity were determined by the following equations ($t_{protein}$: the total amount of protein; $f_{protein}$: the amount of free protein) [72]:

$$EE\ (\%) = \frac{t_{protein} - f_{protein}}{t_{protein}} \times 100\% \qquad \text{(Equation 3.1)}$$

$$loading\ capacity\ (mg/g) = \frac{t_{protein\ (mg)} - f_{protein\ (mg)}}{amount\ of\ nanoparticles} \qquad \text{(Equation 3.2)}$$

This study was performed for **T3** and **T3@PEG3** (section 3.1.2.3.2.2. and 3.1.2.3.3.), and also for **SiQDs@mSiO$_2$, C1** and **C2** (section 3.1.2.4.).

3.1.4. Characterization:

3.1.4.1. Measurements

The UV-Vis absorption spectra were acquired on a *Jasco V-630* spectrophotometer. The fluorescence measurements were recorded using a *FluoroMax4* spectrometer (Horiba Yvon Jobin) at room temperature. The fluorescence quantum yield (Φ_F) of the Si QDs was estimated by comparison with fluorescein in ethanol (Φ_F = 0.79) [98]. DLS to evaluate the particle size and zeta potential was carried out on a *SZ-100 Zetasizer Nano-Instrument* (Horiba). Morphology and size distribution were examined by SEM and TEM. SEM was performed in a *SEM-FIB – Zeiss Auriga CrossBeam*, workstation at Laboratory of Nanofabrication, CENIMAT and TEM images were obtained in a *JEOL JEM 2010F* operating at 200 kV, and collected using a multi-scan camera and a Digital Micrograph software from Gatan. Infrared spectra were recorded on a *PerkinElmer BX* or *PerkinElmer Spectrum Two* spectrometer.

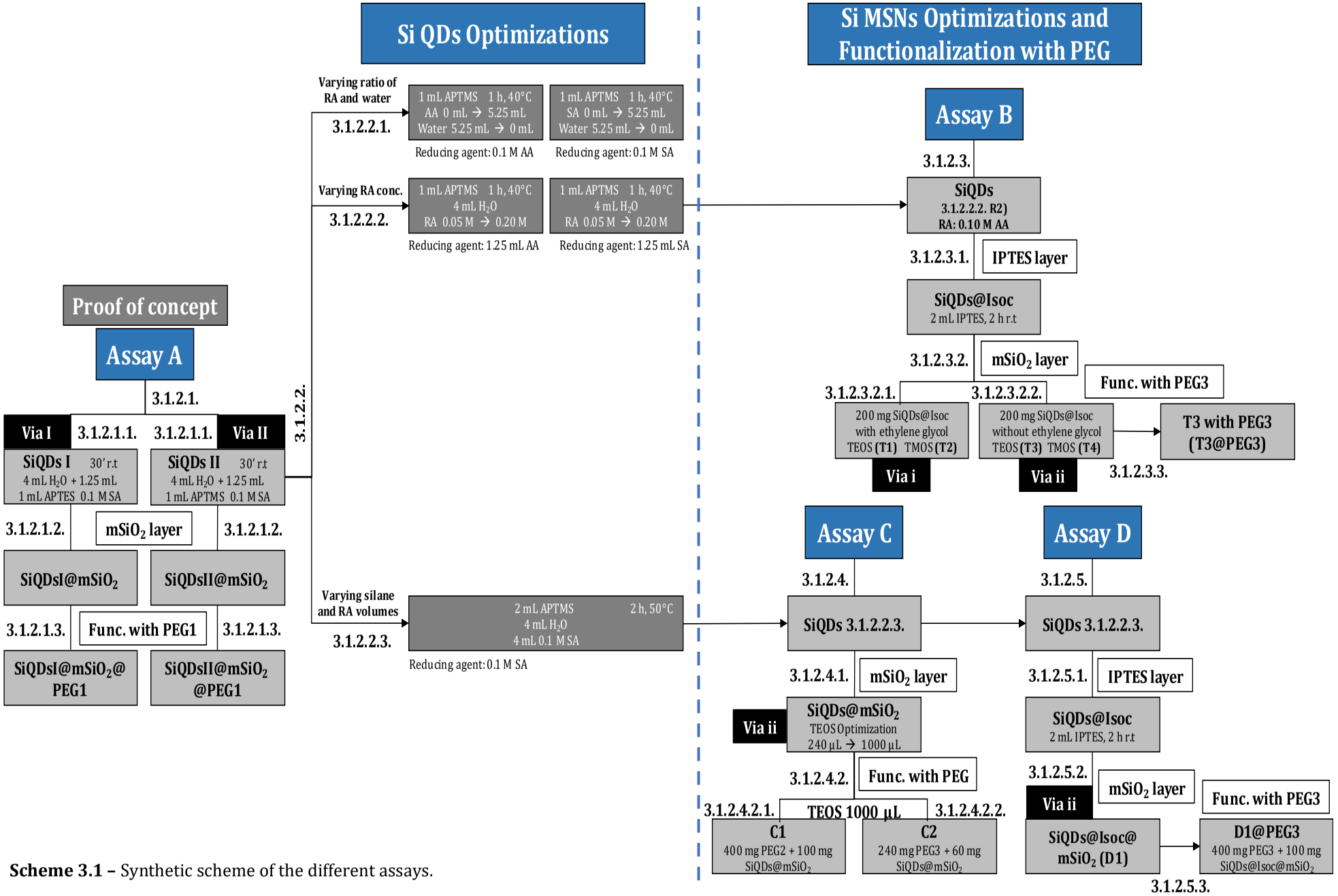

Scheme 3.1 – Synthetic scheme of the different assays.

3.2. RESULTS AND DISCUSSION

Si QDs were synthesized following the method reported by Wang and co-workers [25], however with some modifications. Briefly, Si QDs were obtained in a one-step synthesis, in water and open-air conditions, being further coated with a monolayer of MSNs. A first assay (Assay A) was carried out as a proof-of-concept, and from this point, several modifications concerning the synthesis of Si QDs and their further coating with MSNs were optimized (Assays B-D).

3.2.1. Assay A (proof-of-concept)

Regarding Assay A, APTMS (I) and APTES (II) were used as silica source and SA as a reducing agent, as can be seen in the experimental section 3.1.2.1.1. After 30 min at room temperature, green fluorescent Si QDs were obtained (see Figure 3.1). Both Si QDs show in the absorption spectra (Figure 3.1 – A), two bands, one at 370 nm and another at ca. 520 nm characteristic of its red naked-eye color. As for the emission spectra, a band with a maximum at 510 nm and 501 nm, was obtained for the Si QDs I and II, respectively.

These Si QDs were also characterized by DLS and Φ_F (Figure 3.1 – C). Through DLS analysis both presented a similar size around 3.6-3.8 nm, and the Φ_F values of QDs I and II were of ca. 13%, which was slightly lower than the one reported in the literature (21%) [25]. In the same way, the fluorescence emission bands were blue shifted regarding the 530 nm presented in the literature [25]. The zeta potential showed to be negative with a value ca. –4 mV, revealing the instability of these quantum dots. To overcome such issue and increase the stability, the crude Si QDs were coated with a layer of MSNs.

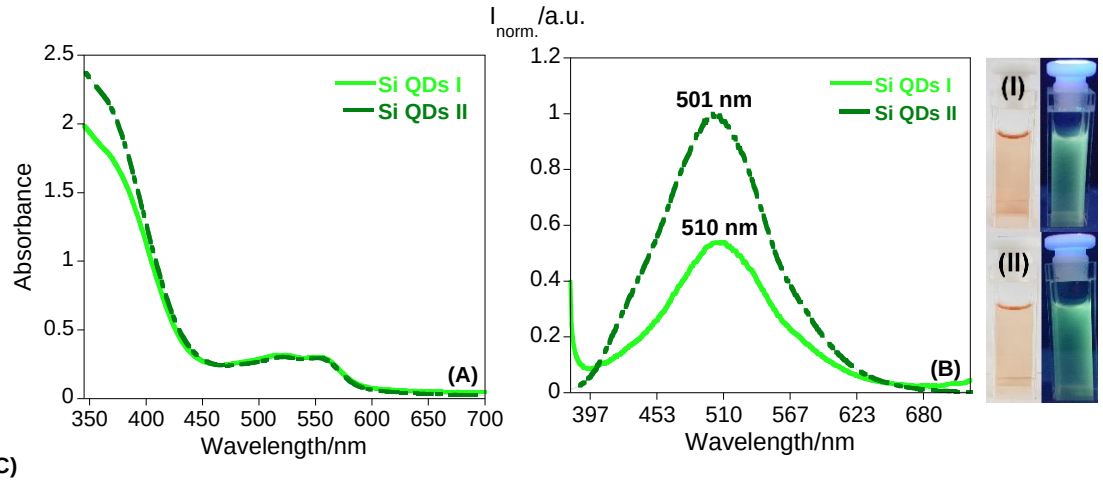

(C)

Si QDs	Size (nm) / PDI	Zeta Potential (mV)	Φ_F (%)
I	3.56 / 0.73	-3.66	12.47
II	3.84 / 0.71	-3.67	13.25

Figure 3.1 – Absorption (A) and fluorescence emission (B) spectra of Si QDs I and II (λ_{exc} = 370 nm) and images of the Si QDs at naked eye and under UV irradiation (λ_{exc} = 365 nm). (C) Size, PDI, zeta potential and Φ_F values of Si QDs I and II.

As can be seen in Figure 3.2, the addition of a layer of MSNs to the crude Si QDs, induces a blue shift in the emission bands of the Si QDs, from 500-510 nm to 467-468 nm. Moreover, the functionalization of PEG also promotes a blue shift in the emission bands to 452-459 nm. Since the mesoporous nanoparticles were not very soluble in water, the obtained hydrodynamic sizes were not very precise, with values of ca. 660 nm for SiQDsI@mSiO_2 and 3375 nm for SiQDsII@mSiO_2. On the other hand, in all cases an inversion of the zeta potential was visualized, from ca. −4 mV to ca. 17-27 mV, confirming the surface coating and further PEG functionalization. Furthermore, the addition of PEG greatly increases the stability of the nanoparticles, obtaining the lowest PDI values of ca. 0.3 for SiQDs@mSiO_2@PEG1 I and II.

The infrared spectra (Figure 3.2 – E) show the characteristic peaks of the silica framework at 1046 cm^{-1} and 1049 cm^{-1}, corresponding to the vibration Si-O-Si. Additionally, in the SiQDsII@mSiO_2 a broad band at 3600-3100 cm^{-1} is associated with absorbed water and silanol groups at the mesoporous surface, and the vibration at ca. 1650 cm^{-1}, indicates the bending modes of physisorbed water. The PEG silane functionalization was confirmed by the appearance of the peaks at 1516-1521 cm^{-1} and 1325 cm^{-1}, corresponding to the vibration NH and CH of the polymer, respectively.

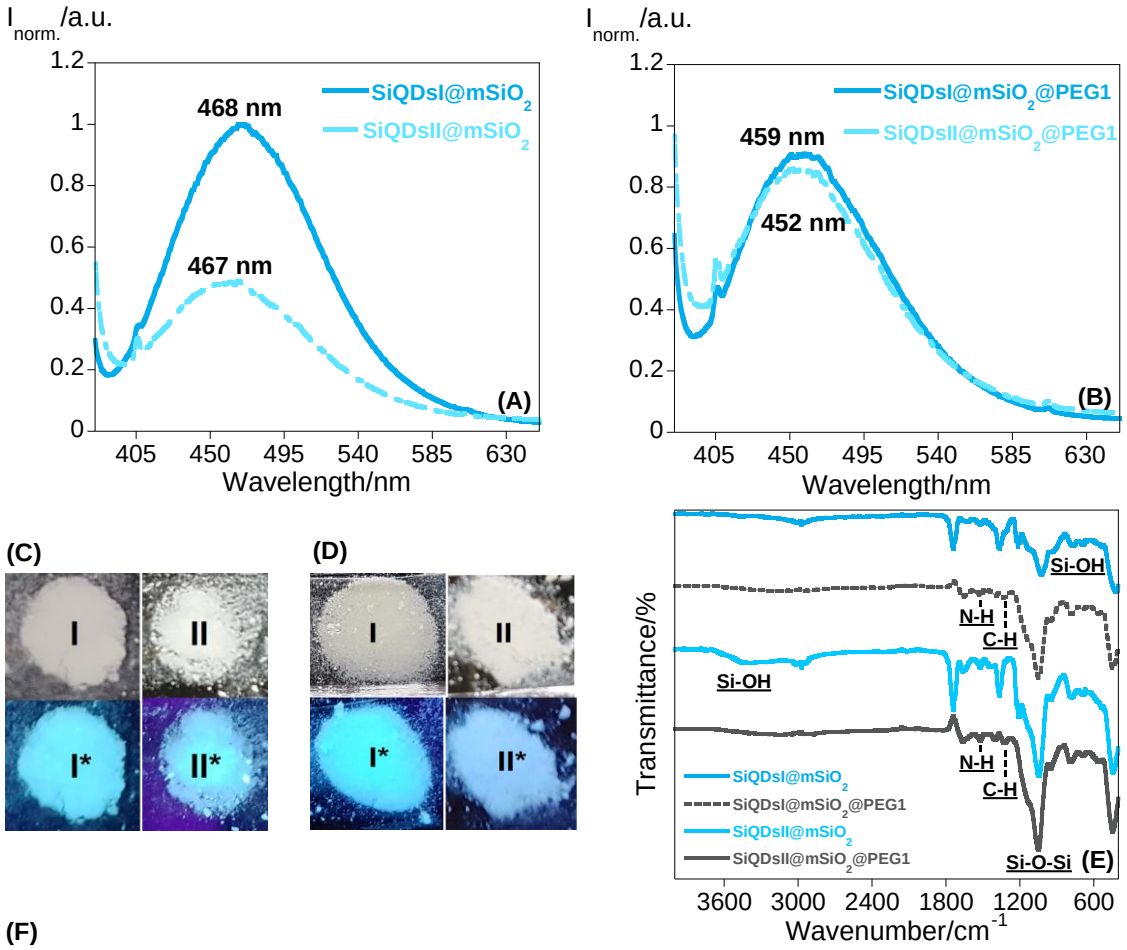

	Size (nm) / PDI	Zeta Potential (mV)
$SiQDsI@mSiO_2$	659.9 / 0.61	26.60
$SiQDsI@mSiO_2$@PEG1	- / 0.31	16.70
$SiQDsII@mSiO_2$	3375 / 0.41	18.00
$SiQDsII@mSiO_2$@PEG1	1151 / 0.29	20.50

Figure 3.2 – (A) $SiQDs@mSiO_2$ I and II, and (B) with PEG1 solid-state emission spectra (λ_{exc} = 370 nm). (I-II) Naked-eye and (I*-II*) under UV irradiation (λ_{exc} = 365 nm) photographs of (C) $SiQDs@mSiO_2$ I and II, and (D) functionalized with PEG1. (E) Infrared spectrum. (F) Size and zeta potential values of $SiQDs@mSiO_2$ I and II and PEGylated $SiQDs@mSiO_2$ I and II (solvent: water). (without template)

To confirm the morphology and size of the MSNs, the sample $SiQDsII@mSiO_2$@PEG1 was analyzed by TEM, and the images are depicted in Figure 3.3. The $SiQDsII@mSiO_2$@PEG1 are quite aggregated, however, they are spherical and with size around 30 nm.

Overall, the spectral changes observed, DLS measurements, TEM and IR peaks, indicate that the syntheses were successfully carried out. Nevertheless some modifications must be taken into consideration to decrease the size, improve the shape and decrease aggregation.

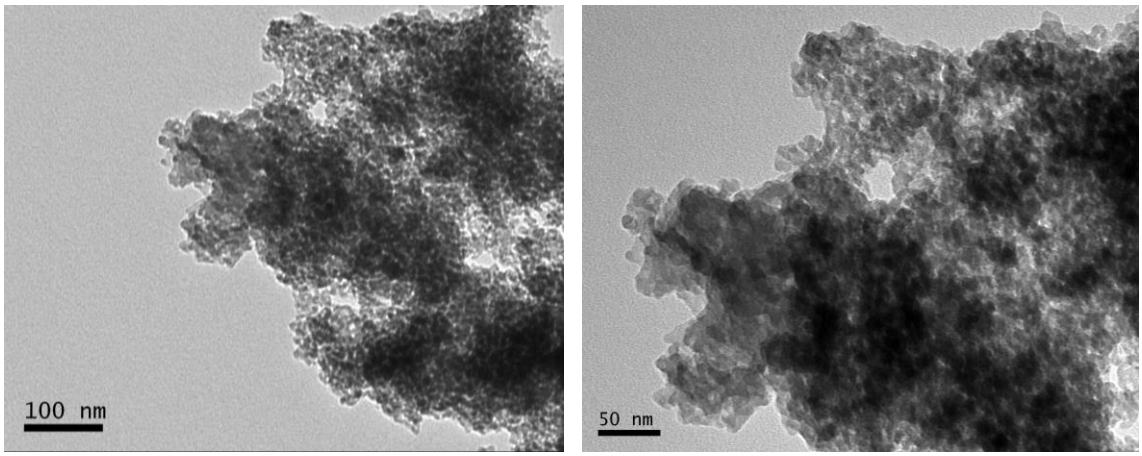

Figure 3.3 – TEM images of SiQDsII@mSiO_2@PEG1 (without template).

3.2.2. Si QDs Optimizations

Given the previous results, the first step was to optimize and improve the stability of the Si QDs. To accomplish that, several experiences were performed with APTMS, changing the reducing agent (AA or SA), temperature and reaction time, as follows: i) the ratio between the reducing agent and water (3.1.2.2.1., Experimental Section, ES), ii) the concentration of the reducing agent (3.1.2.2.2., ES), and finally iii) varying the volumes of the silane source and reducing agent, as well as the temperature and reaction time (3.1.2.2.3., ES).

3.2.2.1. Varying the ratio of reducing agent and water

Figure 3.4 shows the fluorescence emission spectra of Si QDs in aqueous solution with the AA and SA ratios reported in 3.1.2.2.1. ES, as well as their naked-eye and under a UV lamp (λ_{exc} = 365 nm) colors. Additional analysis, concerning the variation of size, PDI, zeta potential and Φ_F of Si QDs are presented in Figure 3.5.

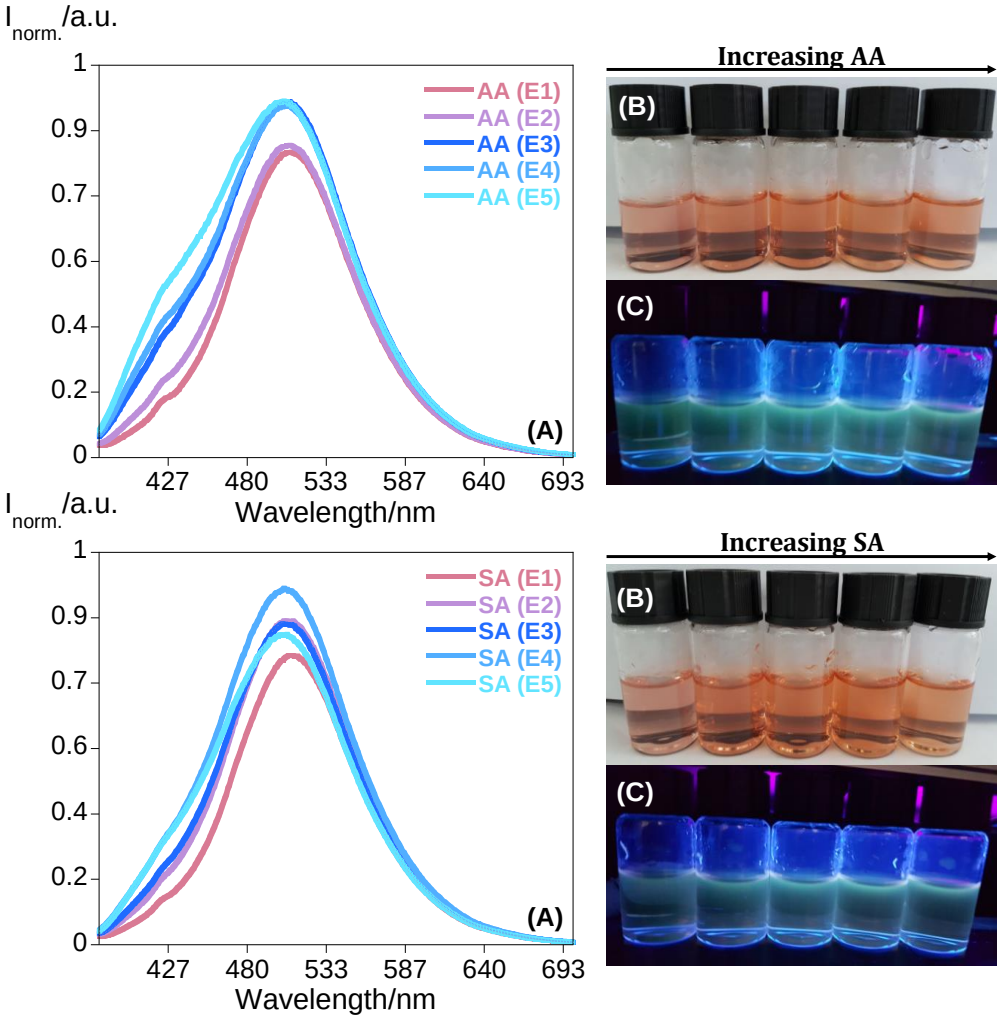

Figure 3.4 – (A) Fluorescence emission spectra of Si QDs (λ_{exc} = 370 nm) while increasing the quantity of AA (above) and SA (below) reducing agents in water. (B) Naked eye and (C) under UV irradiation (λ_{exc} = 365 nm) Si QDs photographs.

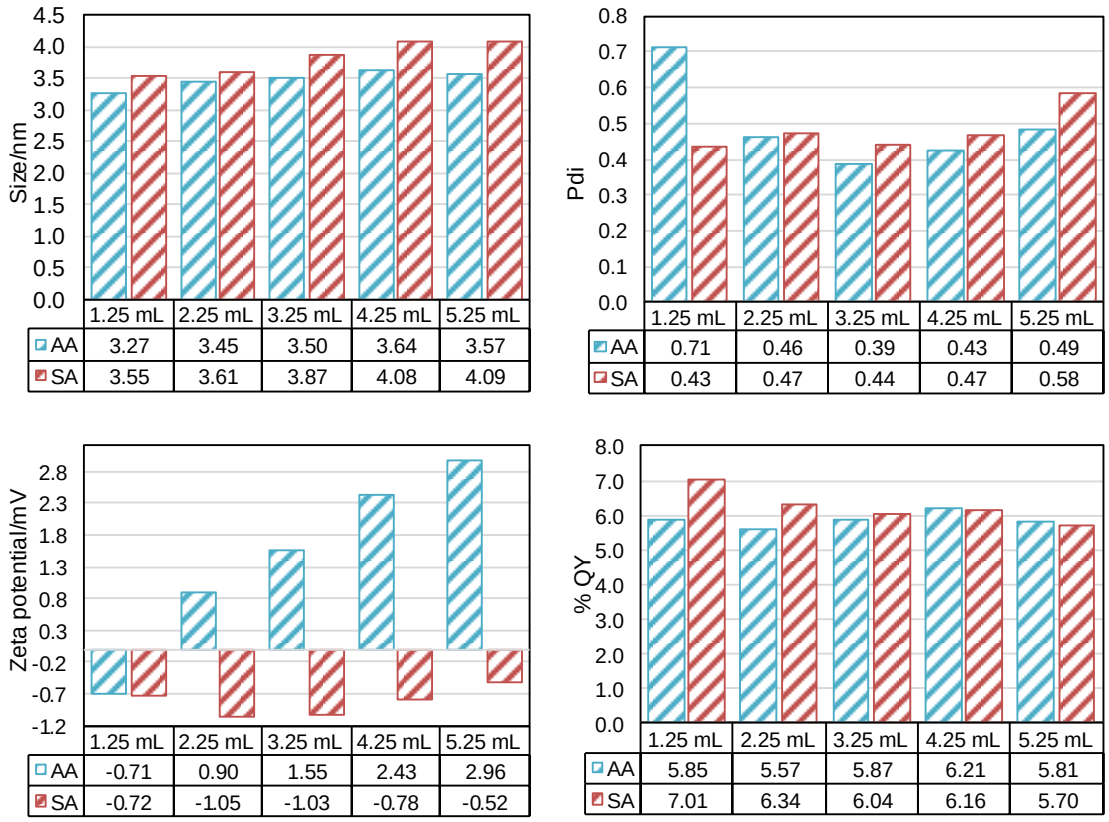

Figure 3.5 – Values of size, PDI, zeta potential and Φ_F of Si QDs at different amounts of reducing agent.

Regarding the fluorescence emission spectra, no significant changes were observed when varying the ratio reducing agent: water. The same behavior was verified in the observed colors, as well as in the size, PDI and Φ_F, with values around 3.5 nm, 0.45, and 6%, respectively. Moreover, by increasing the reaction time (from 30 min to 1 h) and temperature (from room temperature to 40°C), in comparison with the previous synthesis in 3.1.2.1. ES, an improvement in the PDI from 0.7 to 0.45 was detected, yet with a decrease in the Φ_F from 13% to 6%. On the other hand, besides the unchanged zeta potential for SA, an inversion in zeta potential from −0.7 mV to 3 mV was evidenced for high amounts of reducing agent. Overall, this change is not significant from the point of stability, since the value is out of the stability range (>30 mV).

3.2.2.2. Varying the concentration of the reducing agent

In Figures 3.6 and 3.7 are represented the fluorescence emission spectra of Si QDs in aqueous solution, including their naked-eye and under a UV lamp (λ_{exc} = 365 nm) colors, and the variation of size, PDI, zeta potential and Φ_F, while increasing the concentration of reducing agent.

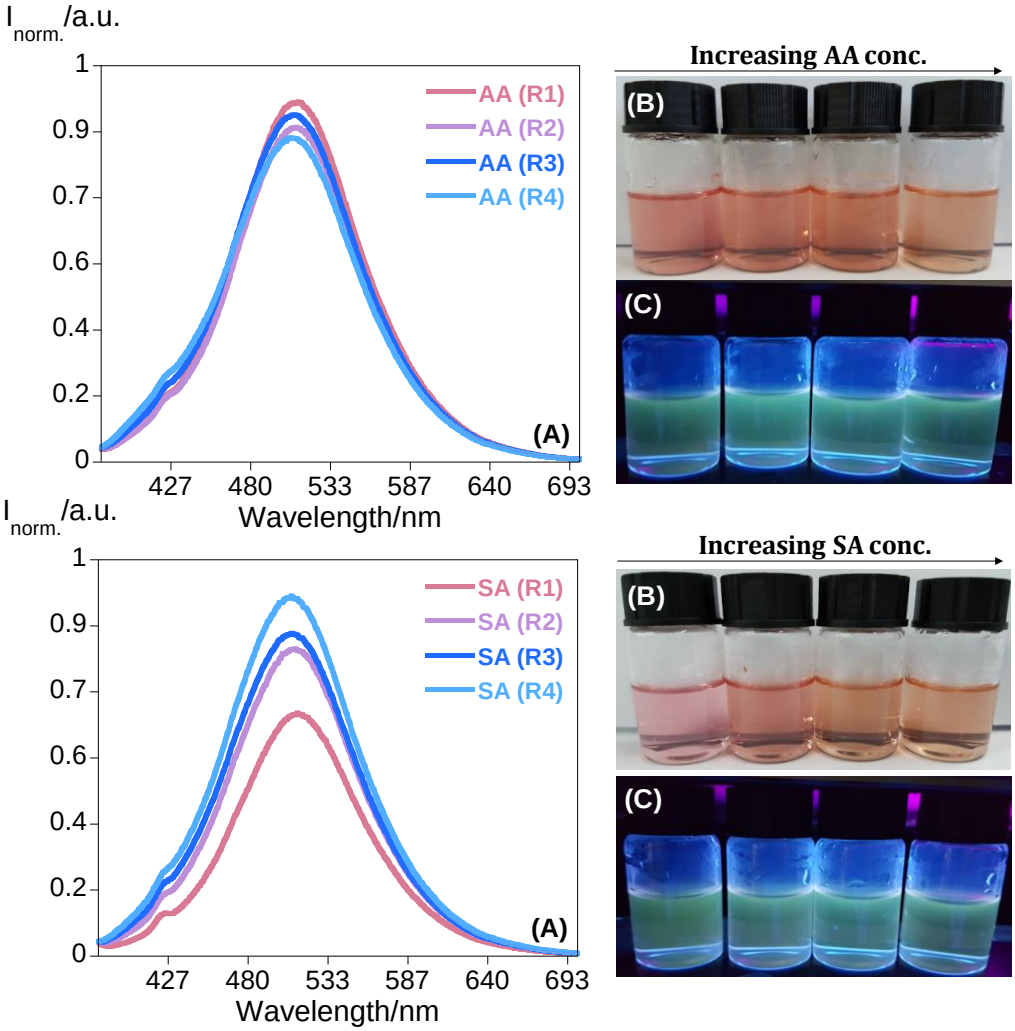

Figure 3.6 – (A) Fluorescence emission spectra of Si QDs (λ_{exc} = 370 nm) while increasing the concentration of AA (above) and SA (below) reducing agents in water. (B) Naked eye and (C) under UV irradiation (λ_{exc} = 365 nm) Si QDs photographs.

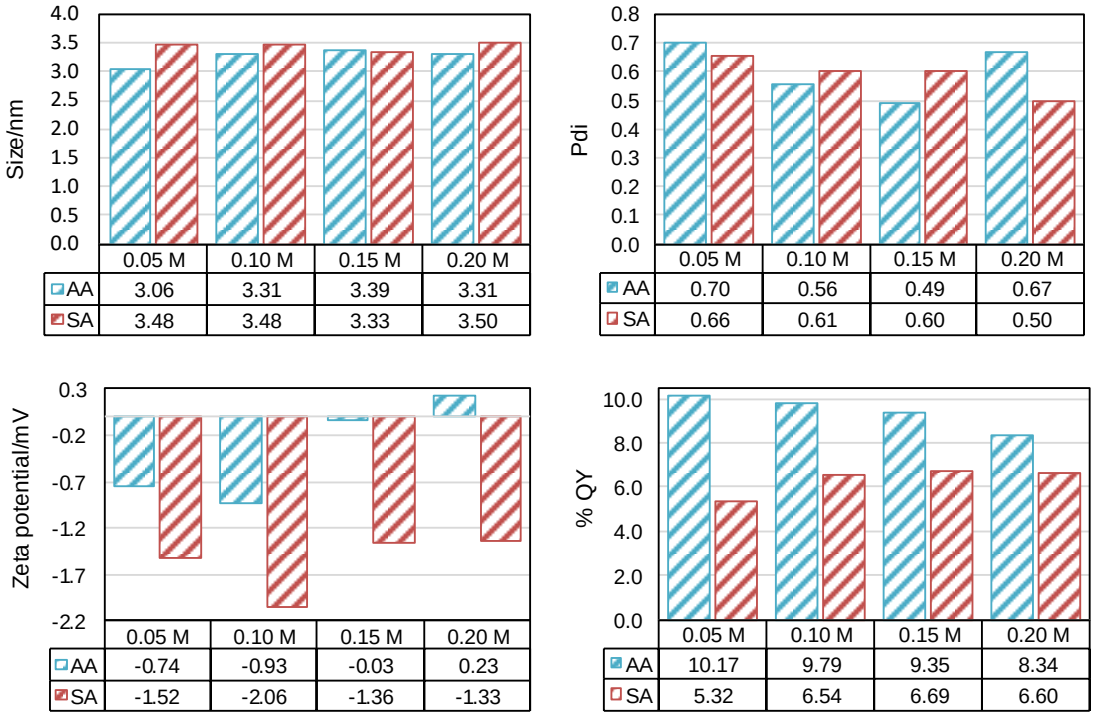

Figure 3.7 – Values of size, PDI, zeta potential and Φ_F Si QDs at different amounts of reducing agent.

Based on Figure 3.7, the size of the quantum dots is not influenced by the concentration of the reducing agent, as well as the PDI, maintaining similar values for all experiments of ca. 0.6. As for the zeta potential, in case of AA it rises to higher positive values, but on the other hand, for SA maintains its negative values, being the most negative for 0.10 M of SA. The fluorescence emission spectra do not present significant alterations for the reducing agent AA and SA, which is also confirmed through the Φ_F with values of ca. 10% and 6% for AA and SA, respectively.

To sum up, based on such results, the increasing amount of reducing agent does not favor the stability, nor the fluorescence signal intensity. Aiming more stable quantum dots, another experiment varying the silane and reducing agent volumes was performed.

3.2.2.3. Varying the silane source and reducing agent volumes

In Figure 3.8 it is represented the fluorescence emission spectra of Si QDs in aqueous solution, and their naked-eye and under a UV lamp (λ_{exc} = 365 nm) colors. Plus, the values of size, PDI, zeta potential and Φ_F of Si QDs are also presented.

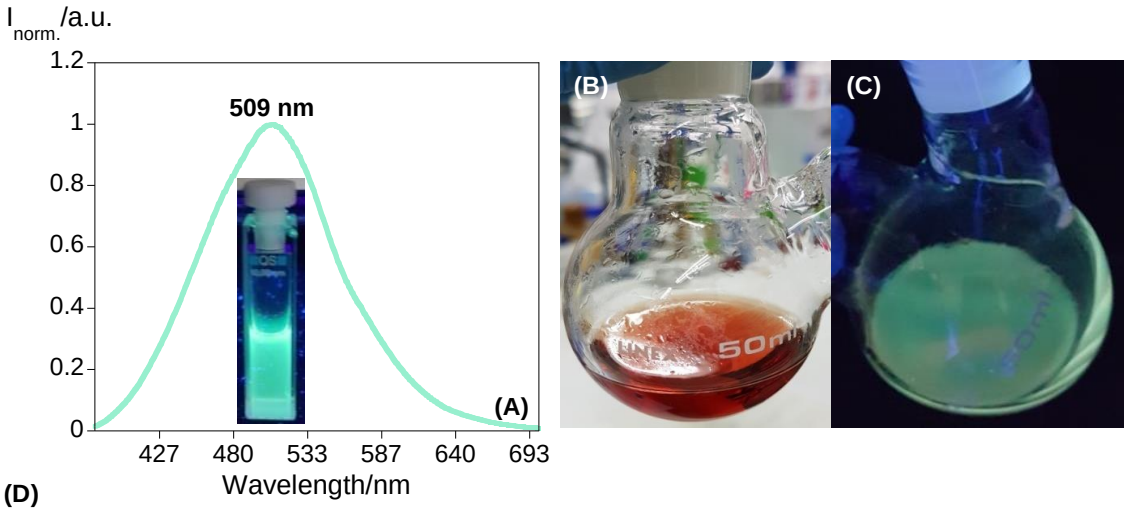

(D)

	Size (nm) / PDI	Zeta Potential (mV)	Φ_F (%)
Silicon QDs	4.01 / 0.19	-1.42	6.39

Figure 3.8 – (A) Fluorescence emission spectra of Si QDs (λ_{exc} = 370 nm). (B) Naked eye and (C) under UV irradiation (λ_{exc} = 365 nm) Si QDs photographs. (D) Size, PDI, zeta potential and Φ_F values of Si QDs.

For the same volume of water (4 mL), 2 mL of APTMS and 4 mL of SA were kept under stirring for 2 h at 50°C. The resulting quantum dots were of green emission with a maximum band centered at 509 nm. A more intense red color was noticed, and a hydrodynamic diameter of ca. 4 nm with a zeta potential of ca. −1.4 mV was obtained. Despite the improvement in the PDI from 0.4 to 0.19, the Φ_F was around 6%, which is lower than the one synthesized in 3.1.2.1. ES.

Based on the previous results, and in order to obtain more stable nanoparticles, the Si QDs produced in 3.1.2.2.2. R2) and in 3.1.2.2.3., in the experimental section were chosen to be firstly functionalized with IPTES and further coated with MSNs – **Assay B** and **D**. Additionally, the Si QDs 3.1.2.2.3. were functionalized with different thicknesses of MSNs – **Assay C**.

3.2.3. Assay B

In this assay, a layer of IPTES was added to the fluorescent Si QDs aiming the creation of a centered core, avoiding further delivery of the QDs through the pore. The addition of IPTES compound led to the formation of a white precipitate, followed by the change of color in the emission from green to blue, with a maximum band centered at ca. 439 nm. After that, a layer of MSNs was added by two different methods, as can be seen in the experimental part, via i (3.1.2.3.2.1.) and via ii (3.1.2.3.2.2.). The main results are gathered in Figure 3.9.

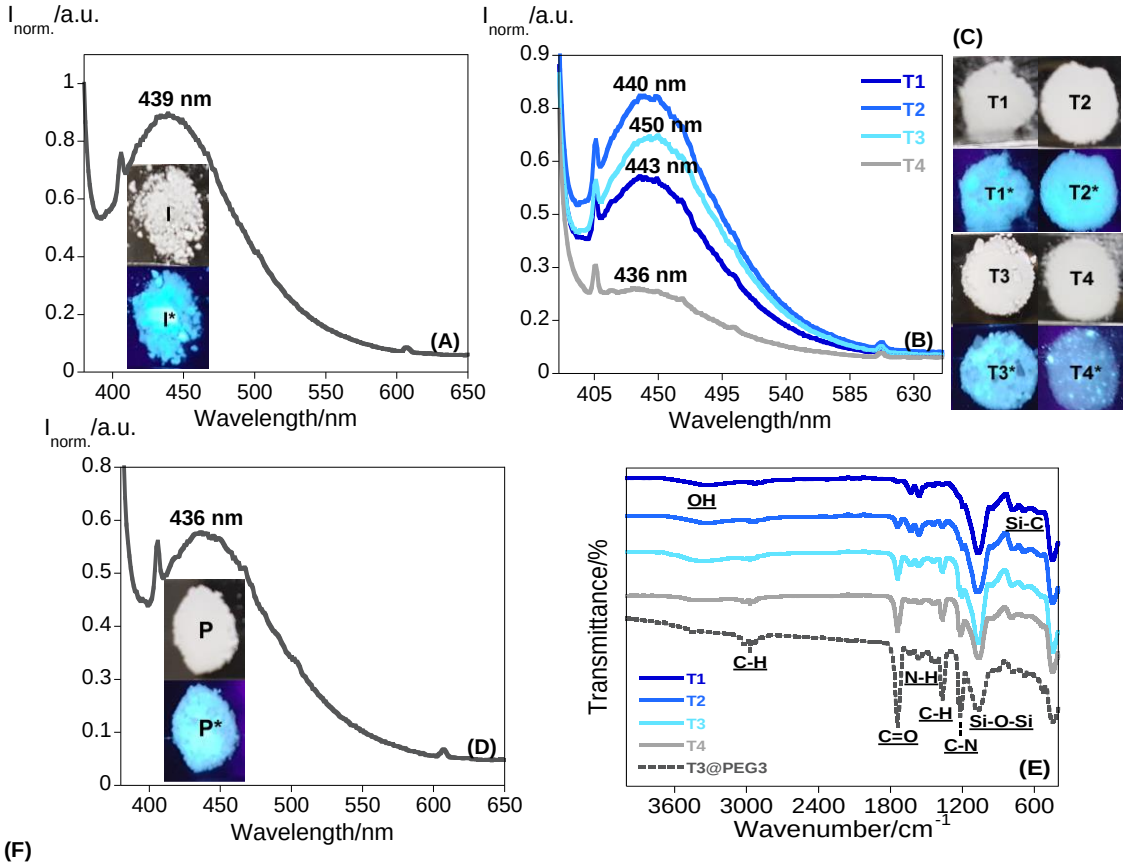

(F)

	Size (nm) / PDI	Zeta Potential (mV)
T1	1275 / 0.66	29.20
T2	807.3 / 0.30	32.37
T3	626.2 / 0.87	28.97
T3@PEG3	1291 / 0.50	34.80
T4	1055 / 0.72	29.03

Figure 3.9 – Solid-state fluorescence emission spectra of (A) SiQDs@Isoc, (B) SiQDs@Isoc@mSiO$_2$ (T1-T4), (D) T3@PEG3 (λ_{exc} = 370 nm). Inset A, D: (I, P) Naked eye and (I*, P*) under UV irradiation (λ_{exc} = 365 nm) SiQDs@Isoc and T3@PEG3 photographs, respectively. (C) (T1-T4) Naked eye and (T1*-T4*) under UV irradiation (λ_{exc} = 365 nm) SiQDs@Isoc@mSiO$_2$ (T1-T4) photographs. (E) Infrared spectrum of SiQDs@Isoc@mSiO$_2$ (T1-T4) and PEGylated SiQDs@Isoc@mSiO$_2$ (T3@PEG3). (F) Size, PDI and zeta potential values of SiQDs@Isoc@mSiO$_2$ (T1-T4) and SiQDs@Isoc@mSiO$_2$ (T3) functionalized with PEG3 (T3@PEG3) (solvent: water). (without template)

Functionalization with IPTES leads to the formation of bigger nanoparticles with a hydrodynamic size around 458 nm.

As mentioned above, a layer of MSNs was added through two different methods, via i and ii, and in each via, two distant sources of silane were tested: TEOS (T1, T3) and TMOS (T2, T4). All the resulting nanoparticles have a white color with emission bands centered at ca. 440-450 nm, shifting just a few nanometers from the initial SiQDs@Isoc. Moreover, a total inversion of the zeta potential is visualized, obtaining all nanoparticles T1 to T4 similar values of ca. 30 mV. Besides the very stable results in the zeta potential, the size and PDI were unstable, mainly because of the difficulty to solubilize these samples.

Through TEM images, were observed that the best samples were the T3, thus to improve its solubility and reduce aggregation, T3 was functionalized with the polymer PEG3, and as a result, improvements in the PDI (from ca. 0.9 to 0.5) and zeta potential (from ca. 29 mV to 35 mV) were evidenced. Additionally, a blue shift from 450 nm to 436 nm in the emission spectra after PEG functionalization indicates the surface coating of the nanoparticles.

All synthetic steps were followed by infrared technique, and according to the IR spectra (Figure 3.9 – E), a typical band of the silica framework at 1070 cm^{-1} (Si-O-Si) was detected. Moreover, the absorption peak at 692.41 cm^{-1} can be attributed to the Si-C stretching vibration. Additionally, in T1, T2 and T3 a broad band at 3600-3100 cm^{-1} is associated with absorbed water, and the vibration at ca. 1635 cm^{-1} in all nanoparticles, indicates the bending modes of physisorbed water. The peak at 1740 cm^{-1} confirms the layer of isocyanate (C=O), as well as, the peaks at ca. 1565 cm^{-1} of NH vibration the functionalization of the PEG polymer. The vibration $-(CH_2CH_2)_n$ is observed at ca. 2974-2874 cm^{-1} and ca. 1443 cm^{-1}, respectively. The additional increment in the mode at ca. 1368 cm^{-1} indicates the deformation vibrations of the polymer backbone (CH). Moreover, an additional absorption peak at ca. 1200 cm^{-1} can be attributed to the C-N stretching vibration of the polymer.

The morphology of all the nanoparticles was confirmed through TEM and SEM images, where sample T3 presented the best results (see Figure 3.10). TEM and SEM images proved the spherical shape of the nanoparticles, as well as their pore in Figure 3.10 – C, represented by the white dots. Through TEM and SEM images, were noticed that T3 nanoparticles have a size around 114 ± 17 nm and ca. 139 ± 18 nm, respectively. Moreover, through the SEM images is possible to observe the size decrease/aggregation of the nanoparticles after functionalization with PEG3, changing from 139 nm to 128 nm.

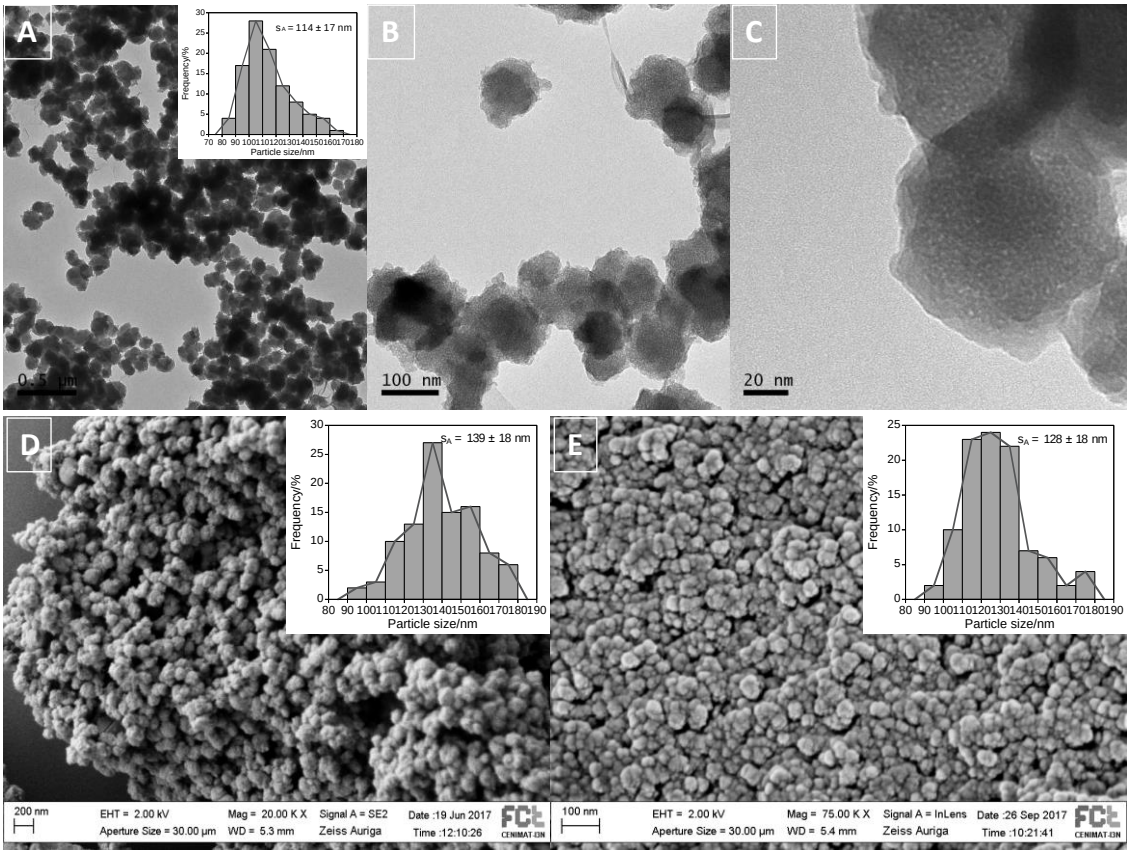

Figure 3.10 – (A-C) TEM images of SiQDs@Isoc@mSiO$_2$ (T3). (D) SEM image of SiQDs@Isoc@mSiO$_2$ (T3) and (E) of SiQDs@Isoc@mSiO$_2$@PEG3 (T3@PEG3). The inset images show the corresponding size distribution.

3.2.3.1. Encapsulation studies on SiQDs@Isoc@mSiO$_2$ (T3) and PEGylated SiQDs@Isoc@mSiO$_2$ (T3@PEG3)

Encapsulation studies of the blue MSNs T3 and T3@PEG3 in physiological pH (PBS, pH = 7.4) with single proteins exhibiting different sizes and pI, such as BSA, LYS, CYT, Myb, Hb, CA and OVA were accomplished. These proteins were selected due to the wide variety of physical properties they collectively presented (Table 3.3 and Table A.1 - Appendix).

The proteins were incubated with the nanoparticles in PBS, with a weight ratio of 1:4 (protein:MSNs) for incubation times of 30 min. EE and the amount adsorbed were determined accordingly with section 3.1.3. in the experimental part, and the obtained results are gathered in Figure 3.11.

Table 3.3 – List of encapsulated proteins and their properties. [a]Geometric dimensions given by published literature [96,97]. [b]The residue count of these proteins come from the Protein Data Bank. PDB codes: BSA, 3V03; LYS, 1DPX; CYT, 1HRC; Myb, 1WLA; Hb, 1A3N; CA, 1V9E; OVA, 1OVA.

Protein	MW (Da)	Size (nm)	pI	Negatively charged residues (%)	Positively charged residues (%)
Bovine Serum Albumin (BSA)	69293	5 x 5 x 9	4.9	6.6	22.7
Lysozyme (LYS)	16239	3 x 3 x 4.5	10–10.5	4.8	28.6
Cytochrome C (CYT)	11833	2.6 x 3.2 x 3.3	11.35	2.9	23.8
Myoglobin (Myb)	17083	ca. 17.6	6.8-7.2	5.2	16.2
Hemoglobin (Hb)	15998	5.3 x 5.4 x 6.5	6.8	4.8	13.6
Carbonic Anhydrase (CA)	28822	3.9 x 4.2 x 5.5	5.9	5.7	16.1
Ovalbumin (OVA)	42881	4 x 5 x 7	4.9	3.6	16.8

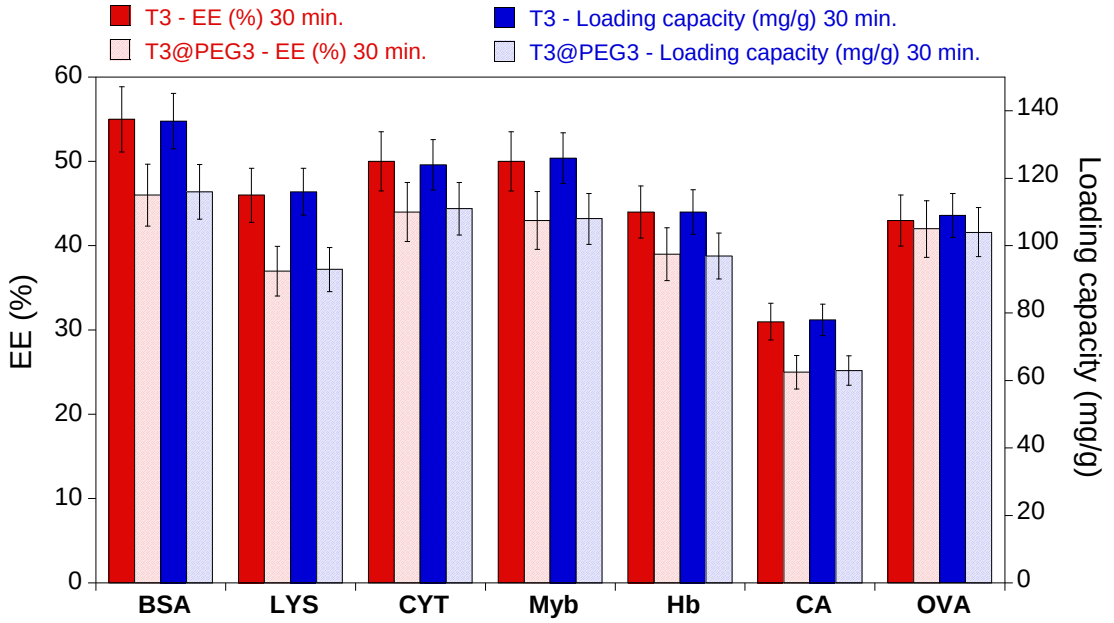

Figure 3.11 – Encapsulation efficiency (EE%) and corresponding loading capacity (mg/g) of several proteins with SiQDs@Isoc@mSiO$_2$ (T3) and PEGylated SiQDs@Isoc@mSiO$_2$ (T3@PEG3), weight ratio of 1:4 (protein:MSNs) in PBS pH = 7.4.

A common tendency is observed for all proteins where they are encapsulated within the nanoparticles. The T3 and T3@PEG3 nanoparticles are positively charged, so it should be expected a higher affinity towards the negatively charged proteins, like BSA, CA and OVA. As a matter of fact, no significant changes were observed in all proteins, with EE around 50%, with the exception of CA that presents a value of 30%. The loading capability is around 100-120 mg/g of nanoparticles. Moreover, the addition of PEG slightly decreases the affinity of the nanoparticles to the proteins.

Considering the initial weight ratio between the proteins and MSNs (1:4), and the EE, these results showed that these nanoparticles could act as nanocarriers to efficiently encapsulate a wide variety of proteins.

3.2.4. Assay C

Concerning assay C, to the crude green Si QDs in 3.1.2.2.3. ES, a layer of MSNs was added through the method via ii (3.1.2.3.2.2.) described in the experimental part., however with a TEOS optimization to 1 mL instead of 500 µL. Furthermore, the previous layer was functionalized with two different PEG polymers, as can be seen in ES, C1 (3.1.2.4.2.1.) and C2 (3.1.2.4.2.2.). The main results are presented in Figure 3.12.

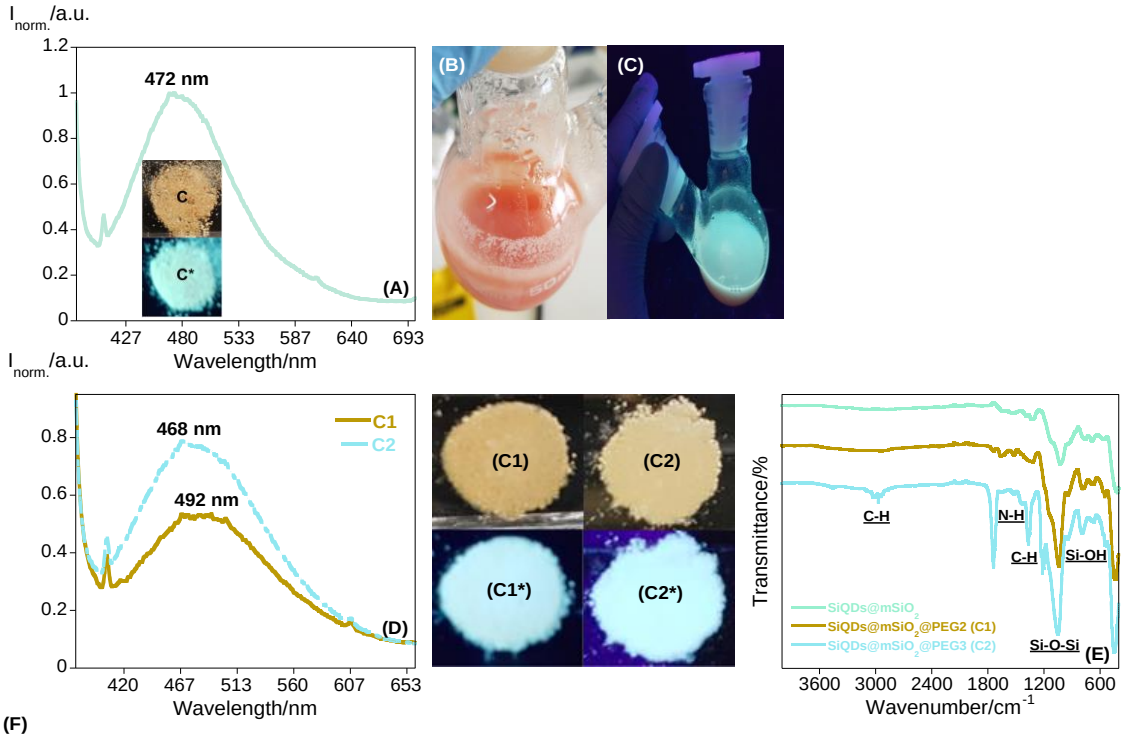

	Size (nm) / PDI	Zeta Potential (mV)
$SiQDs@mSiO_2$	386.0 / 0.55	29.00
$SiQDs@mSiO_2$@PEG2 (C1)	710.4 / 0.61	33.60
$SiQDs@mSiO_2$@PEG3 (C2)	614.6 / 0.27	28.20

Figure 3.12 – Solid-state fluorescence emission spectra of (A) $SiQDs@mSiO_2$, (D) $SiQDs@mSiO_2$@PEG2 (C1) and $SiQDs@mSiO_2$@PEG3 (C2) (λ_{exc} = 370 nm). Inset A: (C) Naked eye and (C*) under UV irradiation (λ_{exc} = 365 nm) $SiQDs@mSiO_2$ powder photographs. (B) Naked eye and (C) under UV irradiation (λ_{exc} = 365 nm) $SiQDs@mSiO_2$ photographs. (C1-C2) Naked eye and (C1*-C2*) under UV irradiation (λ_{exc} = 365 nm) $SiQDs@mSiO_2$@PEG2 (C1) and $SiQDs@mSiO_2$@PEG3 (C2) photographs, respectively. (E) The infrared spectrum of $SiQDs@mSiO_2$ and PEGylated $SiQDs@mSiO_2$ (C1 and C2). (F) Size, PDI and zeta potential values of $SiQDs@mSiO_2$ and PEGylated $SiQDs@mSiO_2$ (C1 and C2) (solvent: water). (without template)

Addition of the layer of MSNs originates a change in color, from green to blue, with a maximum band centered at ca. 472 nm. Moreover, this addition leads to a formation of bigger nanoparticles with a hydrodynamic size around 386 nm, and a total inversion of the zeta potential to positive values with ca. 29 mV, was also observed. However, there was an increment in the PDI, which resulted in poor solubility of the nanoparticles in water. To overcome this issue, $SiQDs@mSiO_2$ were functionalized with two types of polymers PEG2

and PEG3, with different sizes. There was an improvement in the PDI (from ca. 0.6 to 0.3) in C2 with PEG3, yet it is not possible to evidence the same result for C1 with PEG2, which maintained the same PDI. On the other hand, a slight increase of the zeta potential (from 29 mV to 33.6 mV) in C1 was also visualized, unlike C2. Also, a blue shift (from 472 nm to 468 nm) and a red shift (from 472 nm to 492 nm) in the emission spectra after PEG2 and PEG3 functionalization, respectively, indicates the surface coating of the nanoparticles.

Infrared spectra of the nanoparticles (Figure 3.12 – E) was performed to confirm the chemical binding of the products. A typical band of the silica framework at 1022 cm^{-1} (Si-O-Si) was observed. Additionally, the vibration at ca. 1535 cm^{-1} and 1630 cm^{-1}, correspond to NH polymer (C2) and the bending modes of physisorbed water, respectively. In C8 the $-(CH_2CH_2)_n$ vibration is observed at ca. 3019-2947 cm^{-1} and ca. 1444 cm^{-1}. An additional mode at ca. 1367 cm^{-1} (CH) indicates the deformation vibrations of the polymer backbone.

The morphology of the nanoparticles was confirmed through SEM images where sample C2 presented the best results (see Figure 3.13). Through SEM images the spherical shape of the nanoparticles was proved, and it was also possible to observe the size decrease/aggregation of the nanoparticles after functionalization with PEG3, with a size around 44 ± 6 nm.

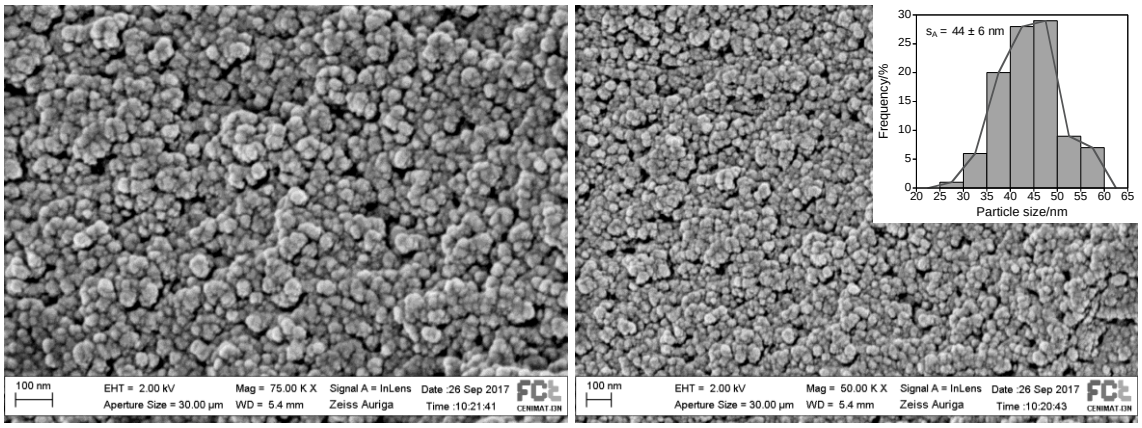

Figure 3.13 – SEM images of SiQDs@mSiO_2@PEG3 (C2). The inset image shows the corresponding size distribution.

3.2.4.1. Encapsulation studies on SiQDs@mSiO_2 and PEGylated SiQDs@mSiO_2 (C1 and C2)

Encapsulation studies of the blue MSNs SiQDs@mSiO_2, C1 and C2 in physiological pH (PBS, pH = 7.4) with single proteins exhibiting different sizes and pI, such as BSA, LYS, CYT, Myb, Hb, CA and OVA were accomplished. These proteins were selected due to the wide

variety of physical properties they collectively presented (Table 3.3 and Table A.1 - Appendix). The proteins were incubated with the nanoparticles in PBS, with a weight ratio of 1:4 (protein:MSNs) for incubation times of 30 min. EE and the amount adsorbed were determined accordingly with section 3.1.3. in the experimental part, and the obtained results are gathered in Figure 3.14.

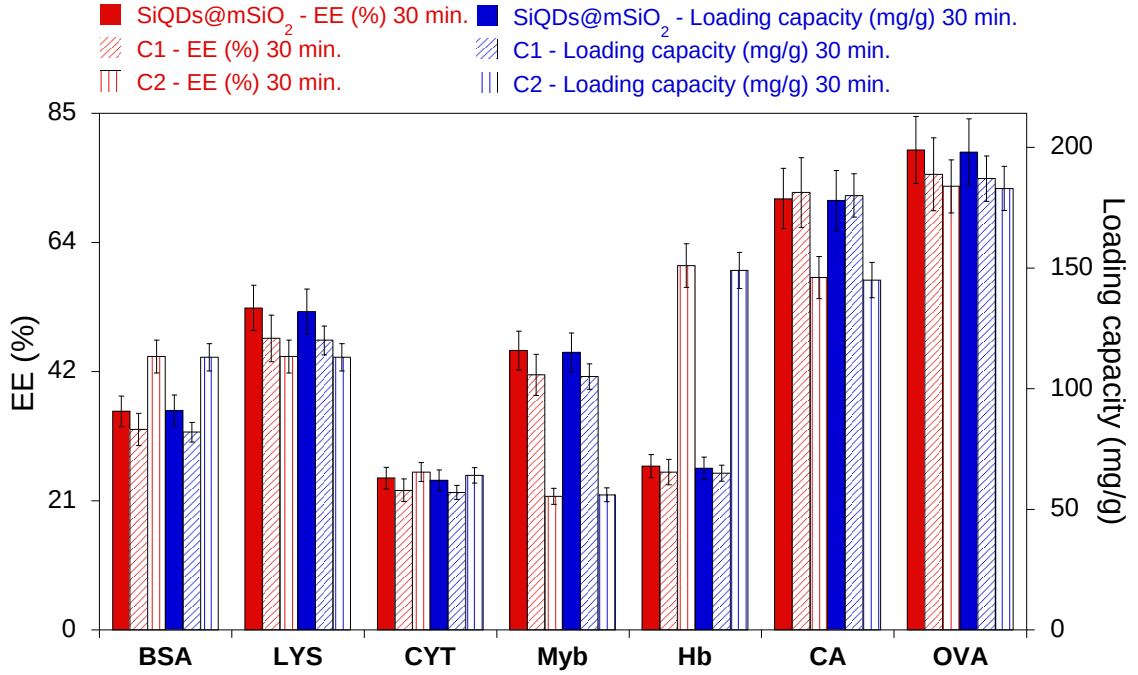

Figure 3.14 – Encapsulation efficiency (EE%) and corresponding loading capacity (mg/g) of several proteins with SiQDs@mSiO$_2$ and PEGylated SiQDs@mSiO$_2$ (C1 and C2), weight ratio of 1:4 (protein:MSNs) in PBS = 7.4.

It was possible to visualize a similar behavior between the samples SiQDs@mSiO$_2$ and C1. Both presented a higher affinity towards the negatively charged proteins CA and OVA, as expected since these nanoparticles are positively charged, thereby having a less affinity towards CYT and Hb proteins, with a decrease around 60% of EE and 100 mg/g of loading capacity. On the other hand, the addition of PEG3 increased the affinity toward BSA and Hb, reducing then its affinity to Myb.

3.2.5. Assay D

In this assay, to the crude green fluorescent Si QDs in 3.1.2.2.3. ES, was added a layer of IPTES with the same purpose of assay B, to avoid the QDs delivery through the pore of the MSNs. Similar as in assay B, a white precipitate was created after the addition of IPTES, followed by the change of color in the emission from green to blue, in this case with a maximum band centered at ca. 467 nm. Consequently, a layer of MSNs was further applied

by via ii (3.1.2.3.2.2.) described in the experimental part. The predominant results are in Figure 3.15.

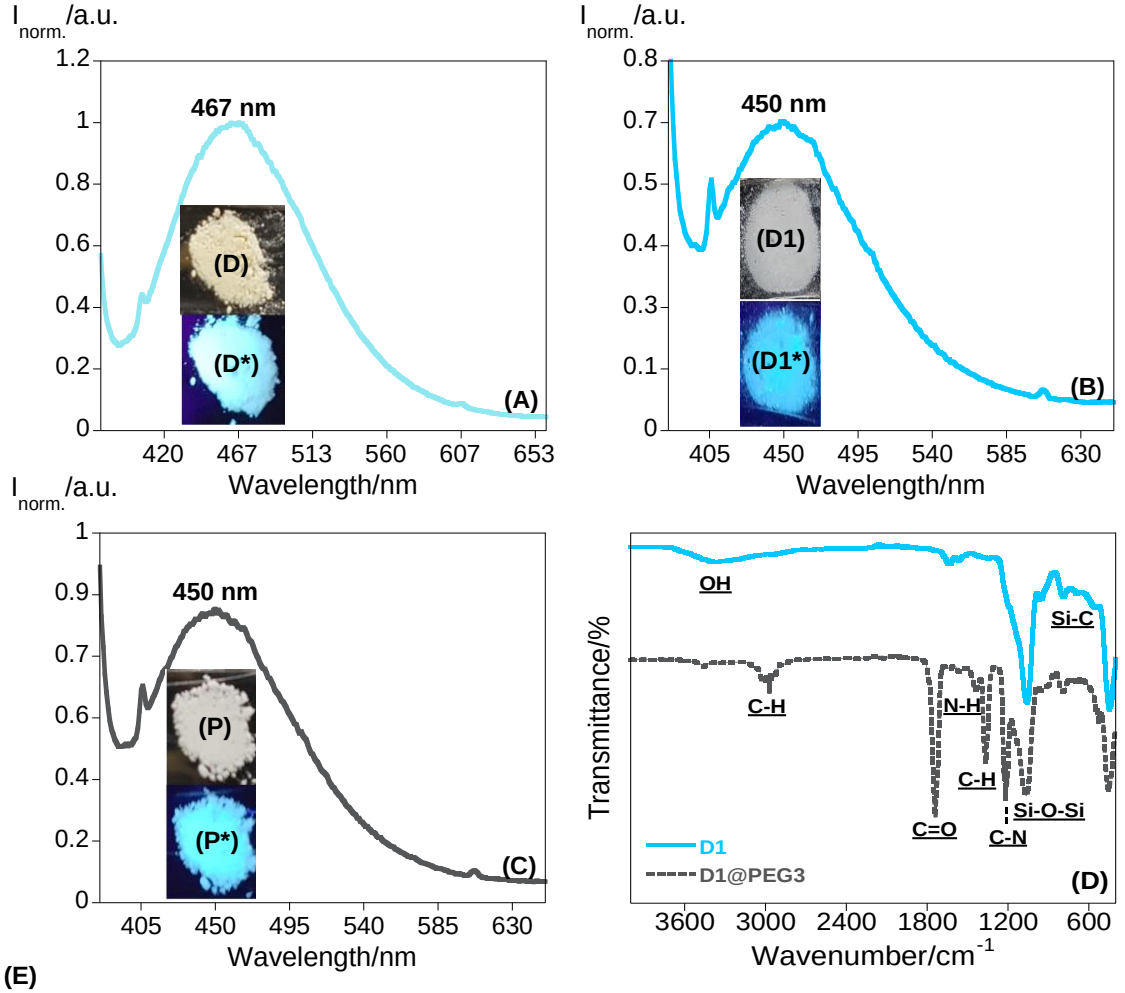

(E)

	Size (nm) / PDI	Zeta Potential (mV)
SiQDs@Isoc	645.2 / 0.73	29.43
SiQDs@Isoc@mSiO$_2$ (D1)	2404 / 0.48	35.57
D1@PEG3	4423 / 0.20	34.13

Figure 3.15 – Solid-state fluorescence emission spectra of (A) SiQDs@Isoc, (B) SiQDs@Isoc@mSiO$_2$ and (C) PEGylated SiQDs@Isoc@mSiO$_2$ (D1@PEG3) (λ_{exc} = 370 nm). Inset A, B, C: (B, D1, P) Naked eye and (B*, D1*, P*) under UV irradiation (λ_{exc} = 365 nm) photographs of SiQDs@Isoc, SiQDs@Isoc@mSiO$_2$ (D1) and PEGylated SiQDs@Isoc@mSiO$_2$ (D1@PEG3), respectively. (D) Infrared spectrum of SiQDs@Isoc@mSiO$_2$ (D1) and PEGylated SiQDs@Isoc@mSiO$_2$ (D1@PEG3). (E) Size, PDI and zeta potential values of SiQDs@Isoc@mSiO$_2$ (D1) and PEGylated SiQDs@Isoc@mSiO$_2$ (D1@PEG3) (solvent: water). (without template)

As expected in comparison with assay B, the functionalization of the Si QDs with IPTES increased the hydrodynamic size of the nanoparticles, in this case to around 645 nm. The same happened with the addition of the mesoporous silica layer to around 2404 nm. The resulting nanoparticles have a maximum band centered at 450 nm, and it was possible to observe a total inversion of the zeta potential from ca. −1.4 mV to 36 mV, confirming then

the surface coating and stability. However, there were still improvements to be done regarding the solubility of the nanoparticles, which can be visualized by the high PDI of ca. 0.5. For this reason, PEG3 was added to the luminescent MSNs to increase its solubility, and results were evidenced by a decrease in the PDI from ca. 0.5 to 0.2.

The infrared spectra (Figure 3.15 – D) showed similar peaks described for the similar system in Assay B.

To confirm the morphology of the mesoporous nanoparticles, the PEGylated SiQDs@Isoc@mSiO_2 (D1@PEG3) was analyzed by SEM and the images are depicted in Figure 3.16. The PEGylated nanoparticles are quite aggregated but are spherical, with a size around 46 ± 11 nm.

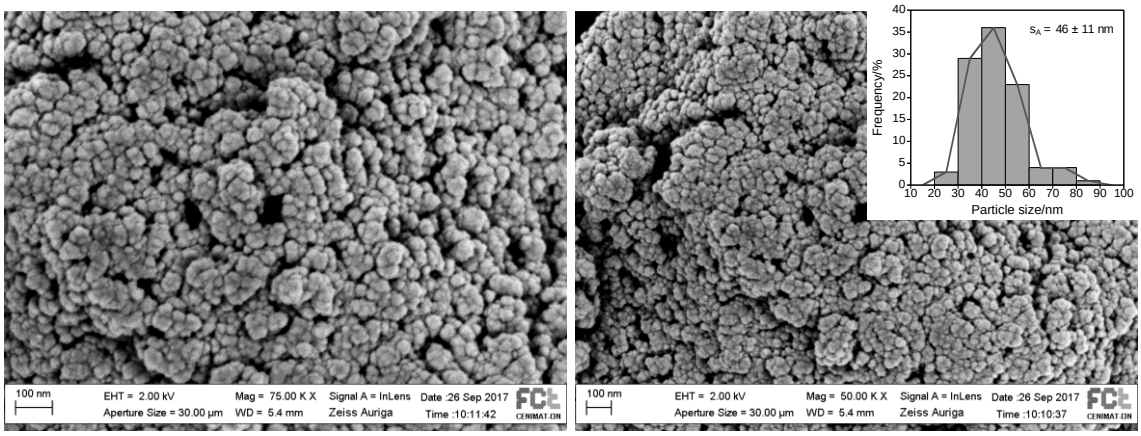

Figure 3.16 – SEM images of PEGylated SiQDs@Isoc@mSiO_2 (D1@PEG3). The inset image shows the corresponding size distribution.

3.3. CONCLUSIONS

In summary, fluorescent Si QDs coated with a monolayer of MSNs have been successfully obtained with good dispersions in water, through the introduction of PEG derivatives. Several techniques were applied to characterize the SiQDS@mSiO_2 and PEGylated nanoparticles. As a proof-of-concept, in the first assay (Assay A) experiments proved that the syntheses were successfully carried out, nevertheless some modifications must be taken in consideration in order to decrease the size, improve the shape and decrease aggregation. From this point, several modifications concerning the synthesis of Si QDs and their further coating with MSNs were optimized (Assays B-D).

Based on such results, the introduction of a layer of IPTES to the green fluorescent Si QDs (Assay B and D) aiming the creation of a centered core, proved to avoid further delivery of the QDs through the pore. However, it led to the formation of bigger

nanoparticles. Moreover, a total inversion of the zeta potential to positive values of ca. 30 mV, was obtained for all nanoparticles in Assay B to D, confirming the surface coating and improvement of stability. TEM and SEM images proved the spherical shape of the nanoparticles. Moreover, through SEM image was possible to observe the size decrease/aggregation of the nanoparticles after functionalization with PEG. Regarding the encapsulation studies, all the resulting nanoparticles in Assay B and C are positive charged, so it should be expected a higher affinity towards the negatively charged proteins, like BSA, CA and OVA. However, in Assay B no significant changes were observed, showing a common tendency for all nanoparticles. On the other hand, in Assay C this observation was demonstrated where both un-PEGylated and PEGylated nanoparticles presented a higher affinity towards CA and OVA, and as expected a less affinity towards CYT and Hb proteins. The nanoparticles functionalized with PEG3 demonstrated a different behavior with an increase of affinity towards BSA and Hb, reducing its affinity to Myb.

To sum up, considering these results it is clearly shown that a promising biocompatible and biodegradable system was created. These nanoparticles can also act as nanocarriers to efficiently encapsulate a wide variety of proteins.

CHAPTER 4

PEG-DERIVATIVES

ABSTRACT

Herein we will focus on the synthesis and characterization of PEG-derivatives and their further application on the functionalization of MSNs surface to increase the solubility of these systems in water. PEG-derivatives were synthesized and optimized according to what was necessary to perform the synthesis.

KEYWORDS: PEG, PEG-Silane derivatives, ^{1}H NMR, Infrared spectroscopy.

4.1. EXPERIMENTAL SECTION

4.1.1. Reagents and Chemicals:

Poly(ethylene glycol) BioUltra 3000, poly(ethylene glycol) BioUltra 6000, poly(ethylene glycol) BioUltra 8000, *p*-toluenesulfonyl chloride ($CH_3C_6H_4SO_2Cl$, ≥98%), hydrochloric acid (HCl, 37%), Magnesium sulfate ($MgSO_4$, ≥99.5%), (3-aminopropyl)trimethoxysilane (APTMS, $H_2N(CH_2)_3Si(OCH_3)_3$, 97%) and (3-aminopropyl)triethoxysilane (APTES, $H_2N(CH_2)_3Si(OC_2H_5)_3$, 99%) were all purchased from Sigma-Aldrich. Sodium hydroxide (NaOH) was produced by Panreac. Tetrahydrofuran (THF, C_4H_8O, ≥99.9%) was purchased from Carlo Erba Reagents. Chloroform ($CHCl_3$) was produced by Merck. All the reagents and solvents were of analytical reagent grade and were used as received.

4.1.2. Syntheses:

4.1.2.1. Synthesis of PEG(3000)-Silane (PEG1)

A solution of 86.4 mg (2.16 mol) NaOH in 4 mL of bi-distilled water was prepared

in a round-bottom flask. Then 1.8 g (0.6 mmol) of the commercially available poly(ethylene glycol) BioUltra 3000 (PEG3000) in 10 mL THF was added to the previous solution. The resulting mixture was stirred for 1 h at 0°C. Then 0.137 g (0.72 mmol) of *p*-toluenesulfonyl chloride in 1 mL of THF was added dropwise to the reaction mixture during 30 min at 0°C. The mixture was stirred for an additional 3 h. After that, a solution of 1 M HCl (2 mL) was added, and the organic phase was extracted three times with chloroform, dried over $MgSO_4$, filtered and the solvent was removed by rotary evaporation. The transparent crude product, showing the substitution of the terminal –OH group with –OTs, was used for the next step without further purification [64].

To the product was added 0.140 mL (0.6 mmol) of APTES in 2.5 mL chloroform and left at 70°C for 8 h under reflux conditions, to bind the silane group to the PEG-OTs moiety through the amino functionality. The organic solvent was removed by rotary evaporation and the obtained raw product was stored at 4°C (Scheme 4.1 and 4.2) [64].

^{1}H-NMR ($CDCl_3$): 3.83 (q, Si(O<u>CH_2</u>CH_3)$_3$), 3.71–3.58 (m, (O<u>CH_2</u><u>CH_2</u>)$_{3000}$), 3.46 (t, <u>CH_2</u>CH_2NH), 0.86 (m, <u>CH_2</u>Si).

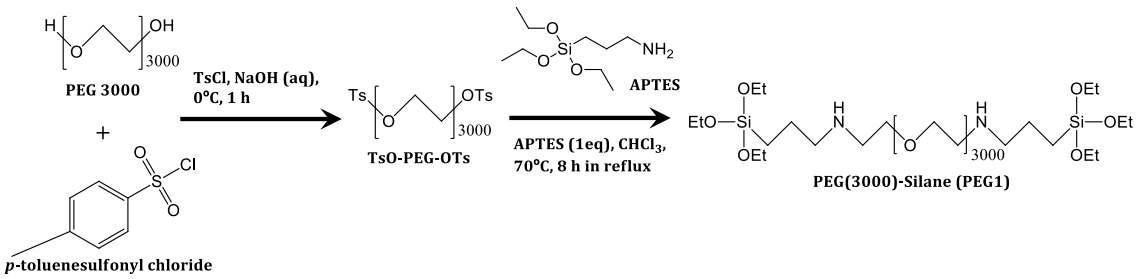

Scheme 4.1– Synthesis of PEG1.

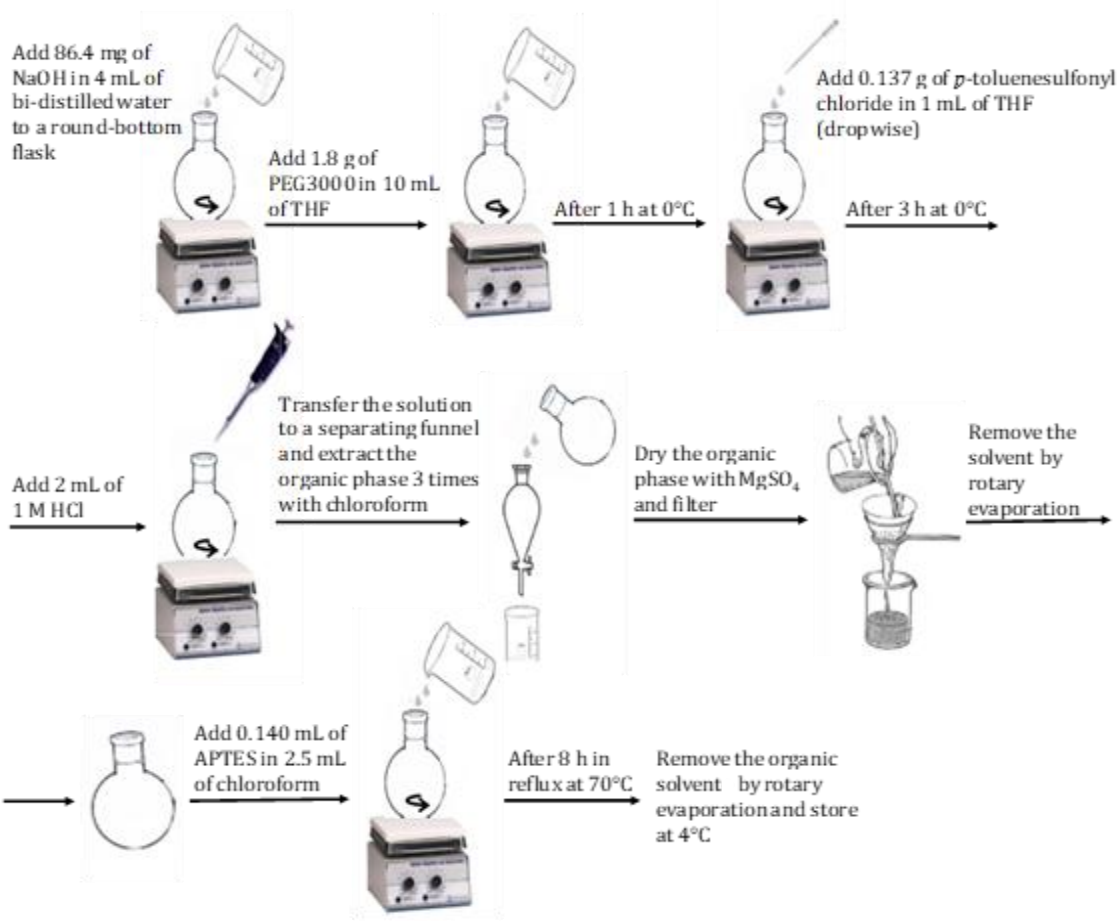

Scheme 4.2 – Procedure applied in the synthesis of PEG1.

4.1.2.2. Synthesis of TsO-PEG-Silane

4.1.2.2.1. Synthesis of TsO-PEG(6000)-Silane (PEG2)

It was performed the same procedure previously described in 4.1.2.1., however using different equivalents.

A solution of 240 mg (6.0 mmol) NaOH in 10 mL of bi-distilled water was prepared in a round-bottom flask. Then 10 g (1.67 mmol) of the commercially available poly(ethylene glycol) BioUltra 6000 in 20 mL THF was added to the previous solution. The resulting mixture was stirred for 1 h at 0°C. Then 1.093 g (5.73 mmol) of *p*-toluenesulfonyl chloride in 1 mL of THF was added dropwise to the reaction mixture during 30 min at 0°C. The mixture was stirred for an additional 3 h. After that a solution of 1 M HCl (10 mL) was added, and the organic phase was extracted three times with chloroform, dried over $MgSO_4$, filtered and the solvent was removed by rotary evaporation. The transparent crude product, showing the substitution of the terminal –OH group with –OTs, was used for the next step without further purification.

115 µL (0.49 mmol, 1eq) of APTES in 2 mL chloroform was added TsO-PEG(6000)-OTs dissolved in 10 mL of chloroform and stirred at 70°C for 8 h under reflux conditions, to bind the silane group to the PEG-OTs moiety through the amino functionality. The organic solvent was removed by rotary evaporation and the obtained raw product was stored at 4°C (Scheme 4.3).

^{1}H-NMR ($CDCl_3$): 7.95 (d, ring CH, $-SO_3$ side), 7.82 (d, ring CH, CH_3- side), 3.84 (q, $Si(OCH_2CH_3)_3$), 3.71–3.58 (m, $(OCH_2CH_2)_{6000}$), 3.49 (t, $(OCH_2CH_2)_{6000}OCH_2$), 2.49 (d, CH_2NH), 2.37 (t, $NHCH_2$), 1.84 (s, CH_3 tosyl), 1.65 (m, $NHCH_2CH_2$), 1.27 (m, $Si(OCH_2CH_3)_3$), 0.90 (t, CH_2Si).

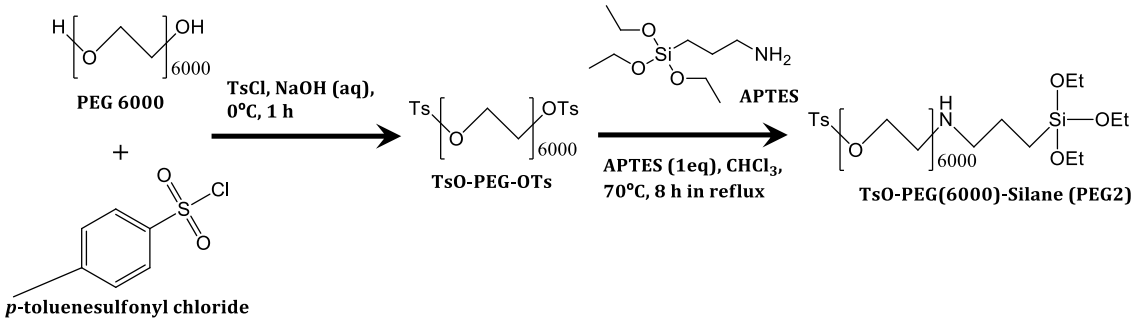

Scheme 4.3 – Synthesis of PEG2.

4.1.2.2.2. Synthesis of TsO-PEG(8000)-Silane (PEG3)

The same procedure described in section 4.1.2.2.1. was performed; however, it was used a solution of 180 mg (4.5 mmol) NaOH in 8.33 mL of bi-distilled water. Then 10 g (1.25 mmol) of the commercially available poly(ethylene glycol) BioUltra 8000, 0.9342 g (4.9 mmol) of *p*-toluenesulfonyl chloride in 1 mL of THF and 130 µL (0.73 mmol, 1 eq) of APTMS in 2 mL chloroform was added to 6.061 g (0.73 mmol, 1eq) of TsO-PEG(8000)-OTs (Scheme 4.4).

^{1}H-NMR ($CDCl_3$): 7.95 (d, ring CH, $-SO_3$ side), 7.82 (d, ring CH, CH_3- side), 3.71–3.58 (m, $(OCH_2CH_2)_{8000}$), 3.49 (m, $(OCH_2CH_2)_{8000}OCH_2$), 2.50 (d, CH_2NH), 2.37 (t, $NHCH_2$), 1.79 (s, CH_3 tosyl), 1.65 (m, $NHCH_2CH_2$), 1.28 (m, $Si(OCH_3)_3$), 0.90 (t, CH_2Si).

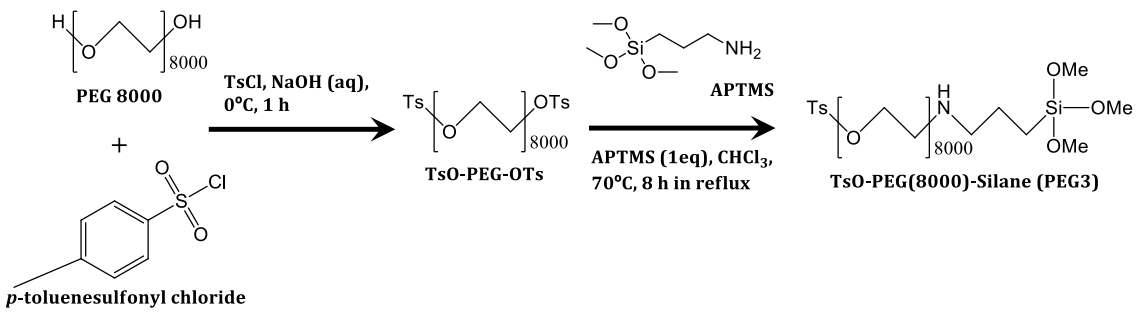

Scheme 4.4 – Synthesis of PEG3.

4.1.3. Characterization:

4.1.3.1. Measurements

Infrared spectra were recorded on a *PerkinElmer BX* or *PerkinElmer Spectrum Two* spectrometer. ^{1}H NMR spectra were recorded on a Bruker Avance III 400 at FCT-University Nova of Lisbon, Portugal. The NMR spectrometers are part of The National NMR Facility, supported by Fundação para a Ciência e a Tecnologia (RECI/BBB-BQB/0230/2012).

4.2. RESULTS AND DISCUSSION

Aiming an improvement of water solubility of the different nanoparticles described in Chapter 2 and 3, PEG-derivatives were needed to be synthetized following the method reported by Cauda and co-workers [64]. Specifically, three types of PEG-derivatives were synthesized, having three different PEG-chain lengths with (i) M_w 3000, (ii) M_w 6000, and (iii) M_w 8000. Briefly, PEG-derivatives were obtained by first preparing an intermediate leaving group, poly(ethylene glycol) tosylate, being further combined with two different sources of silica, as can be seen in the experimental part, APTES in 4.1.2.1. and 4.1.2.2.1., and APTMS in 4.1.2.2.2., to create the linear PEG-Silanes with different lengths.

PEG was converted to bitosyl-PEG which reacted with APTES or APTMS to obtain the linear PEG-Silane. The structures of PEG1, PEG2 and PEG3 compared with PEG3000 were identified by ^{1}H NMR analysis, Figure 4.1.

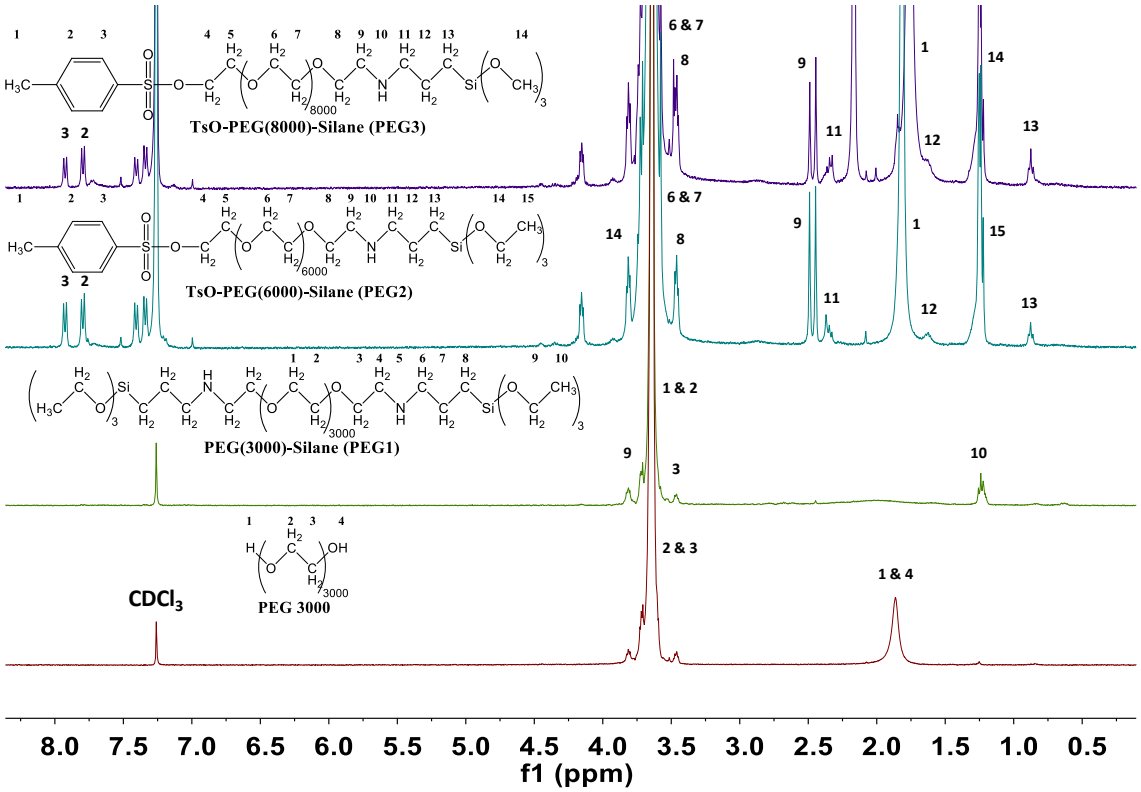

Figure 4.1 – ^{1}H NMR (400 MHz) spectra of PEG3000, PEG1, PEG2, and PEG3.

The chemical shifts for protons from position 1 to 4 in the PEG3000, from 1 to 10 in the PEG1, from 1 to 15 in the PEG2, and from 1 to 14 in the PEG3 are shown in the previous figure (the expansions of the undistinguished spectra peaks at regular scale are shown in the Appendix, section A.2.3.). The molecular structure of the different PEG-derivatives was confirmed by the presence of all the characteristic peaks and peak integration.

To further verify the successful synthesis of the PEG-derivatives, infrared spectra were also collected, as shown in Figure 4.2.

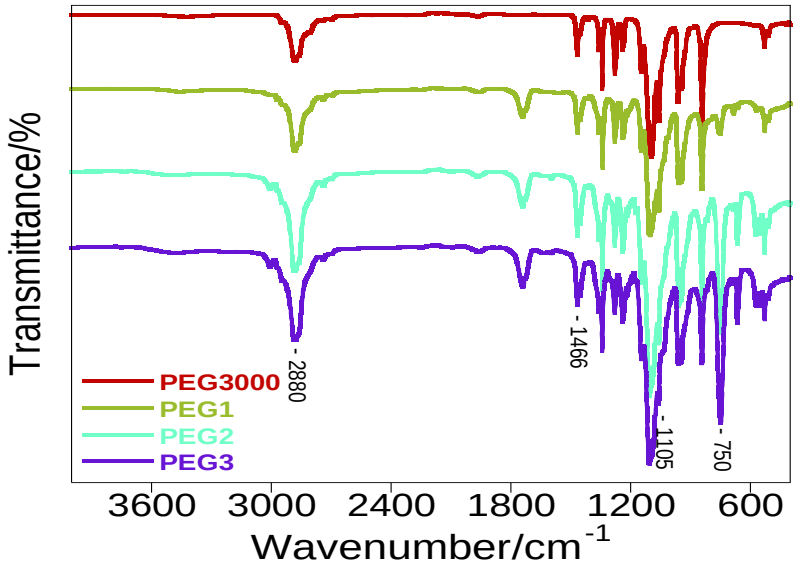

Figure 4.2 – Infrared spectra of PEG3000, PEG1, PEG2 and PEG3.

Regarding the infrared spectra in Figure 4.2, all PEG-derivatives show the characteristic peaks at 2880 cm^{-1}, 1466 cm^{-1} and 1097-1105 cm^{-1} related to the vibration $-(CH_2CH_2)_n$ and C-O ether bending vibration of the polymer. Moreover, the bending vibration of the benzene ring at 748-752 cm^{-1} in PEG1-3 also indicate that PEG had reacted with the TsCl.

4.3. CONCLUSIONS

In summary, three different types of PEG-derivatives have been successfully obtained, and in addition, it allowed to acquire good dispersions in water through the functionalization of these PEG-derivatives in luminescent MSNs, as it was possible to verify in the previous Chapters 2 and 3. Different techniques were applied to characterize these PEG-derivatives, such as FT-IR and NMR, which proved the introduction of the terminal group OTs, that were further combined with a source of silica, such as APTES or APTMS, creating the linear PEG-Silane. Due to these results, it is possible to conclude that with this inexpensive technique, large quantities of silane-modified PEG can be obtained, which can be used to covalently attach to MSNs or other surfaces, creating a system with possible biological applications.

CHAPTER 5

FINAL REMARKS

The use of biodegradable luminescent inorganic MSNs as a therapeutic tool promises an evolution in drug delivery and protein loading/extraction, as well as a major advantage the use of environmentally friendly nano-tools. Regarding such aspect, the synthesis and characterization of luminescent inorganic mesoporous nanomaterials (QDs@$mSiO_2$), and their further application for protein loading/extraction were explored.

In summary, fluorescent QDs coated with MSNs have been successfully obtained, and improvements in water solubility were observed with the functionalization of PEG-derivatives into the mesoporous surface. Several techniques were performed to characterize the different nanoparticles.

On Chapter 2 experiments proved that photo-stability of the CdTe QDs was improved by MSNs coating. Also, Green CdTeQDs@$mSiO_2$ and CdTeQDs@$mSiO_2$@PEG1 have demonstrated a large affinity for proteins, such as Hb, CA and OVA.

As for Chapter 3 after several modifications, concerning the synthesis of the Si QDs and their further coating with MSNs, there was an improvement of stability after a total inversion of the zeta potential. Further experiments led to discover that the introduction of a layer of IPTES can decrease post-delivery of the QDs through the mesoporous pore. All nanoparticles are positively charged and encapsulation studies demonstrated a common tendency to encapsulate all proteins, with the exception of Assay C presenting a different behavior towards specific proteins, where SiQDs@$mSiO_2$ and C1 present a higher affinity towards the negatively charged proteins CA and OVA, with a decrease towards CYT and Hb proteins. And also, C2 with an increase of affinity towards BSA and Hb, reducing its affinity to Myb.

In common with Chapter 2 and 3, TEM and SEM images proved the spherical shape of the nanoparticles. Moreover, the size decrease/aggregation of the nanoparticles after functionalization with PEG.

Concerning Chapter 4, the synthesis of three different types of PEG-derivatives was successfully carried out. PEG-derivatives were obtained using a two-step synthesis where firstly was prepared an intermediate leaving group with a terminal group OTs and then further combined with APTES or APTMS by heating at 70°C for 8 h, as confirmed by FT-IR and NMR. Through this method large quantities of silane-modified PEG were obtained using an inexpensive, straightforward technique, which can be used to attach PEG to MSNs or other surfaces covalently. The preparation of these different PEG-silane polymers allowed to synthesize luminescent MSNs with high colloidal stability in aqueous solutions, making them suitable for several biological applications.

To sum up, there are still some improvements to be made regarding the decrease of aggregation and water solubility, yet these systems proved to be promising nanocarriers for a wide range of applications in protein loading/extraction and possibly drug delivery and diagnostics.

REFERENCES

[1] Z. Li, Q. Sun, Y. Zhu, B. Tan, Z. P. Xu, and S. X. Dou, "Ultra-small fluorescent inorganic nanoparticles for bioimaging," *J. Mater. Chem. B*, vol. 2, no. 19, p. 2793, 2014.

[2] W. C. Chan, "Quantum Dot Bioconjugates for Ultrasensitive Nonisotopic Detection," *Science (80-.).*, vol. 281, no. 5385, pp. 2016–2018, 1998.

[3] M. Bruchez Jr., "Semiconductor Nanocrystals as Fluorescent Biological Labels," *Science (80-.).*, vol. 281, no. 5385, pp. 2013–2016, 1998.

[4] M. F. Frasco and N. Chaniotakis, "Semiconductor quantum dots in chemical sensors and biosensors," *Sensors*, vol. 9, no. 9, pp. 7266–7286, 2009.

[5] S. J. Byrne *et al.*, "Optimisation of the synthesis and modification of CdTe quantum dots for enhanced live cell imaging," *J. Mater. Chem.*, vol. 16, no. 28, p. 2896, 2006.

[6] H. Bao, Y. Gong, Z. Li, and M. Gao, "Enhancement Effect of Illumination on the Photoluminescence of Water-Soluble CdTe Nanocrystals : Toward Highly Fluorescent CdTe / CdS Core - Shell Structure," *Chem. Mater.*, vol. 16, no. 15, pp. 3853–3859, 2004.

[7] C. Wang, H. Zhang, J. Zhang, M. Li, H. Sun, and B. Yang, "Application of ultrasonic irradiation in aqueous synthesis of highly fluorescent CdTe/CdS core-shell nanocrystals," *J. Phys. Chem. C*, vol. 111, pp. 2465–2469, 2007.

[8] L. Li *et al.*, "Rapid synthesis of highly luminescent CdTe nanocrystals in the aqueous phase by microwave irradiation with controllable temperature," *Chem. Commun.*, vol. 281, no. 4, p. 528, 2005.

[9] Y. He *et al.*, "Microwave-assisted synthesis of water-dispersed CdTe nanocrystals with high luminescent efficiency and narrow size distribution," *Chem. Mater.*, vol. 19, no. 3, pp. 359–365, 2007.

[10] H. Zhang, L. Wang, H. Xiong, L. Hu, B. Yang, and W. Li, "Hydrothermal Synthesis for High-Quality CDTe Nanocrystals," *Adv. Mater.*, vol. 15, no. 20, pp. 1712–1715, 2003.

[11] S. Wu, J. Dou, J. Zhang, and S. Zhang, "A simple and economical one-pot method to synthesize high-quality water soluble CdTe QDs," *J. Mater. Chem.*, vol. 22, no. 29, p. 14573, 2012.

[12] A. M. Derfus, W. C. W. Chan, and S. N. Bhatia, "Probing the Cytotoxicity of Semiconductor Quantum Dots, Supp. Info.," *Nano Lett.*, vol. 4, no. 1, pp. 11–18, 2004.

[13] C. Kirchner *et al.*, "Cytotoxicity of colloidal CdSe and CdSe/ZnS nanoparticles," *Nano Lett.*, vol. 5, no. 2, pp. 331–338, 2005.

[14] Y. Yu, C. E. Rowland, R. D. Schaller, and B. A. Korgel, "Synthesis and Ligand Exchange of Thiol-Capped Silicon Nanocrystals," *Langmuir*, vol. 31, no. 24, pp. 6886–6893,

2015.

[15] C. Song *et al.*, "Peptide-Conjugated Fluorescent Silicon Nanoparticles Enabling Simultaneous Tracking and Specific Destruction of Cancer Cells," *Anal. Chem.*, vol. 87, no. 13, pp. 6718–6723, 2015.

[16] J. M. J. Paulusse, M. W. F. Nielen, and H. Zuilhof, "Preparation, Characterization, and Surface Modi fi cation of Tri fl uoroethyl Ester-Terminated Silicon Nanoparticles," *Am. Chem. Soc.*, vol. 24, p. 4311−4318, 2012.

[17] J. L. Heinrich, C. L. Curtis, G. M. Credo, M. J. Sailor, and K. L. Kavanagh, "Luminescent colloidal silicon suspensions from porous silicon.," *Science*, vol. 255, no. 5040, pp. 66–68, 1992.

[18] F. Hua, F. Erogbogbo, M. T. Swihart, and E. Ruckenstein, "Organically capped silicon nanoparticles with blue photoluminescence prepared by hydrosilylation followed by oxidation," *Langmuir*, vol. 22, no. 9, pp. 4363–4370, 2006.

[19] X. Li, Y. He, and M. T. Swihart, "Surface functionalization of silicon nanoparticles produced by laser-driven pyrolysis of silane followed by HF- HNO3 etching," *Langmuir*, vol. 20, no. 11, pp. 4720–4727, 2004.

[20] L. Mangolini, E. Thimsen, and U. Kortshagen, "High-Yield Plasma Synthesis of Luminescent Silicon Nanocrystals," *Nano*, 2005.

[21] J. P. Wilcoxon and G. a. Samara, "Tailorable, visible light emission from silicon nanocrystals," *Appl. Phys. Lett.*, vol. 74, no. 21, p. 3164, 1999.

[22] Y. Zhong *et al.*, "Large-scale aqueous synthesis of fluorescent and biocompatible silicon nanoparticles and their use as highly photostable biological probes," *J. Am. Chem. Soc.*, vol. 135, no. 22, pp. 8350–8356, 2013.

[23] Y. Zhong *et al.*, "Facile, Large-Quantity Synthesis of Stable, Tunable-Color Silicon Nanoparticles and Their Application for Long-Term Cellular Imaging," *ACS Nano*, vol. 9, no. 6, pp. 5958–5967, 2015.

[24] Q. Li *et al.*, "Surface-modified silicon nanoparticles with ultrabright photoluminescence and single-exponential decay for nanoscale fluorescence lifetime imaging of temperature," *J. Am. Chem. Soc.*, vol. 135, no. 40, pp. 14924–14927, 2013.

[25] J. Wang, D.-X. Ye, G.-H. Liang, J. Chang, J.-L. Kong, and J.-Y. Chen, "One-step synthesis of water-dispersible silicon nanoparticles and their use in fluorescence lifetime imaging of living cells," *J. Mater. Chem. B*, vol. 2, no. 27, p. 4338, 2014.

[26] S. D. Ma, Y. L. Chen, J. Feng, J. J. Liu, X. W. Zuo, and X. G. Chen, "One-Step Synthesis of Water-Dispersible and Biocompatible Silicon Nanoparticles for Selective Heparin Sensing and Cell Imaging," *Anal. Chem.*, vol. 88, no. 21, pp. 10474–10481, 2016.

[27] C. T. Kresge, M. E. Leonowicz, W. J. Roth, J. C. Vartuli, and J. S. Beck, "Ordered

mesoporous molecular sieves synthesized by a liquid-crystal template mechanism," *Nature*, vol. 359, no. 6397, pp. 710–712, 1992.

[28] J. S. Beck *et al.*, "A New Family of Mesoporous Molecular Sieves Prepared with Liquid Cristal Templates," *J. Am. Chem. Soc.*, vol. 114, no. 14, pp. 10834–10843, 1992.

[29] U. Ciesla and F. Schüth, "Ordered mesoporous materials," *Microporous Mesoporous Mater.*, vol. 27, no. 2, pp. 131–149, 1999.

[30] C. D. Nunes, M. Pillinger, A. A. Valente, and I. S. Gonc, "Synthesis and Characterization of Methyltrioxorhenium (VII) Immobilized in Bipyridyl-Functionalized Mesoporous Silica," *Eur. J. Inorg. Chem.*, no. Vii, pp. 1100–1107, 2002.

[31] X. Hu, P. Zrazhevskiy, and X. Gao, "Encapsulation of single quantum dots with mesoporous silica," *Ann. Biomed. Eng.*, vol. 37, no. 10, pp. 1960–1966, 2009.

[32] T. Yanagisawa, T. Shimizu, K. Kuroda, and C. Kato, "The preparation of alkyltrimethylammonium-kanemite complexes and their conversion to microporous materials," *Bulletin of the Chemical Society of Japan*, vol. 63, no. 4. pp. 988–992, 1990.

[33] L. Zhou, C. Gao, X. Hu, and W. Xu, "One-pot large-scale synthesis of robust ultrafine silica-hybridized CdTe quantum dots," *ACS Appl. Mater. Interfaces*, vol. 2, no. 4, pp. 1211–1219, 2010.

[34] Z. Xu, P. Deng, S. Tang, D. Kuang, F. Zhang, and J. Li, "Preparation of 2D molecularly imprinted materials based on mesoporous silicas via click reaction," *J. Mater. Chem. B*, vol. 2, no. 47, pp. 8418–8426, 2014.

[35] D. Li, X. He, Y. Chen, W. Li, and Y. Zhang, "Novel Hybrid Structure Silica/CdTe/Molecularly Imprinted Polymer: Synthesis, Specific Recognition, and Quantitative Fluorescence Detection of Bovine Hemoglobin," *ACS Appl. Mater. Interfaces*, vol. 5, pp. 12609–12616, 2013.

[36] A. Wolcott *et al.*, "Silica-coated CdTe quantum dots functionalized with thiols for bioconjugation to IgG proteins," *J. Phys. Chem. B*, vol. 110, no. 11, pp. 5779–5789, 2006.

[37] Y. Song, Y. Cao, P. Chen, Q. Zhao, and G. Shen, "Fabrication od mesoporous CdTe/ZnO@SiO2 core/shell nanostructures with tunable dual emission and ultrasensitive flourescence response to metal ions," *Chem. Mater.*, vol. 21, no. 68, pp. 68–77, 2009.

[38] X. Hu, P. Zrazhevskiy, and X. Gao, "Encapsulation of Single Quantum Dots with Mesoporous Silica," *Ann. Biomed. Eng.*, vol. 37, no. 10, pp. 1960–1966, 2010.

[39] S. Zhou *et al.*, "Mesoporous silica-coated quantum dots functionalized with folic acid for lung cancer cell imaging," *Anal. Methods*, vol. 7, no. 22, pp. 9649–9654, 2015.

[40] P. Wang, Y. Zhu, X. Yang, C. Li, and H. L. Du, "Synthesis of CdSe nanoparticles into the

pores of mesoporous silica microspheres," *Acta Mater.*, vol. 56, no. 5, pp. 1144–1150, 2008.

[41] J. Sha, C. Tong, H. Zhang, L. Feng, B. Liu, and C. L??, "CdTe QDs functionalized mesoporous silica nanoparticles loaded with conjugated polymers: A facile sensing platform for cupric (II) ion detection in water through FRET," *Dye. Pigment.*, vol. 113, pp. 102–109, 2015.

[42] Y. Gao *et al.*, "Decorating CdTe QD-embedded mesoporous silica nanospheres with Ag NPs to prevent bacteria invasion for enhanced anticounterfeit applications," *ACS Appl. Mater. Interfaces*, vol. 7, no. 18, pp. 10022–10033, 2015.

[43] J. C. Santos *et al.*, "Stable CdTe nanocrystals grown in situ in thiol-modified MCM-41 mesoporous silica: Control synthesis and electrochemical detection of Cu^{2+}," *Microporous Mesoporous Mater.*, vol. 221, pp. 48–57, 2016.

[44] D. R. Radu, C. Lai, K. Jeftinija, E. W. Rowe, S. Jeftinija, and V. S. Lin, "Communication A Polyamidoamine Dendrimer-Capped Mesoporous Silica Nanosphere-Based Gene Transfection Reagent A Polyamidoamine Dendrimer-Capped Mesoporous Silica Nanosphere-Based," *Communication*, no. lane 2, pp. 13216–13217, 2004.

[45] J. Liu, A. Stace-naughton, X. Jiang, and C. J. Brinker, "Porous Nanoparticle Supported Lipid Bilayers (Protocells) as Delivery Vehicles Porous Nanoparticle Supported Lipid Bilayers (Protocells) as Delivery," pp. 1354–1355, 2009.

[46] V. Cauda *et al.*, "Colchicine-loaded lipid bilayer-coated 50 nm mesoporous nanoparticles efficiently induce microtubule depolymerization upon cell uptake," *Nano Lett.*, vol. 10, no. 7, pp. 2484–2492, 2010.

[47] L. S. Wang *et al.*, "Biofunctionalized phospholipid-capped mesoporous silica nanoshuttles for targeted drug delivery: Improved water suspensibility and decreased nonspecific protein binding," *ACS Nano*, vol. 4, no. 8, pp. 4371–4379, 2010.

[48] J. M. H. S. Zalipsky, *Poly(ethyleneglycol): chemistry and biological applications*, vol. 680. 1997.

[49] J. H. Lee, H. B. Lee, and J. D. Andrade, "Blood compatibility of polyethylene oxide surfaces," *Prog. Polym. Sci.*, vol. 20, no. 6, pp. 1043–1079, 1995.

[50] V. Cauda, A. Schlossbauer, and T. Bein, "Bio-degradation study of colloidal mesoporous silica nanoparticles: Effect of surface functionalization with organo-silanes and poly(ethylene glycol)," *Microporous Mesoporous Mater.*, vol. 132, no. 1–2, pp. 60–71, 2010.

[51] J. L. Texas and S. P. Texas, "Hyaluronic Acid-decorated PLGA-PEG Nanoparticles for Targeted Delivery of SN-38 to Ovarian Cancer . Hyaluronic Acid-decorated PLGA-PEG Nanoparticles for Targeted Delivery of SN-38 to Ovarian Cancer," vol. 2434, no. JUNE,

pp. 2425–2434, 2013.

[52] M. V Cleveland, D. P. Flavin, R. A. Ruben, R. M. Epstein, and G. E. Clark, "New polyethylene glycol laxative for treatment of constipation in adults: A randomized, double-blind, placebo-controlled study," *South. Med. J.*, vol. 94, no. 5, pp. 478–481, 2001.

[53] D. Oupicky, M. Ogris, K. a Howard, P. R. Dash, K. Ulbrich, and L. W. Seymour, "Importance of lateral and steric stabilization of polyelectrolyte gene delivery vectors for extended systemic circulation.," *Mol. Ther.*, vol. 5, no. 4, pp. 463–72, 2002.

[54] K. Knop, R. Hoogenboom, D. Fischer, and U. S. Schubert, "Poly(ethylene glycol) in drug delivery: Pros and cons as well as potential alternatives," *Angew. Chemie - Int. Ed.*, vol. 49, no. 36, pp. 6288–6308, 2010.

[55] C. E. Astete and C. M. Sabliov, "Synthesis and characterization of PLGA nanoparticles.," *J. Biomater. Sci. Polym. Ed.*, vol. 17, no. 3, pp. 247–289, 2006.

[56] M. Muthu, "Nanoparticles Based on PLGA and its Co-Polymer: An Overview," *Asian J. Pharm.*, vol. 3, no. December, pp. 266–273, 2009.

[57] J. M. Lu *et al.*, "Current advances in research and clinical applications of PLGA-based nanotechnology," *Expert Rev. Mol. Diagn.*, vol. 9, no. 4, pp. 325–341, 2009.

[58] M. J. Roberts, M. D. Bentley, and J. M. Harris, "Chemistry for peptide and protein PEGylation.pdf," *Adv. Drug Deliv. Rev.*, vol. 54, no. 4, pp. 459–476, 2002.

[59] J. M. Harris, "Journal of Macromolecular Science , Part C : Polymer Reviews LABORATORY SYNTHESIS OF POLYETHYLENE GLYCOL DERIVATIVES," *J. Macromol. Sci.*, no. April 2012, pp. 37–41, 2007.

[60] Y. Akiyama, H. Otsuka, Y. Nagasaki, M. Kato, and K. Kataoka, "Selective Synthesis of Heterobifunctional Poly(ethylene glycol) Derivatives Containing Both Mercapto and Acetal Terminals," *Bioconjugate Chem*, vol. 11, pp. 947–950, 2000.

[61] J. Li and W. J. Kao, "Synthesis of polyethylene glycol (PEG) derivatives and PEGylated-peptide biopolymer conjugates.," *Biomacromolecules*, vol. 4, no. 4, pp. 1055–1067, 2003.

[62] L. R. Hirsch *et al.*, "Nanoshell-mediated near-infrared thermal therapy of tumors under magnetic resonance guidance," *Proc. Natl. Acad. Sci.*, vol. 100, no. 23, pp. 13549–13554, 2003.

[63] A. Jayagopal, P. K. Russ, and F. R. Haselton, "Surface engineering of quantum dots for in vivo vascular imaging," *Bioconjug. Chem.*, vol. 18, no. 5, pp. 1424–1433, 2007.

[64] V. Cauda, C. Argyo, and T. Bein, "Impact of different PEGylation patterns on the long-term bio-stability of colloidal mesoporous silica nanoparticles," *J. Mater. Chem.*, vol. 20, no. 39, p. 8693, 2010.

[65] R. Tian *et al.*, "Selective extraction of peptides from human plasma by highly ordered mesoporous silica particles for peptidome analysis," *Angew. Chemie - Int. Ed.*, vol. 46, no. 6, pp. 962–965, 2007.

[66] J. M. Kisler, G. W. Stevens, and A. J. O. Connor, "Adsorption of Proteins on Mesoporous Molecular Sieves," *Mater. Phys. Mech.*, vol. 4, pp. 89–93, 2001.

[67] R. Tian, M. Ye, L. Hu, X. Li, and H. Zou, "Selective extraction of peptides in acidic human plasma by porous silica nanoparticles for peptidome analysis with 2-D LC-MS/MS," *J. Sep. Sci.*, vol. 30, no. 14, pp. 2204–2209, 2007.

[68] P. Yang, S. Gai, and J. Lin, "Functionalized mesoporous silica materials for controlled drug delivery," *Chem. Soc. Rev.*, vol. 41, no. 9, p. 3679, 2012.

[69] F. Tang, L. Li, and D. Chen, "Mesoporous silica nanoparticles: Synthesis, biocompatibility and drug delivery," *Adv. Mater.*, vol. 24, no. 12, pp. 1504–1534, 2012.

[70] Q. He and J. Shi, "Mesoporous silica nanoparticle based nano drug delivery systems: synthesis, controlled drug release and delivery, pharmacokinetics and biocompatibility," *J. Mater. Chem.*, vol. 21, no. 16, p. 5845, 2011.

[71] M. Manzano and M. Vallet-Regí, "New developments in ordered mesoporous materials for drug delivery," *J. Mater. Chem.*, vol. 20, no. 27, p. 5593, 2010.

[72] J. Tu *et al.*, "Mesoporous Silica Nanoparticles with Large Pores for the Encapsulation and Release of Proteins," *ACS Appl. Mater. Interfaces*, vol. 8, no. 47, pp. 32211–32219, 2016.

[73] Y. S. Chaudhary, S. K. Manna, S. Mazumdar, and D. Khushalani, "Protein encapsulation into mesoporous silica hosts," *Microporous Mesoporous Mater.*, vol. 109, no. 1–3, pp. 535–541, 2008.

[74] Z. Li, J. C. Barnes, A. Bosoy, J. F. Stoddart, and J. I. Zink, "Mesoporous silica nanoparticles in biomedical applications," *Chem. Soc. Rev.*, vol. 41, no. 7, p. 2590, 2012.

[75] J. Lei, L. Wang, and J. Zhang, "Superbright multifluorescent core - Shell mesoporous nanospheres as trackable transport carrier for drug," *ACS Nano*, vol. 5, no. 5, pp. 3447–3455, 2011.

[76] X. Kang *et al.*, "Core-shell structured up-conversion luminescent and mesoporous NaYF4:Yb3+/Er3+@nSiO2@mSiO2 nanospheres as carriers for drug delivery," *J. Phys. Chem. C*, vol. 115, no. 32, pp. 15801–15811, 2011.

[77] S. L. Flegler, J. Heckman, and K. L. Klomparents, *Scanning and Transmission Electron Microscopy - An Introduction*. Oxford University Press, 1995.

[78] V. Kazmiruk, *Scanning Electron Microscopy*. InTech, 2012.

[79] D. B. Williams and C. B. Carter, *Transmission Electron Microscopy: A Textbook for*

Materials Science. Springer, 2009.

[80] "Atomic world - TEM." [Online]. Available: http://www.hk-phy.org/atomic_world/tem/tem02_e.html.

[81] "Scanning Electron Microscope," 2017. [Online]. Available: http://imgarcade.com/scanning-electron-microscope.html.

[82] "Electron Microscope Diagram Of A Scanning Electron Microscope Diagram." [Online]. Available: http://picphotos.net/electron-microscope-diagram-of-a-scanning-electron-microscope-diagram/.

[83] H. P. Klug and L. E. Alexander, *X-ray diffraction procedures for polycrystalline and amorphous materials*, Second Edi. New York: Wiley, 1974.

[84] J. Grebenkemper, "Powder X-ray Diffraction," 2017. [Online]. Available: https://chem.libretexts.org/Core/Analytical_Chemistry/Instrumental_Analysis/Diffraction_Scattering_Techniques/Powder_X-ray_Diffraction.

[85] P. C. Hiemenz and R. Rajagopalan, *Principles of Colloid and Surface Chemistry*, Third Edit. CRC Press, 1997.

[86] D. J. Shaw, *Introduction to colloid and surface chemistry*. Butterworth-Heine-mann, 1992.

[87] SelectScience, "The Art of Particles," 2017. [Online]. Available: http://www.selectscience.net/SelectScience-TV/Videos/the-art-of-particles/?videoID=3363.

[88] P. R. Griffiths and J. A. De Haseth, *Fourier Transform Infrared Spectrometry*. John Wiley & Sons, 2007.

[89] "Spectrum Two FT-IR spectrometer." [Online]. Available: http://www.perkinelmer.co.uk/product/spectrum-two-ft-ir-sp10-software-l160000a.

[90] J. D. Ingle and S. R. Crouch, *Spectrochemical Analysis*. Prentice Hall, 1988.

[91] "V-630Bio UV-Vis Spectrophotometer from Jasco." [Online]. Available: https://www.news-medical.net/V-630Bio-UV-Vis-Spectrophotometer-from-Jasco.

[92] "Spectrofluorometer, Compact." [Online]. Available: http://www.acalbfi.com/nl/Photonics/Spectroscopy/Grating-based-spectrometer/p/Spectrofluorometer--Compact/0000002C51.

[93] M. Bouchoucha, M. F. Côté, R. C-Gaudreault, M. A. Fortin, and F. Kleitz, "Size-Controlled Functionalized Mesoporous Silica Nanoparticles for Tunable Drug Release and Enhanced Anti-Tumoral Activity," *Chem. Mater.*, vol. 28, no. 12, pp. 4243–4258, 2016.

[94] J. Olmsted, "Calorimetric determinations of absolute fluorescence quantum yields," *J.*

Phys. Chem., vol. 83, no. 20, pp. 2581–2584, 1979.

[95] F. L. Arbeloa, P. R. Ojeda, and I. L. Arbeloa, "Flourescence self-quenching of the molecular forms of Rhodamine B in aqueous and ethanolic solutions," *J. Lumin.*, vol. 44, no. 1–2, pp. 105–112, 1989.

[96] S. P. Hudson *et al.*, "Proteins in mesoporous silicates," *ACS Symp. Ser.*, vol. 986, pp. 49–60, 2008.

[97] A. E. Eriksson, T. A. Jones, and A. Liljas, "Refined structure of human carbonic anhydrase II at 2.0 A resolution.," *Proteins*, vol. 4, no. 2, pp. 274–282, 1988.

[98] R. E. Kellogg and R. G. Bennett, "Radiationless Intermolecular Energy Transfer. III. Determination of Phosphorescence Efficiencies," *J. Chem. Phys.*, vol. 41, no. 10, pp. 3042–3045, 1964.

APPENDIX A

APPENDIX

In this section, a few complementary information regarding the main experimental results and analysis is presented. The following Appendix is divided in two main subdivisions: Experimental section (A.1.) and Experimental results (A.2.).

A.1, Table A.1 – describes the amino acid composition of all the proteins used in the encapsulation studies concerning Chapter 2 and 3. It contains the total amount of residues, available side-chain amines that participate in electrostatic interactions with the nanoparticles, and the percentage of charged residues.

A.2, Figures A.1 – A.5 – present supplementary Green CdTeQDs@mSiO_2@PEG1 TEM images acquired in Chapter 2.

A.2, Figures A.6 – A.9 – exhibit additional Green CdTeQDs@mSiO_2@PEG1 SEM images acquired in Chapter 2.

A.2, Figures A.10 – A.13 – show the infrared spectra of SiQDs@mSiO_2 I and II (with and without template) performed in Assay A, Chapter 3. These spectra allow the confirmation of the assignment described in the main discussion.

A.2, Figures A.14 – A.17 – present T1 TEM images acquired in Assay B, Chapter 3.

A.2, Figures A.18 – A.21 – present T2 TEM images collected in Assay B, Chapter 3.

A.2, Figures A.22 – A.25 – gather additional TEM and SEM images of T3 performed in Assay B, Chapter 3.

A.2, Figures A.26 – A.29 – exhibit T4 TEM images acquired in Assay B, Chapter 3.

A.2, Figure A.30 – A.31 – show the ^{1}H NMR (400 MHz) spectra expansions of the PEG-Derivatives PEG1, PEG2 and PEG3, performed in Chapter 4.

A.1. Experimental section (Chapter 2 and 3)

Table A.1 – Amino acid composition of all the proteins used in the encapsulation studies, showing the total amount of residues, available side-chain amines to participate in electrostatic interactions with the nanoparticles, and respective content of positive and negatively charged residues, in percentage.

AA	Amine side-chain residues	Bovine Serum Albumine (BSA)			Lysozyme (LYS)			Cytochrome C (CYT c)			Myoglobin (Myb)			Hemoglobin (Hb)			Carbonic Anhydrase (CA)			Ovalbumin (OVA)		
		# AA	% AA	# side-chain amines	# AA	% AA	# side-chain amines	# AA	% AA	# side-chain amines	# AA	% AA	# side-chain amines	# AA	% AA	# side-chain amines	# AA	% AA	# side-chain amines	# AA	% AA	# side-chain amines
Ala	0	48	7.9%	0	14	9.5%	0	6	5.7%	0	15	9.7%	0	15	10.2%	0	21	8.0%	0	35	9.1%	0
Arg	3	26	4.3%	78	12	8.2%	36	2	1.9%	6	2	1.3%	6	3	2.0%	9	8	3.1%	24	15	3.9%	45
Asn	1	14	2.3%	14	14	9.5%	14	5	4.8%	5	2	1.3%	2	6	4.1%	6	18	6.9%	18	17	4.4%	17
Asp	1	40	6.6%	40	7	4.8%	7	3	2.9%	3	8	5.2%	8	7	4.8%	7	15	5.7%	15	14	3.6%	14
Cys	0	35	5.8%	0	9	6.1%	0	2	1.9%	0	0	0.0%	0	2	1.4%	0	1	0.4%	0	6	1.6%	0
Gln	1	20	3.3%	20	3	2.0%	3	3	2.9%	3	6	3.9%	6	3	2.0%	3	9	3.4%	9	15	3.9%	15
Glu	0	59	9.7%	0	2	1.4%	0	9	8.6%	0	13	8.4%	0	8	5.4%	0	13	5.0%	0	33	8.5%	0
Gly	0	17	2.8%	0	13	8.8%	0	12	11.4%	0	15	9.7%	0	13	8.8%	0	17	6.5%	0	19	4.9%	0
His	2	17	2.8%	34	1	0.7%	2	3	2.9%	6	11	7.1%	22	9	6.1%	18	11	4.2%	22	7	1.8%	14
Ile	0	15	2.5%	0	7	4.8%	0	6	5.7%	0	9	5.8%	0	0	0.0%	0	10	3.8%	0	25	6.5%	0
Leu	0	65	10.7%	0	15	10.2%	0	6	5.7%	0	17	11.0%	0	18	12.2%	0	24	9.2%	0	32	8.3%	0
Lys	1	60	9.9%	60	6	4.1%	6	19	18.1%	19	19	12.3%	19	11	7.5%	11	18	6.9%	18	20	5.2%	20
Met	0	5	0.8%	0	3	2.0%	0	3	2.9%	0	3	1.9%	0	2	1.4%	0	1	0.4%	0	17	4.4%	0
Phe	0	30	4.9%	0	4	2.7%	0	4	3.8%	0	7	4.5%	0	8	5.4%	0	11	4.2%	0	20	5.2%	0
Pro	0	28	4.6%	0	3	2.0%	0	4	3.8%	0	4	2.6%	0	7	4.8%	0	19	7.3%	0	14	3.6%	0
Ser	0	32	5.3%	0	11	7.5%	0	0	0.0%	0	5	3.2%	0	5	3.4%	0	26	10.0%	0	38	9.8%	0
Thr	0	34	5.6%	0	7	4.8%	0	10	9.5%	0	7	4.5%	0	7	4.8%	0	9	3.4%	0	15	3.9%	0
Trp	1	3	0.5%	3	6	4.1%	6	1	1.0%	1	2	1.3%	2	2	1.4%	2	6	2.3%	6	3	0.8%	3
Tyr	0	21	3.5%	0	3	2.0%	0	4	3.8%	0	2	1.3%	0	3	2.0%	0	7	2.7%	0	10	2.6%	0
Val	0	38	6.3%	0	7	4.8%	0	3	2.9%	0	7	4.5%	0	18	12.2%	0	17	6.5%	0	31	8.0%	0
Total AA		607			147			105			154			147			261			386		
Total amine side-chain residues		249			74			43			65			56			112			128		
Molecular weight		69293			16239			11833			17083			15998			28822			42881		
Total negatively charged residues (Asp + Glu):		40			7			3			8			7			15			14		
Total positively charged residues (Arg + Lys):		138			42			25			25			20			42			65		

A.2. Experimental results

A.2.1. Experimental results (Chapter 2)

A.2.1.1. Green CdTeQDs@mSiO$_2$@PEG1

TEM

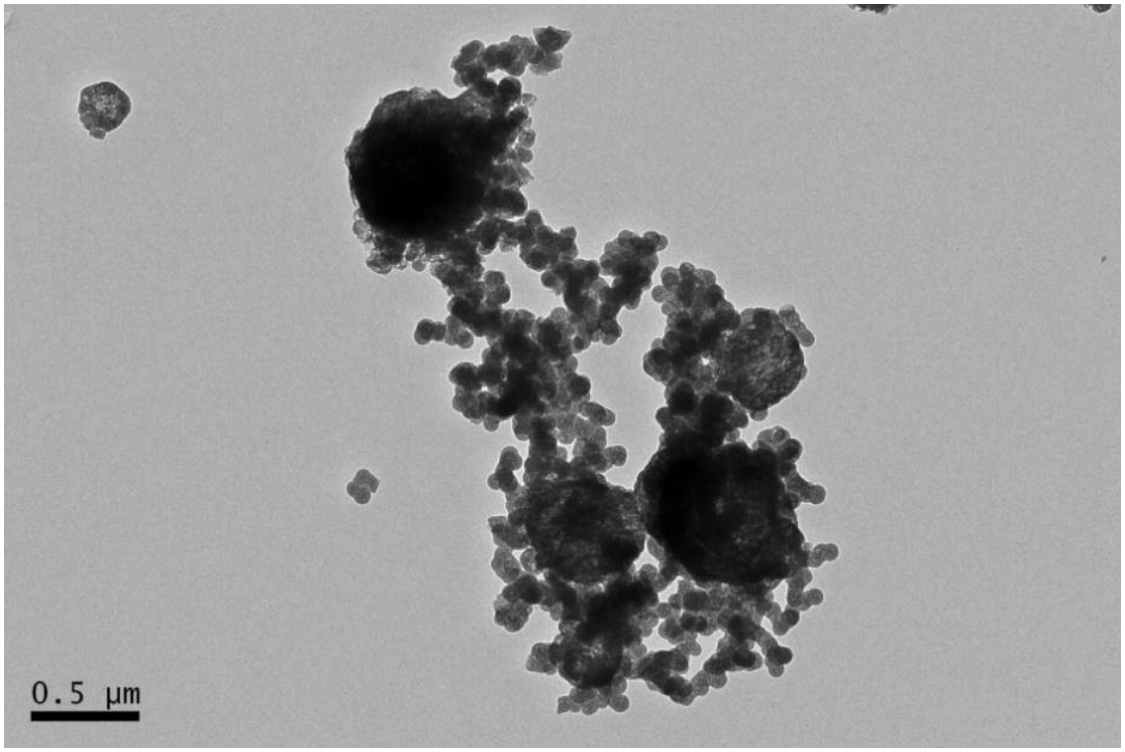

Figure A.1

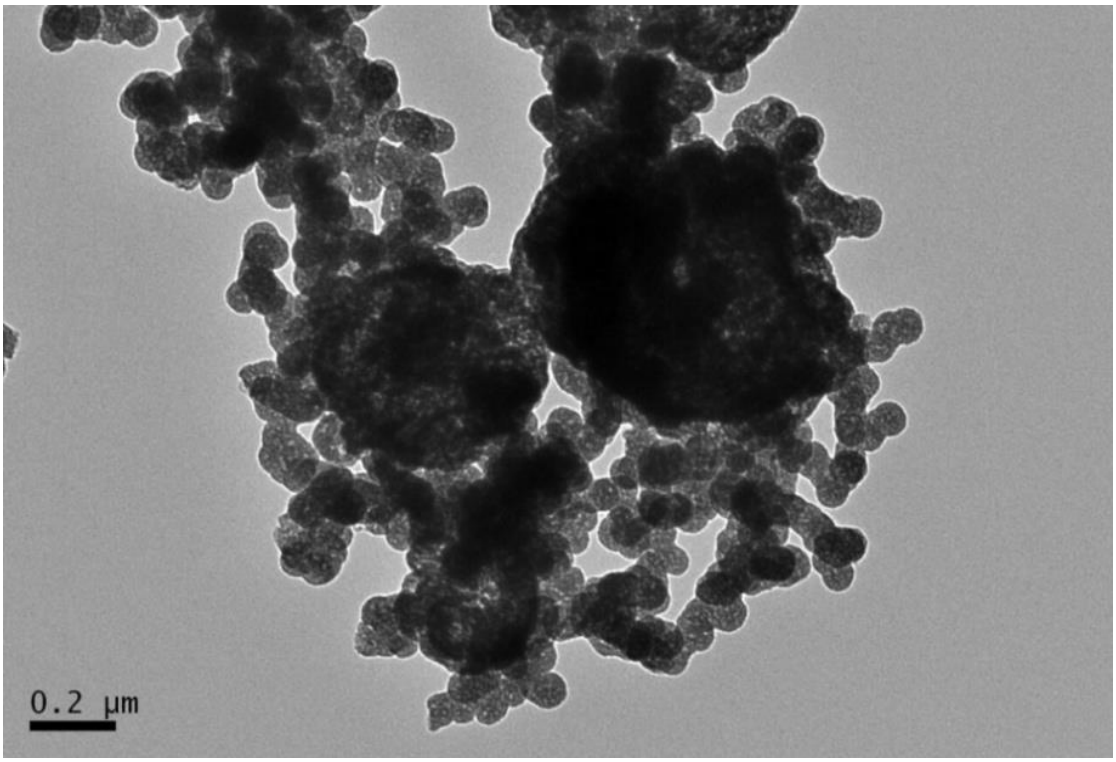

Figure A.2

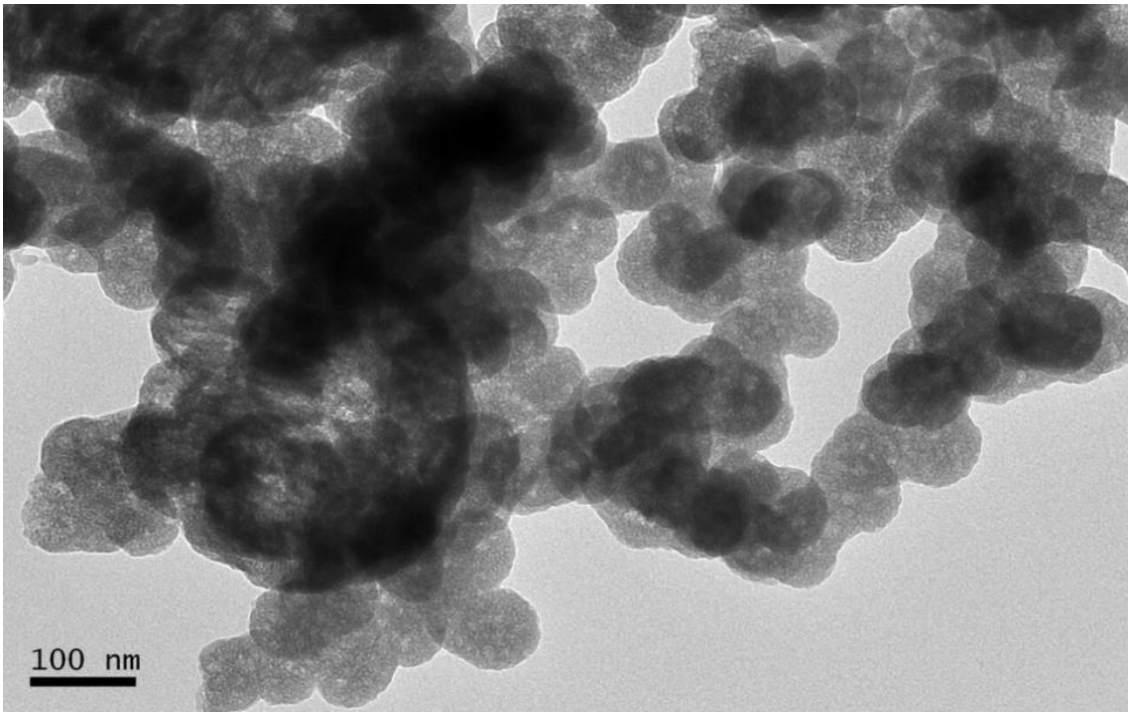

Figure A.3

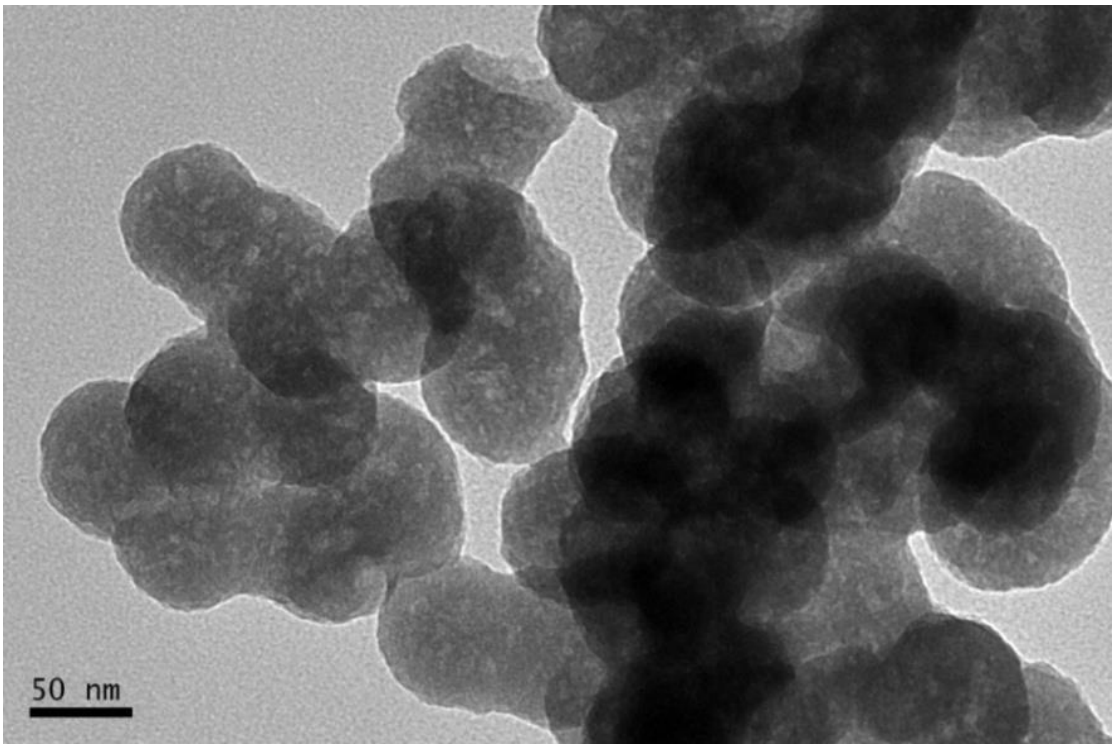

Figure A.4

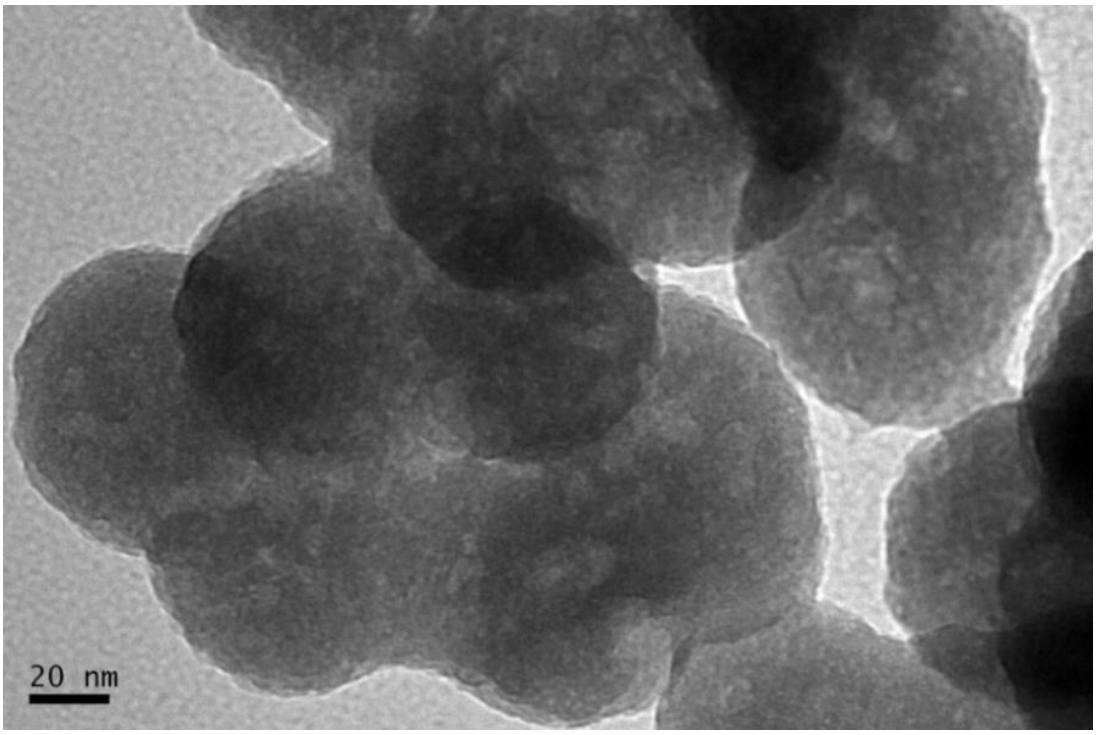

Figure A.5

SEM

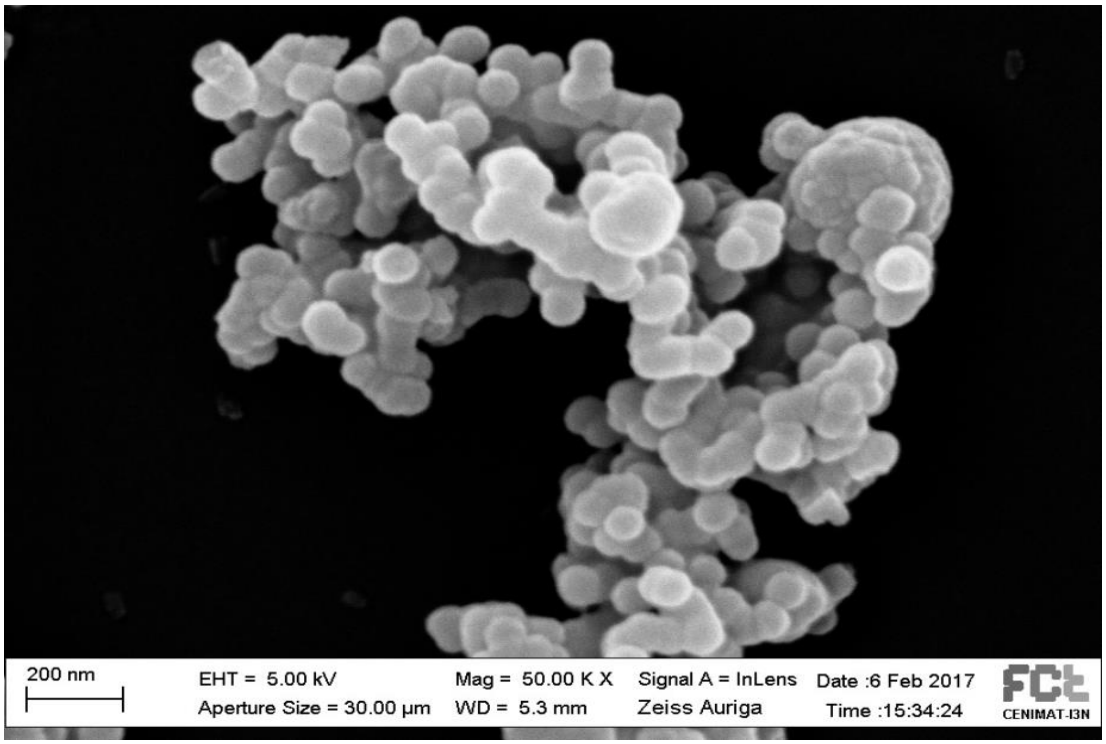

Figure A.6

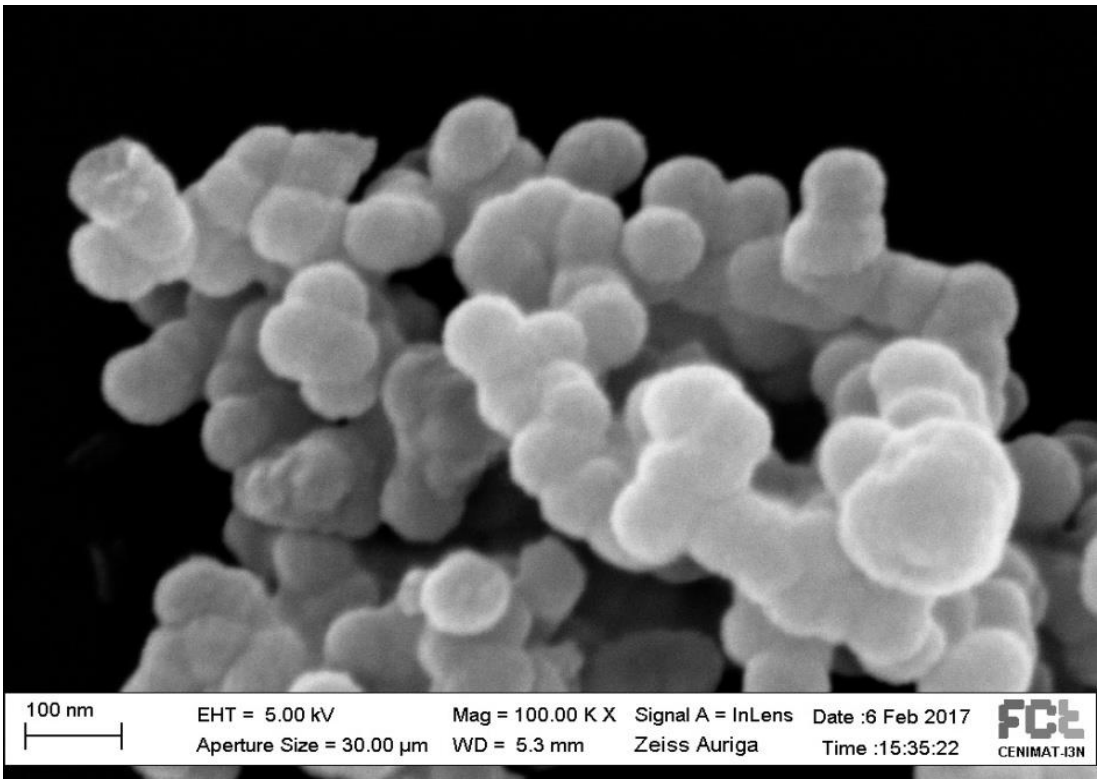

Figure A.7

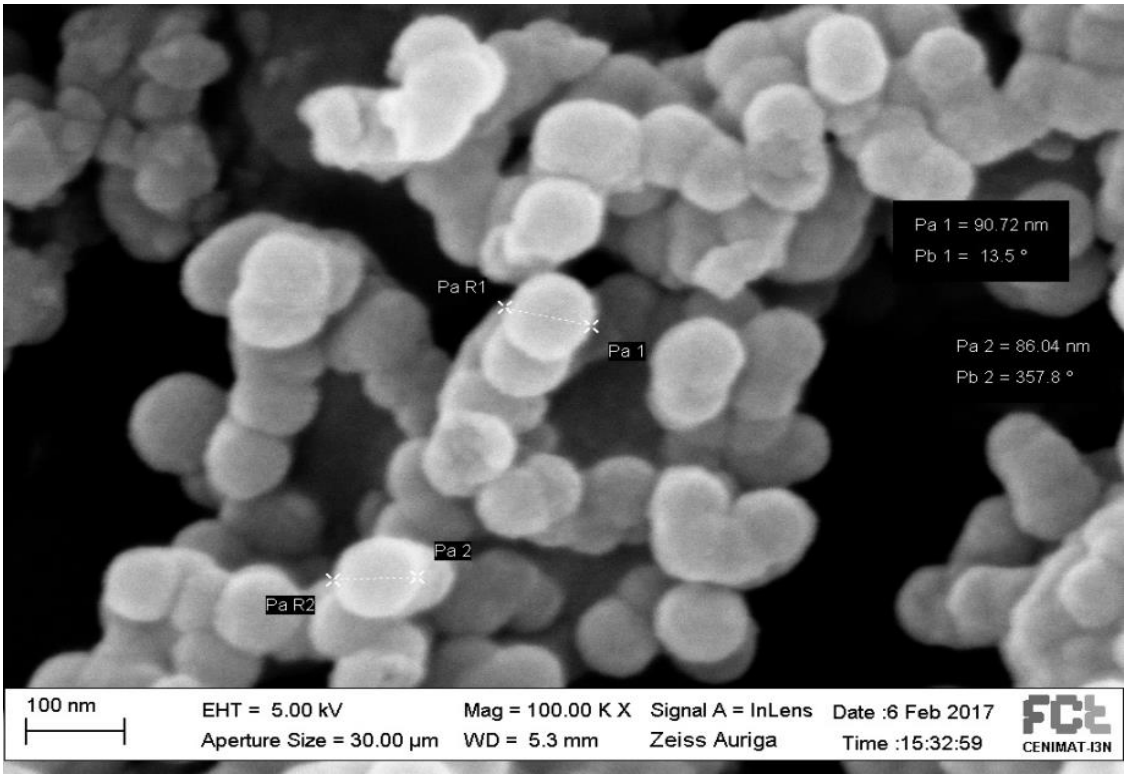

Figure A.8

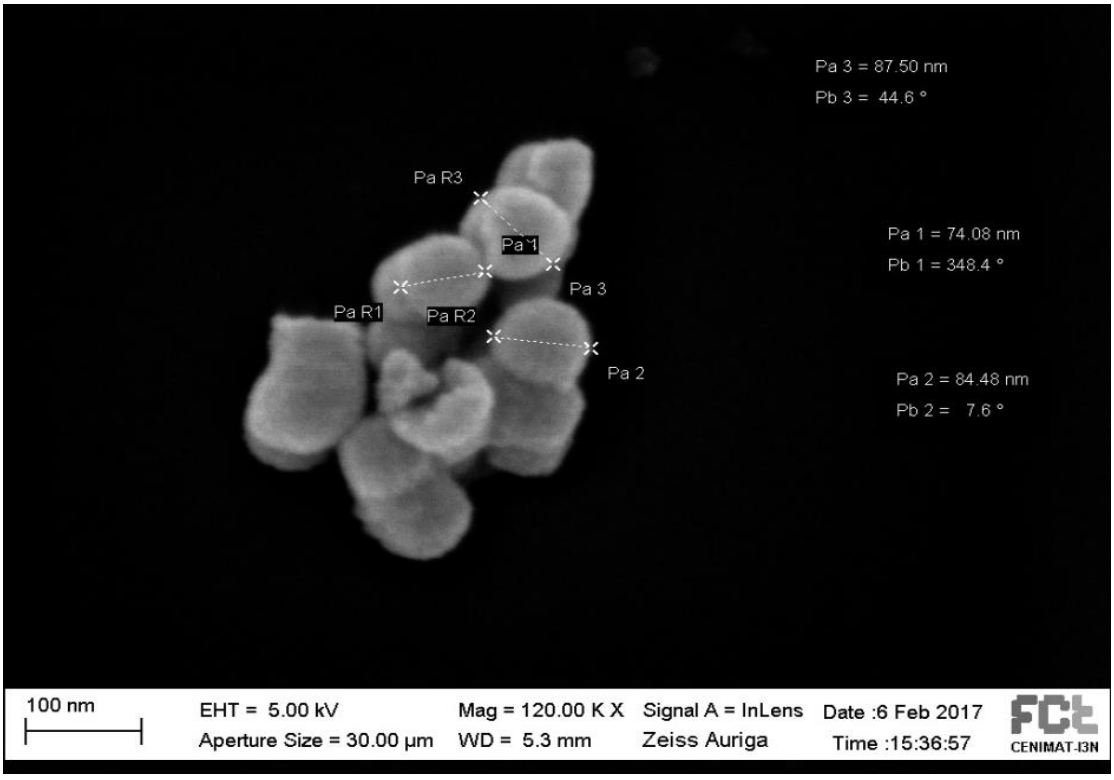

Figure A.9

A.2.2. Experimental results (Chapter 3)

A.2.2.1. Assay A

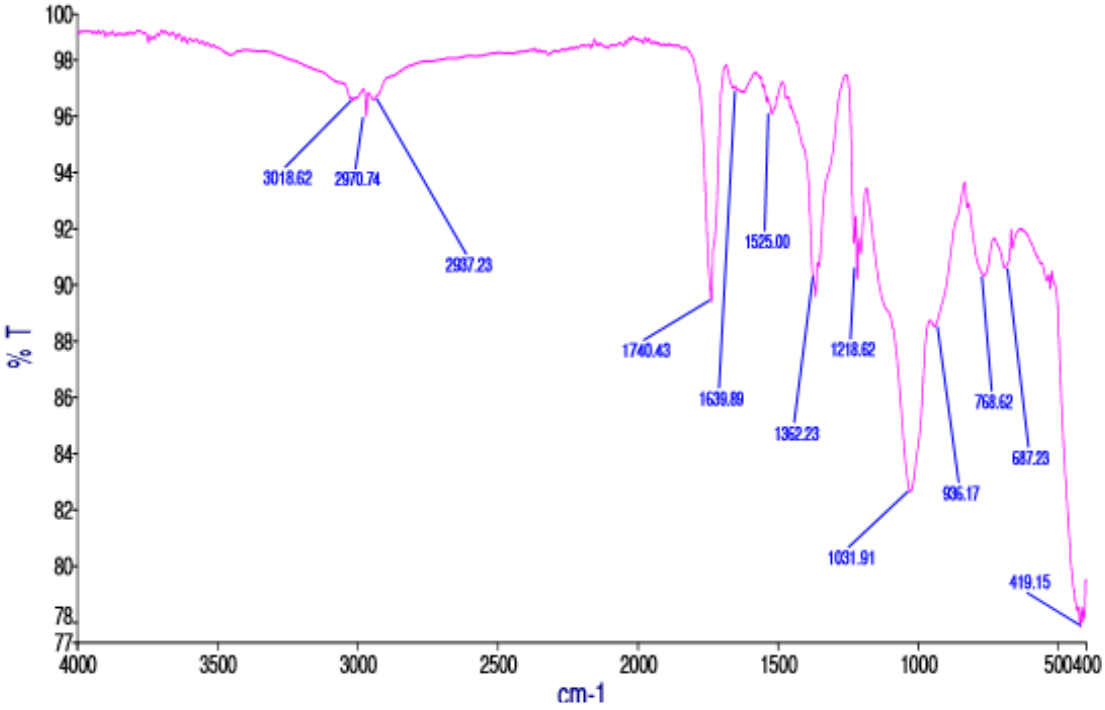

Figure A.10 - Infrared spectrum of SiQDsI@mSiO$_2$ (without template).

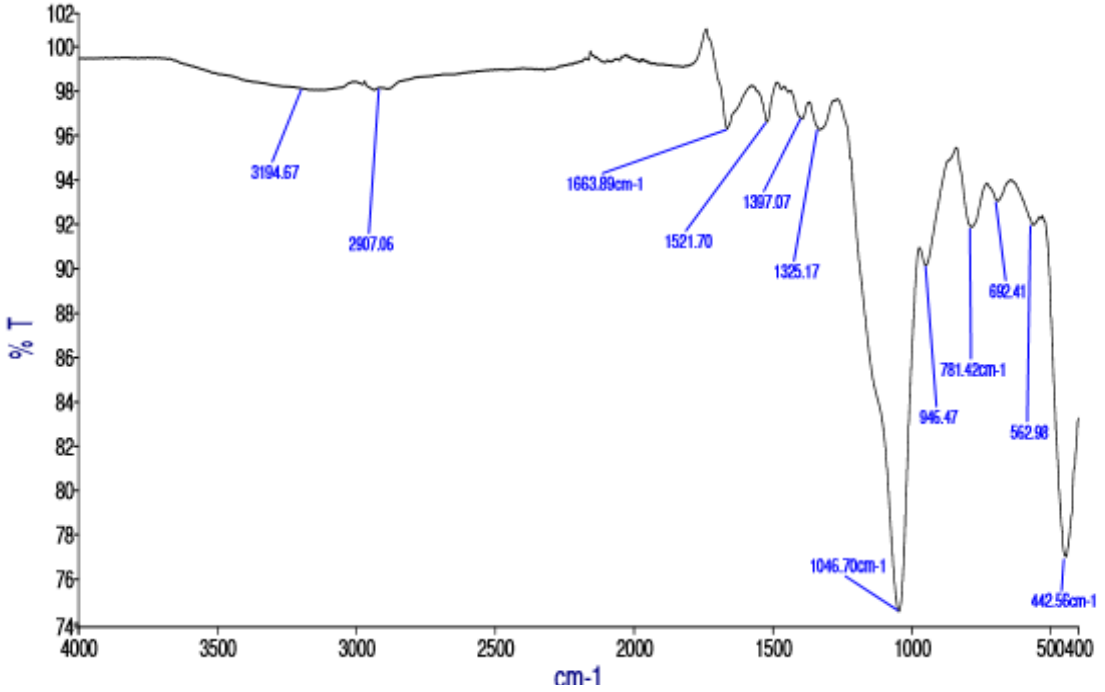

Figure A.11 - Infrared spectrum of SiQDsI@mSiO$_2$@PEG1 (without template).

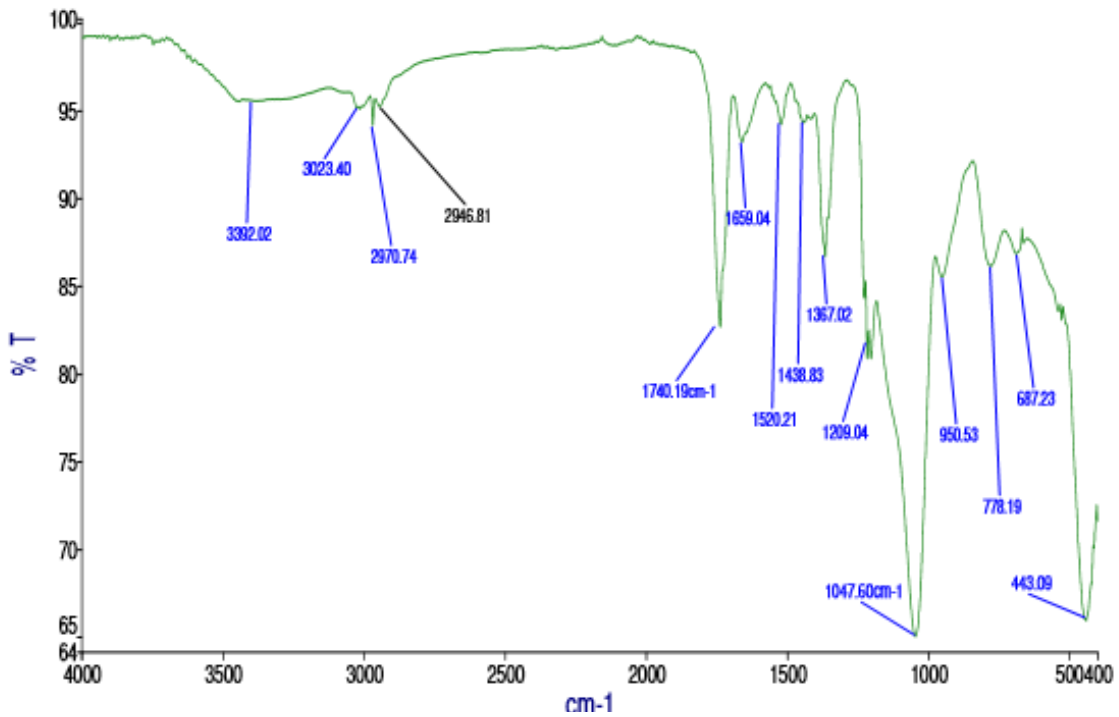

Figure A.12 - Infrared spectrum of SiQDsII@mSiO$_2$ (without template).

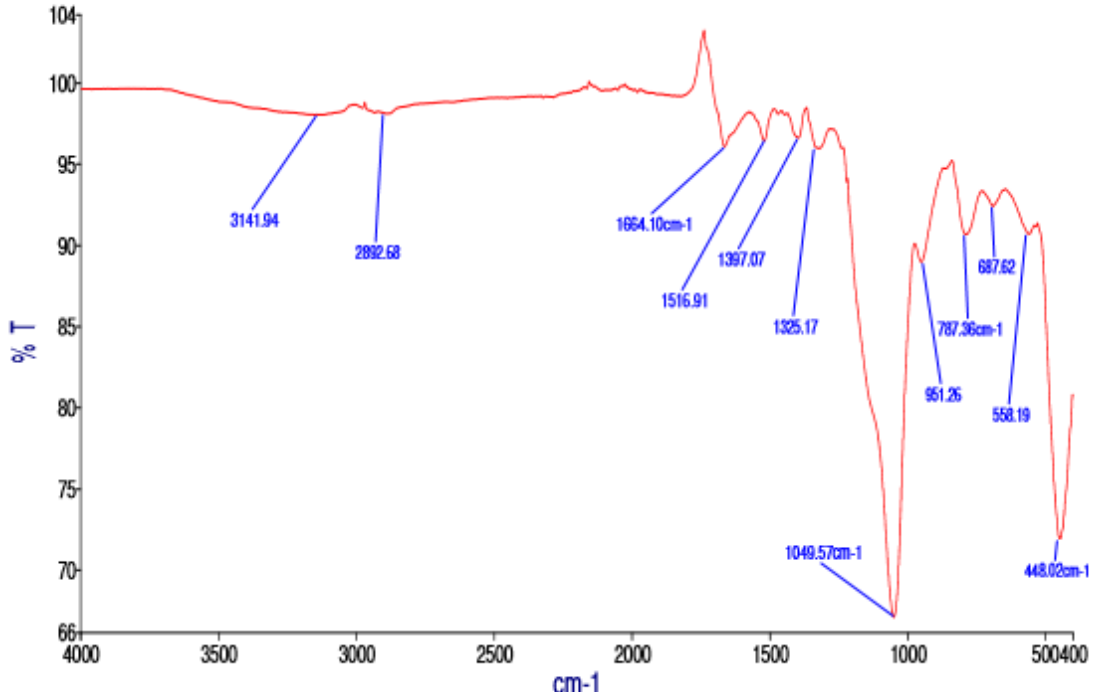

Figure A.13 - Infrared spectrum of SiQDsII@mSiO$_2$@PEG1 (without template).

A.2.2.2. Assay B

A.2.2.2.1. T1

TEM

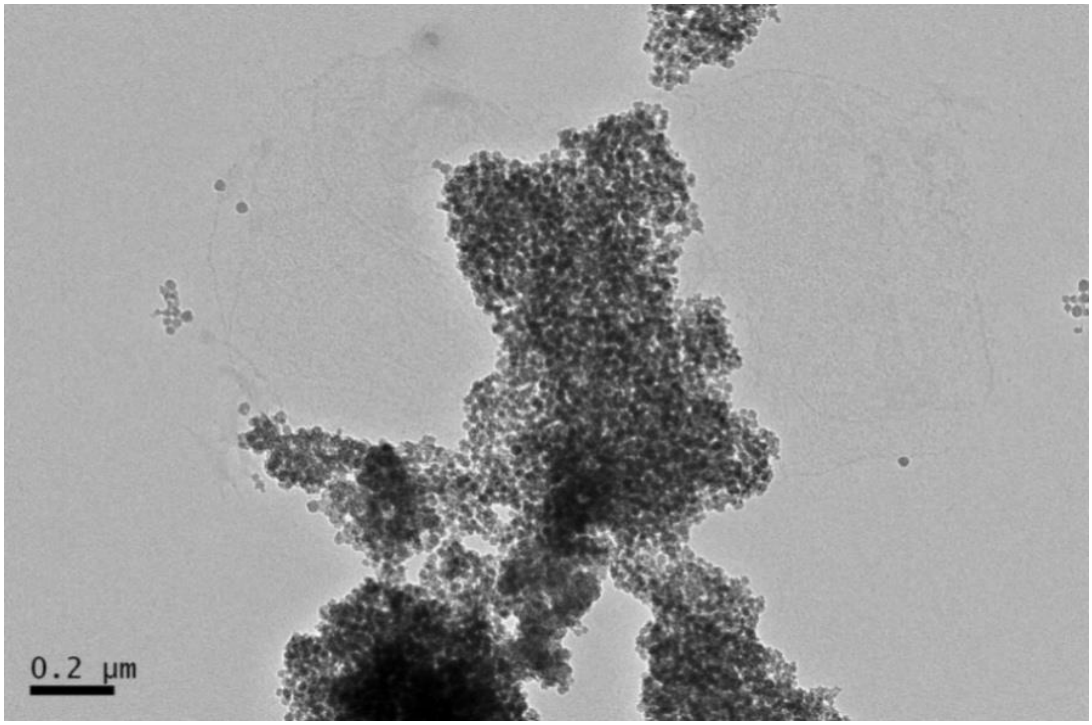

Figure A.14

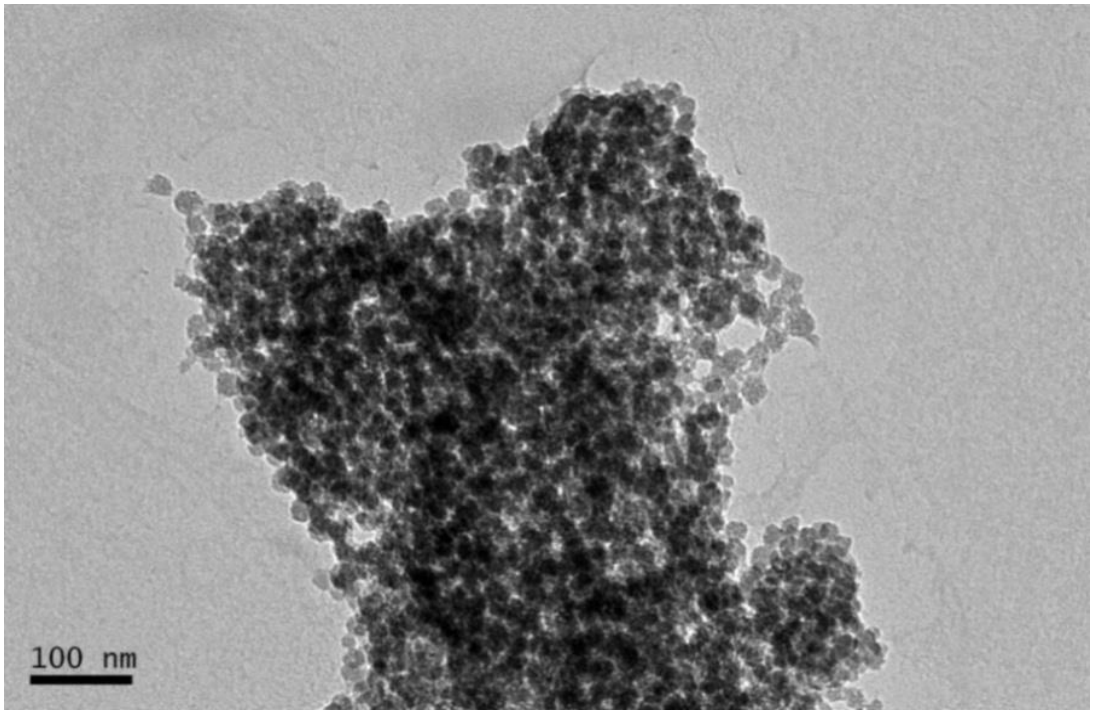

Figure A.15

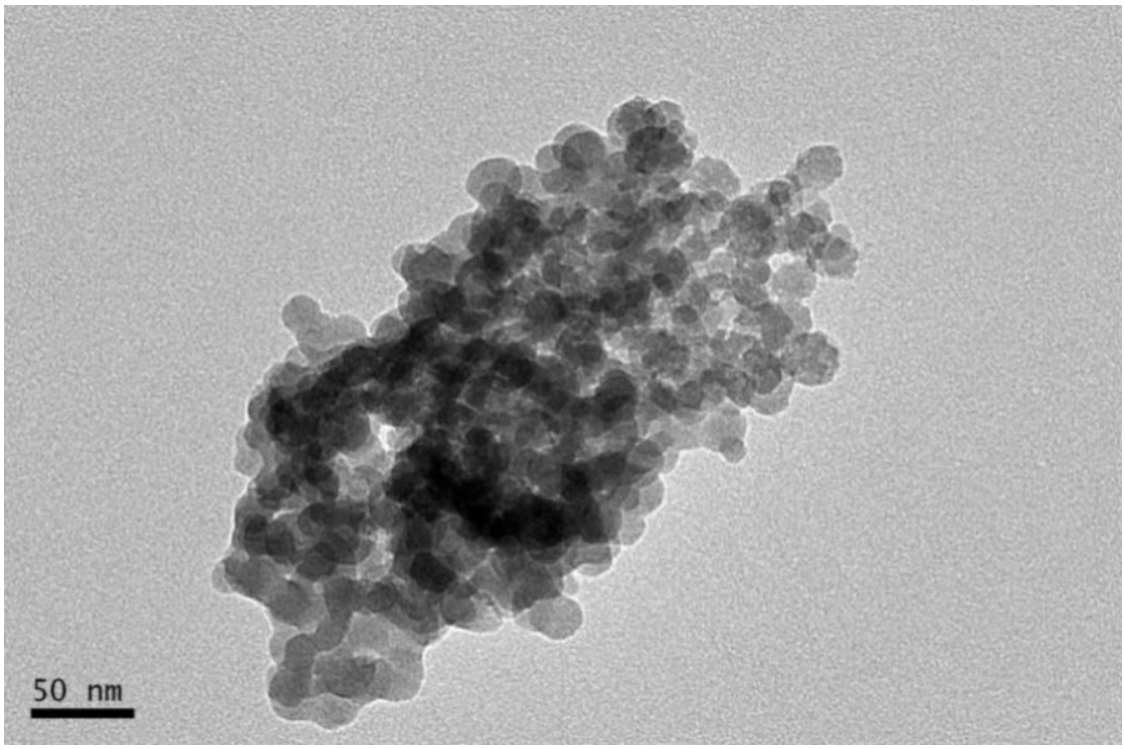

Figure A.16

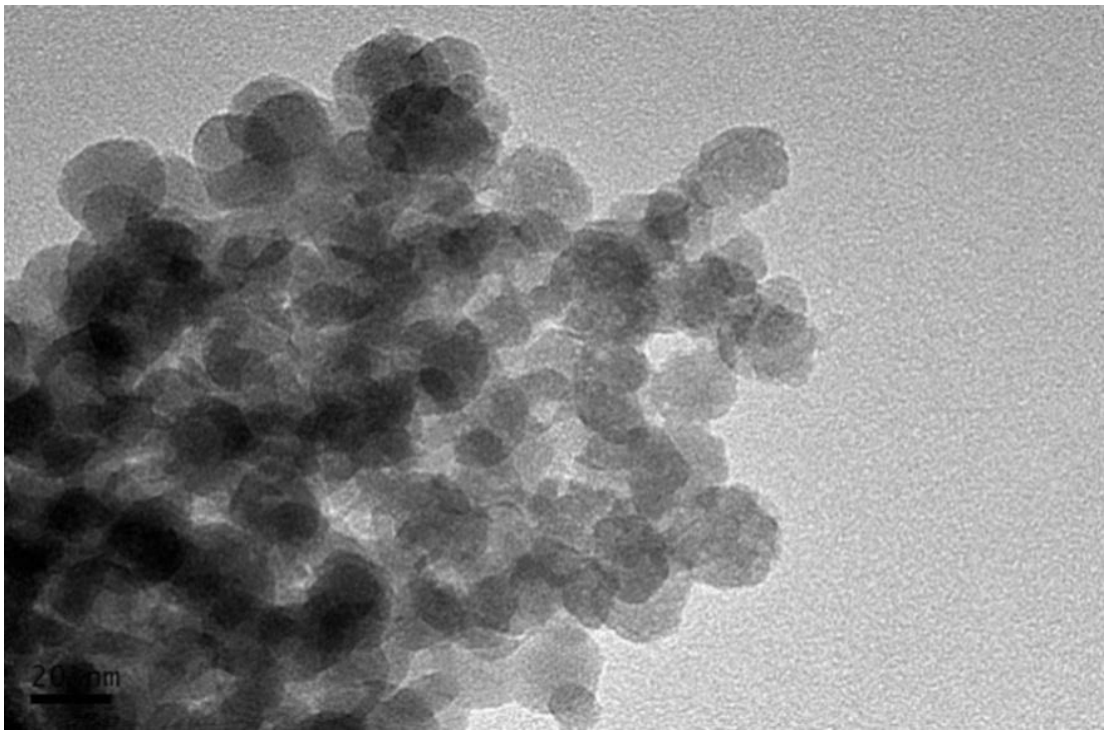

Figure A.17

A.2.2.2.2. T2

TEM

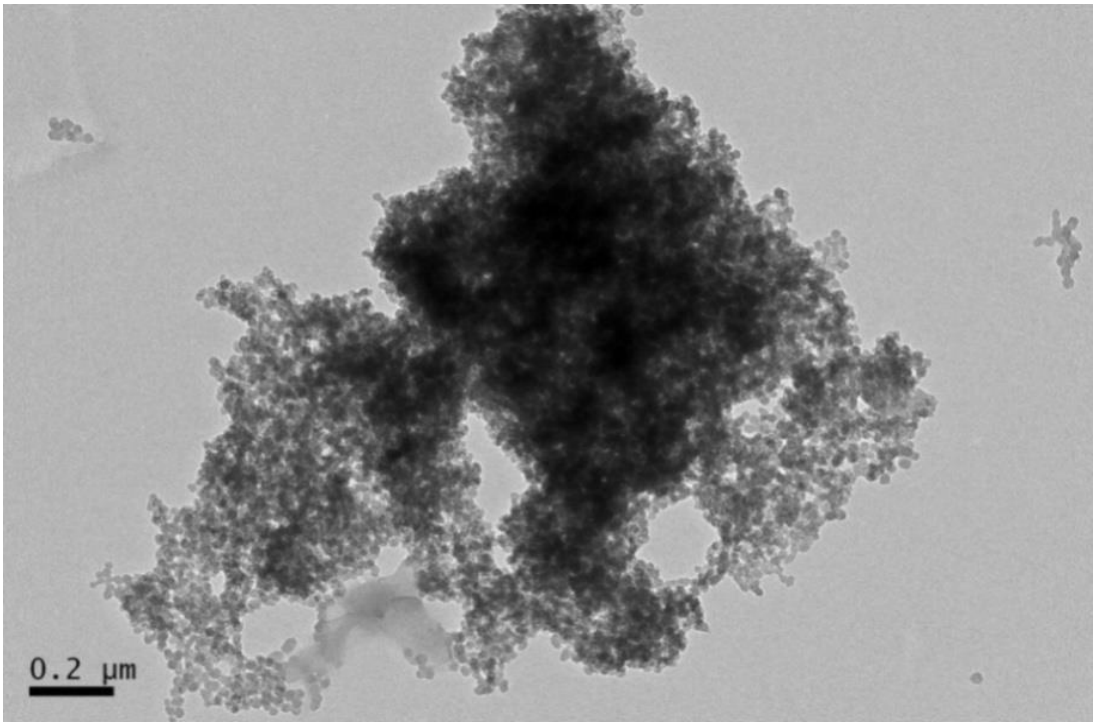

Figure A.18

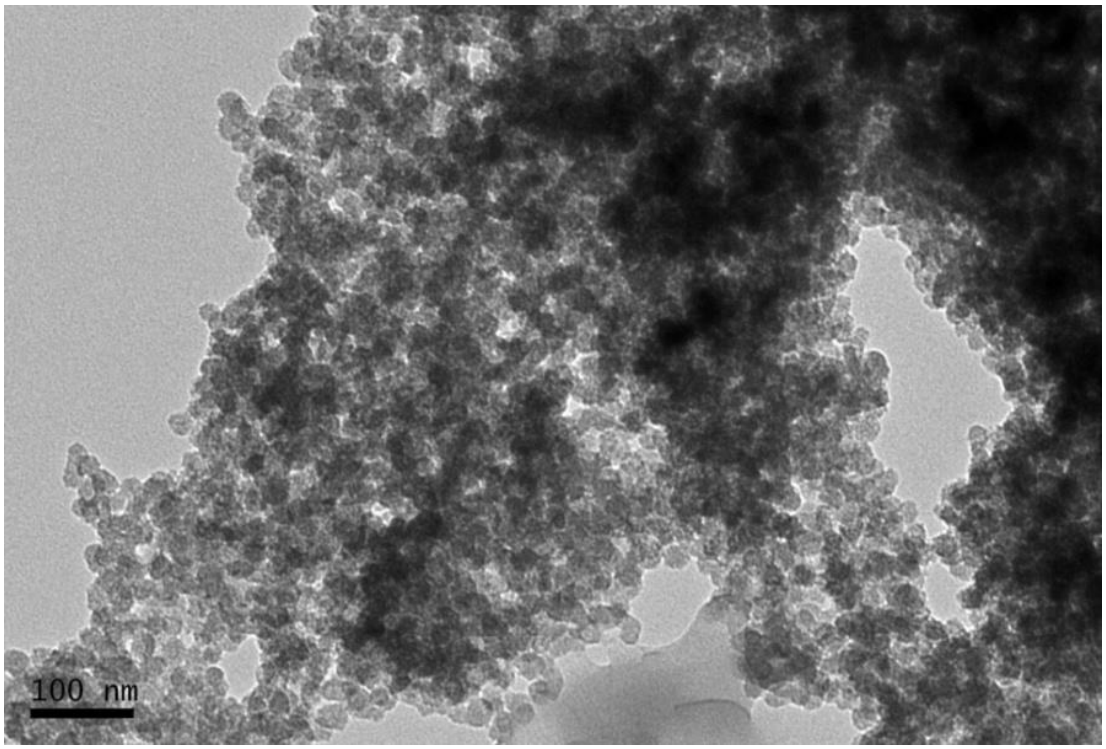

Figure A.19

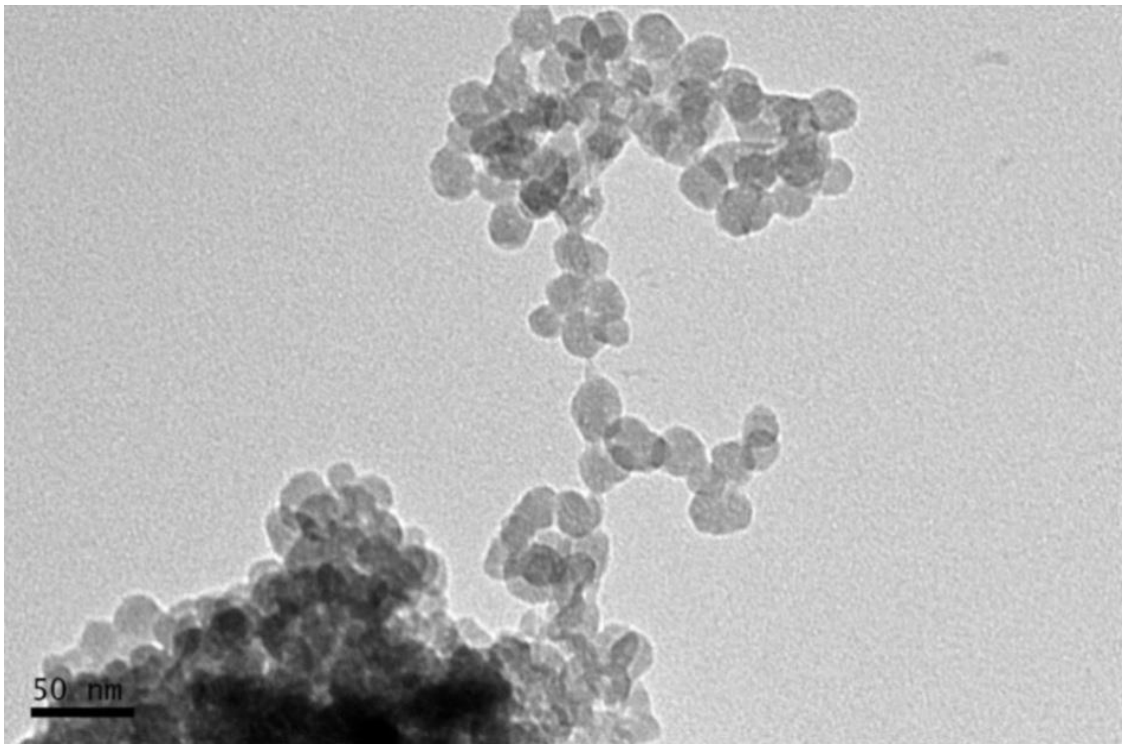

Figure A.20

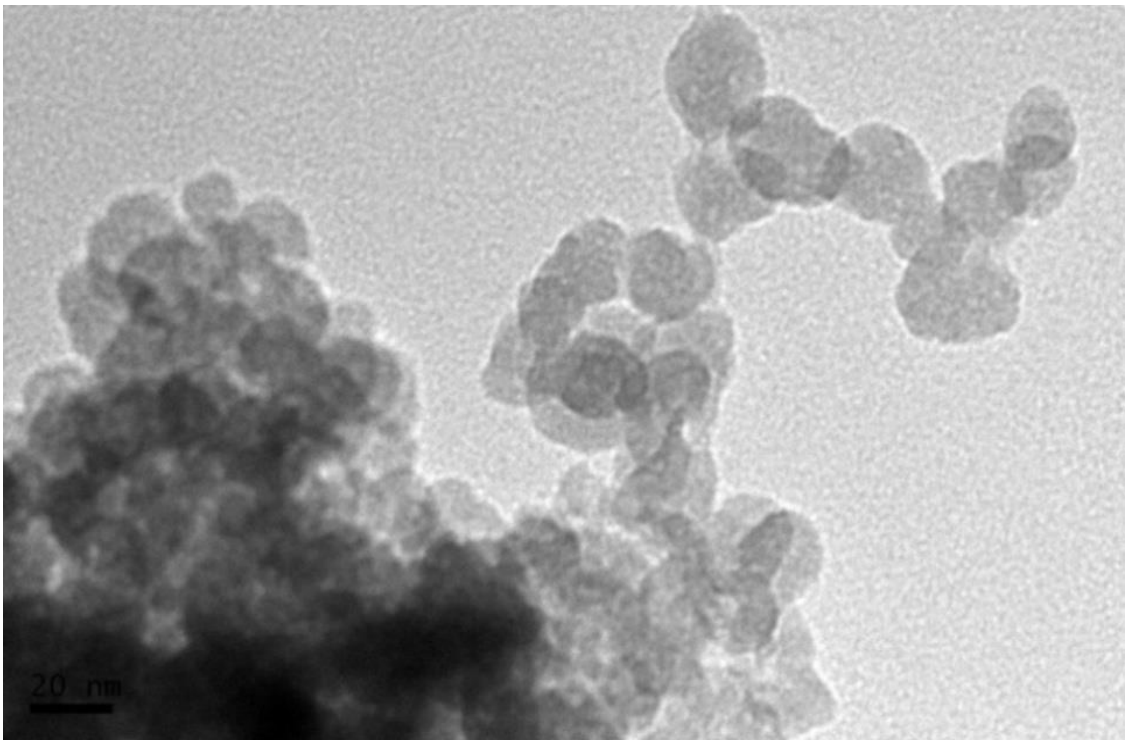

Figure A.21

A.2.2.2.3. T3

TEM

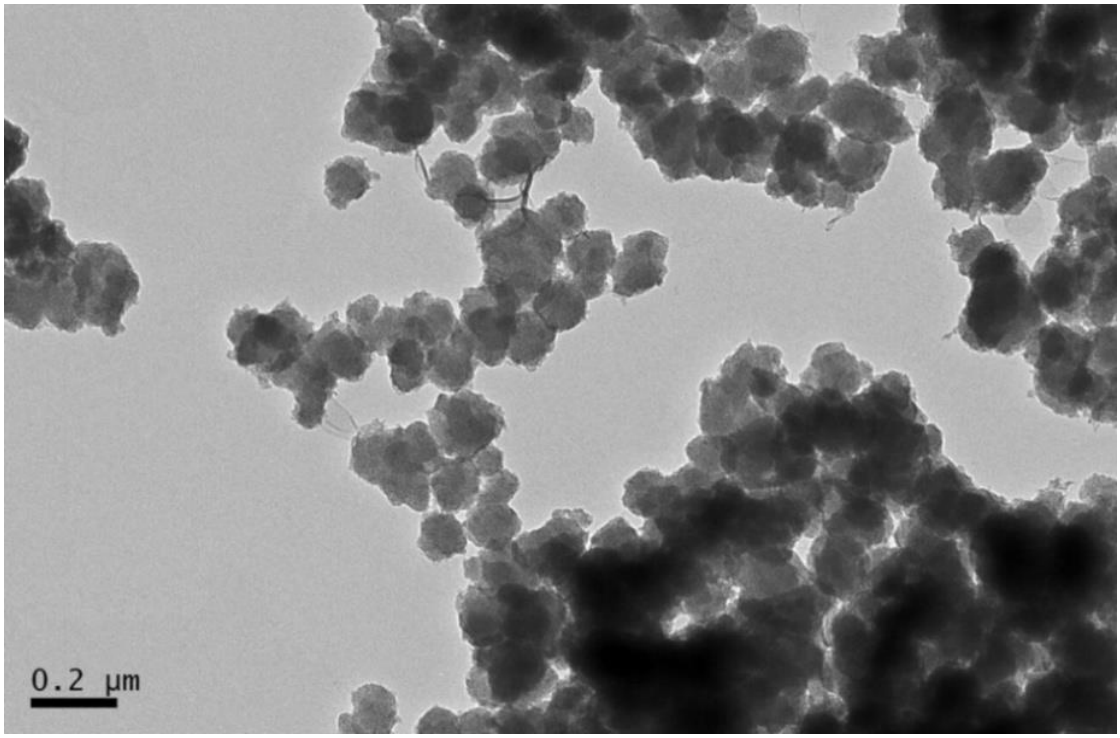

Figure A.22

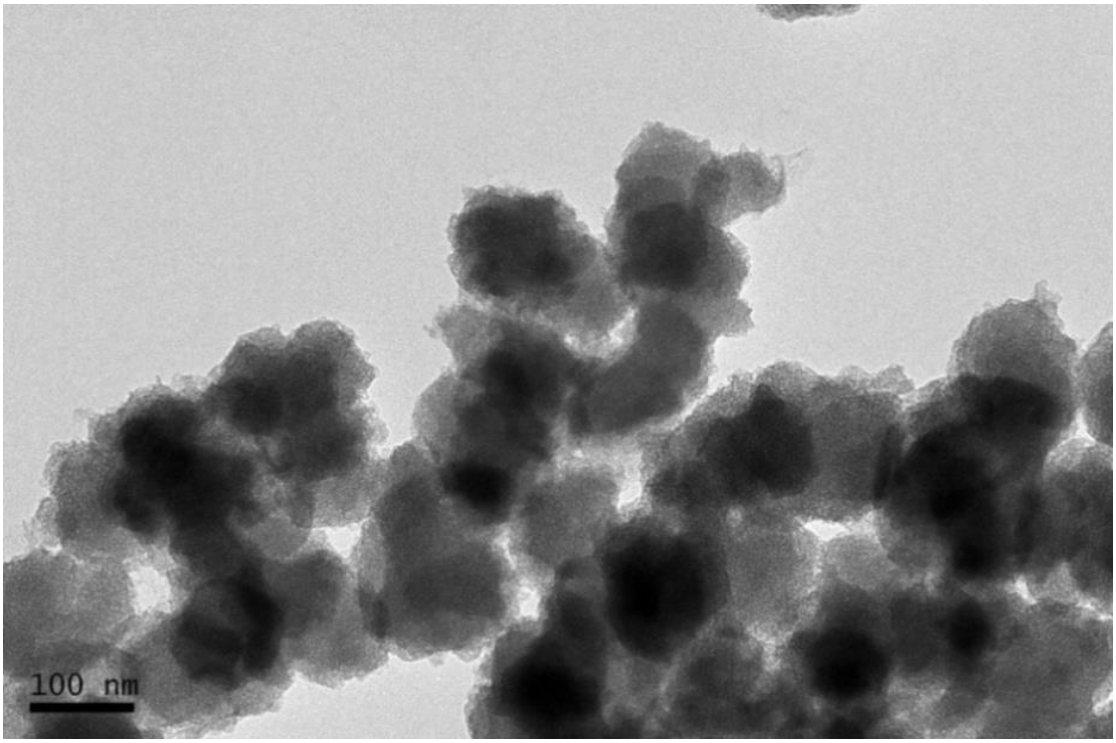

Figure A.23

SEM

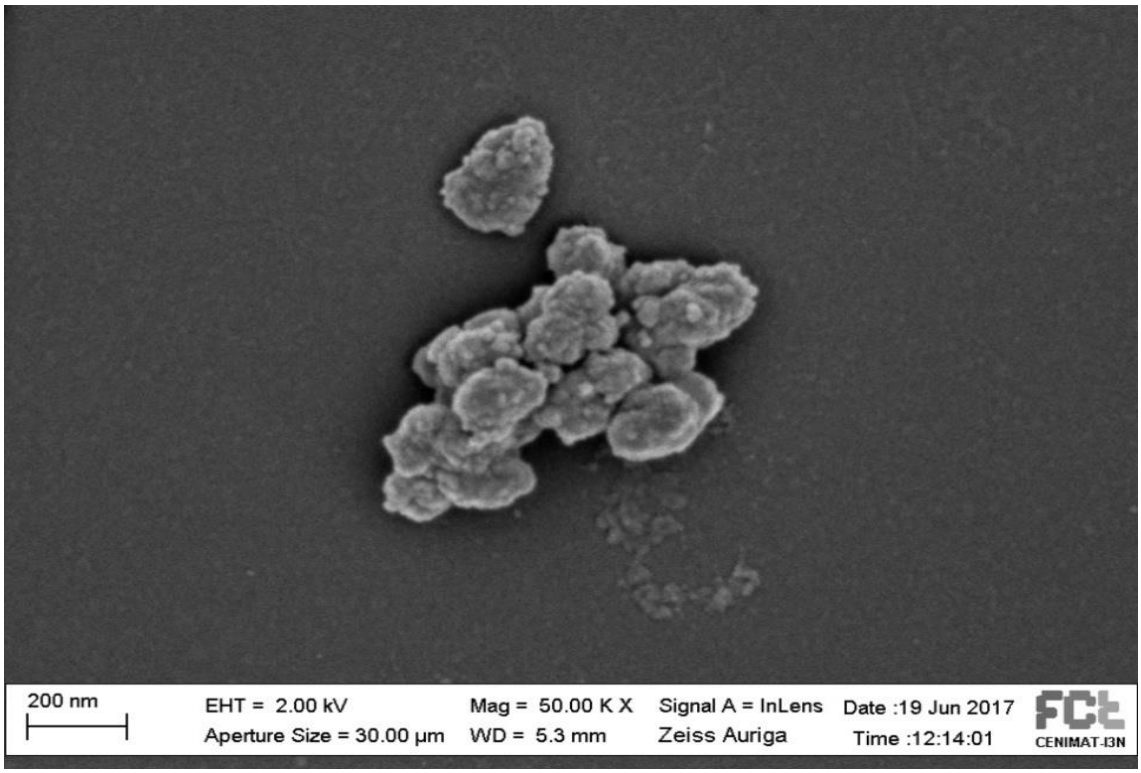

Figure A.24

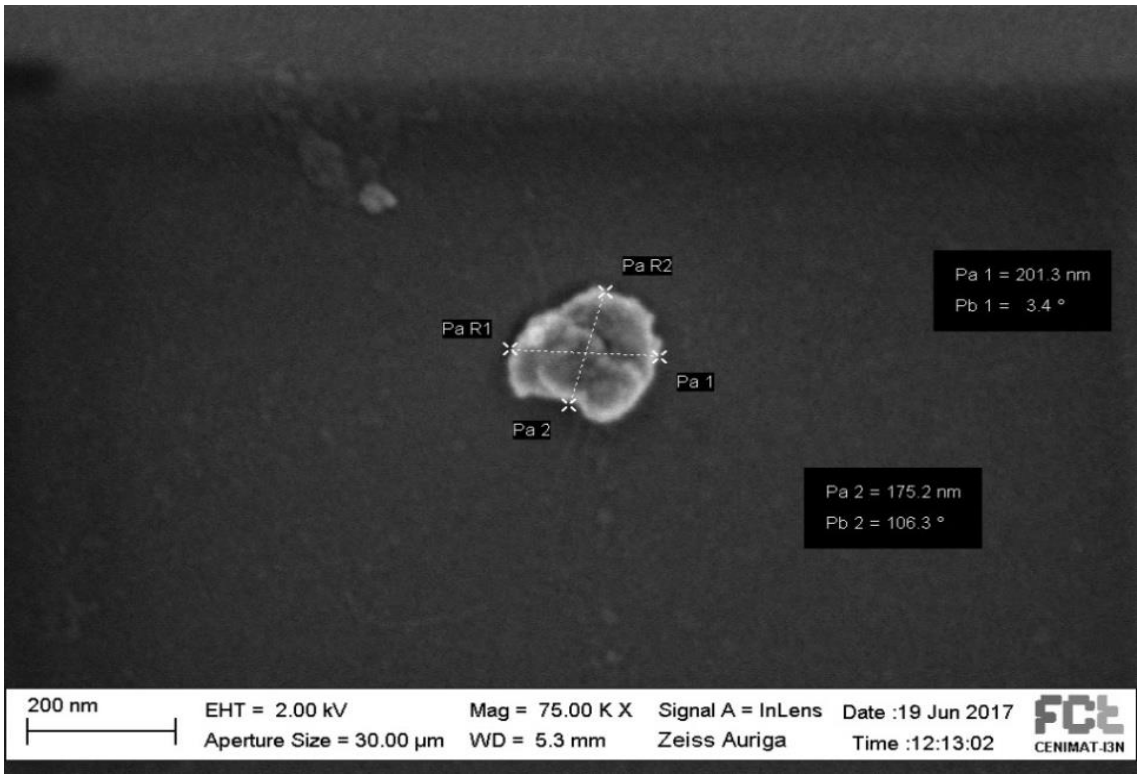

Figure A.25

A.2.2.2.4. T4

TEM

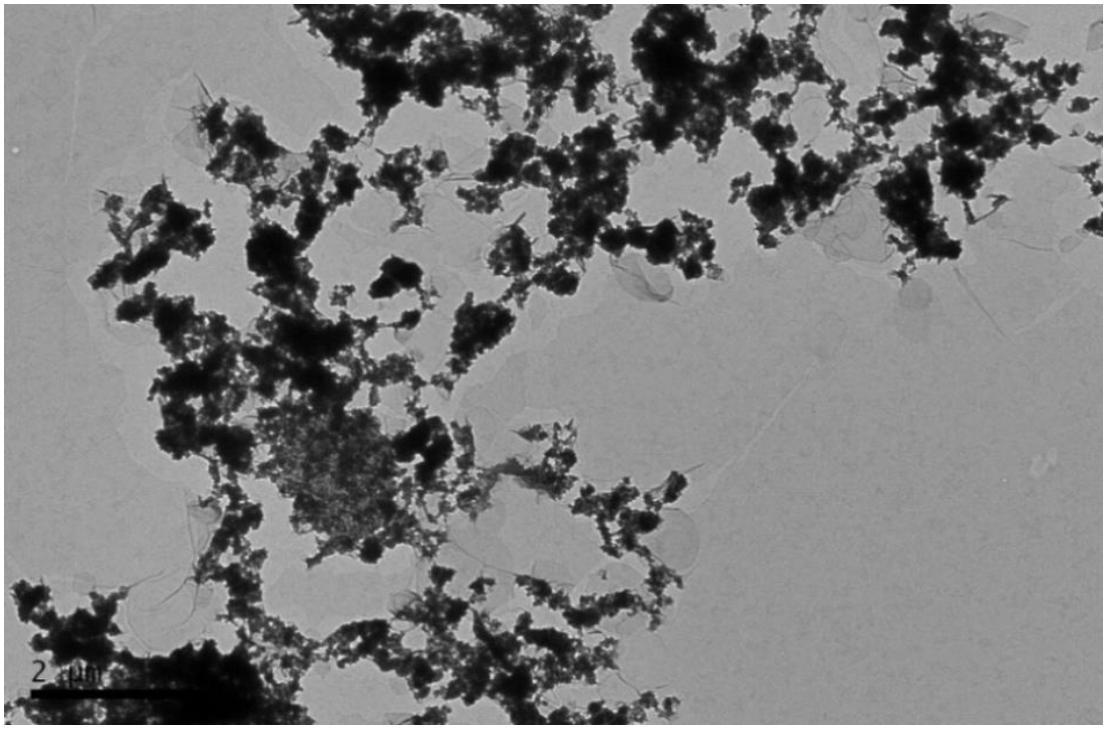

Figure A.26

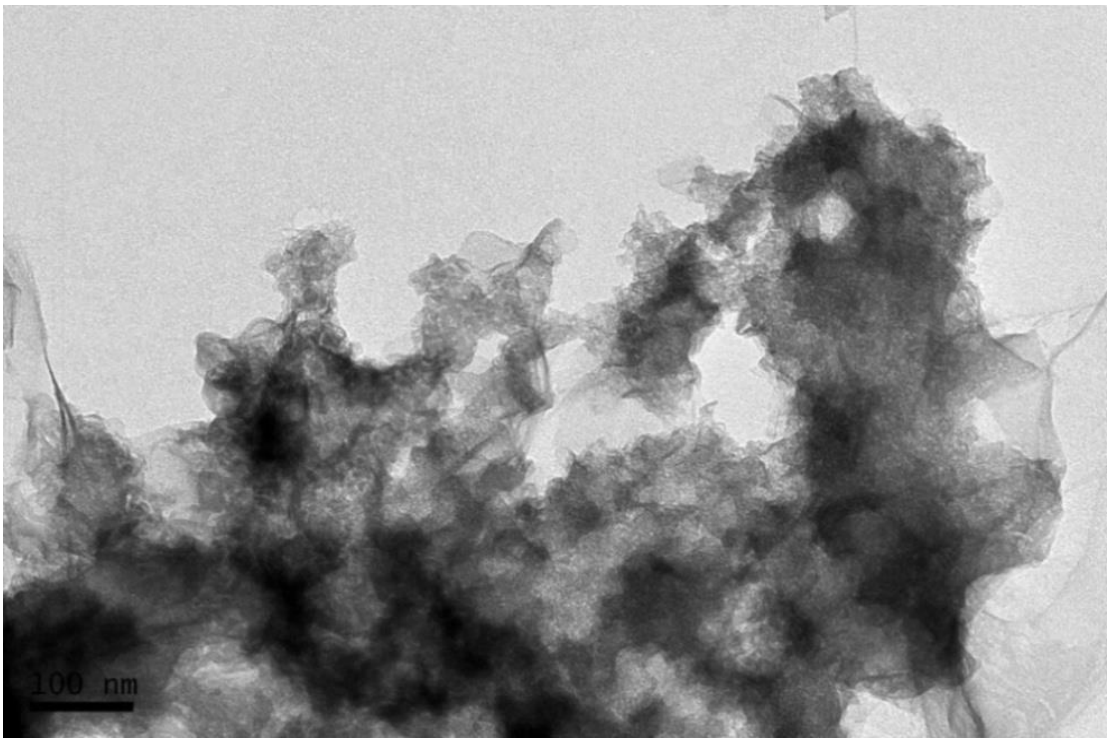

Figure A.27

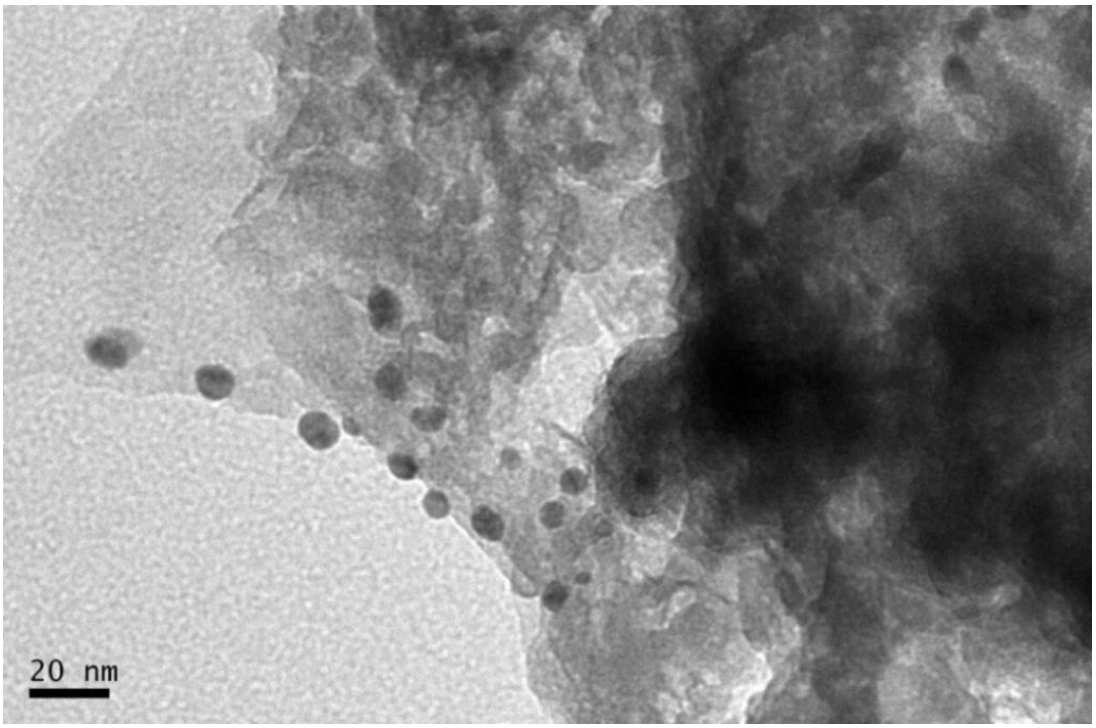

Figure A.28

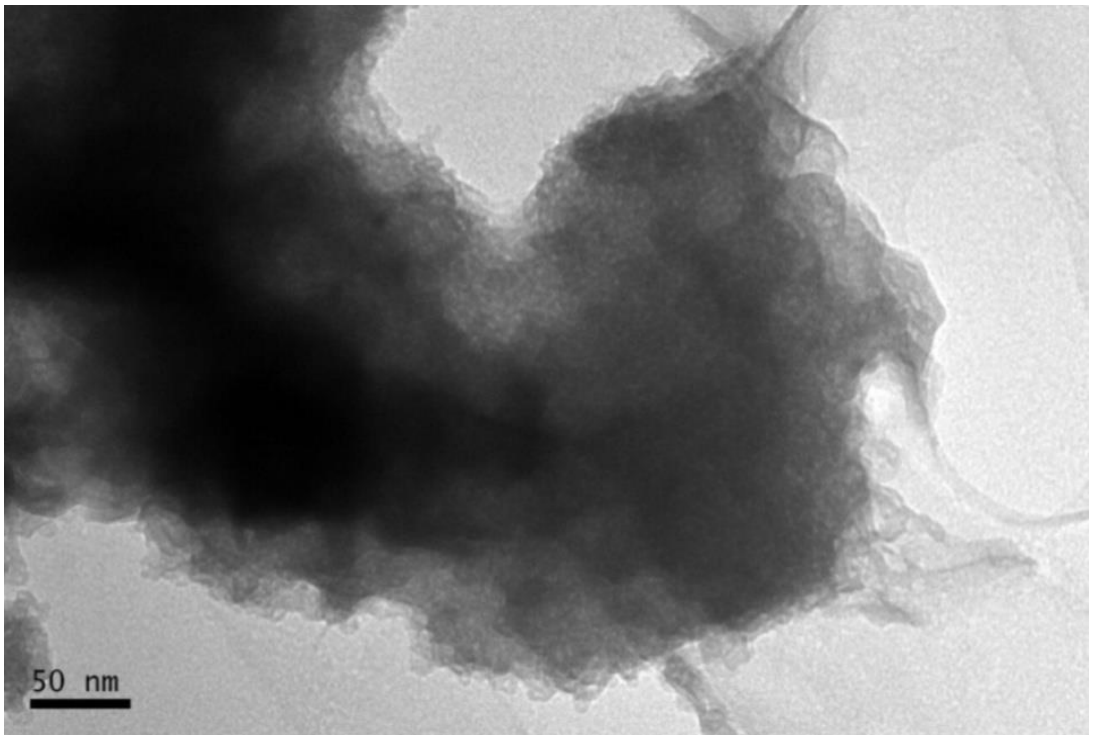

Figure A.29

A.2.3. Experimental results (Chapter 4)

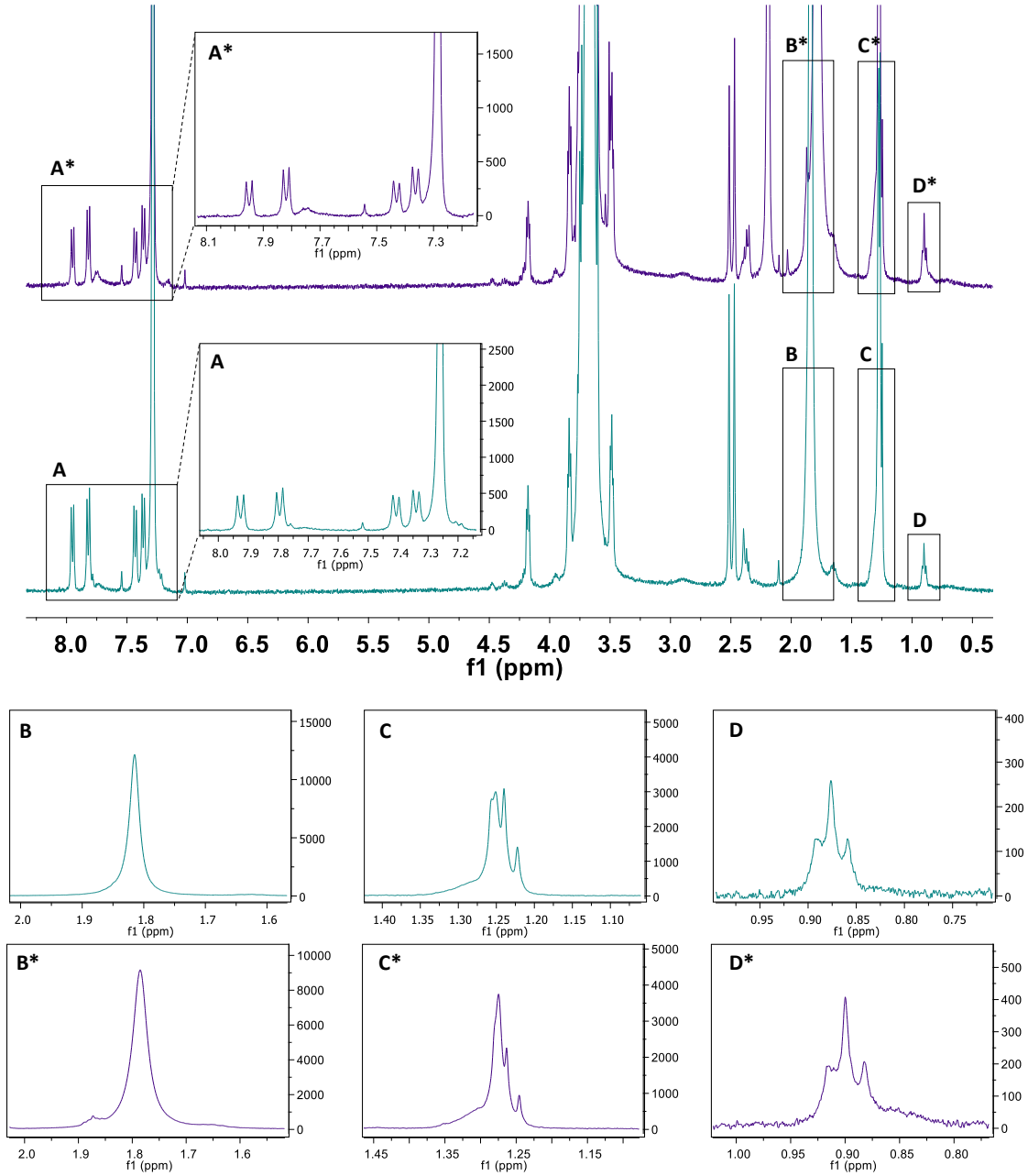

Figure A.30 – ^{1}H NMR (400 MHz) spectra of PEG2 (blue) and PEG3 (purple), with expansions.

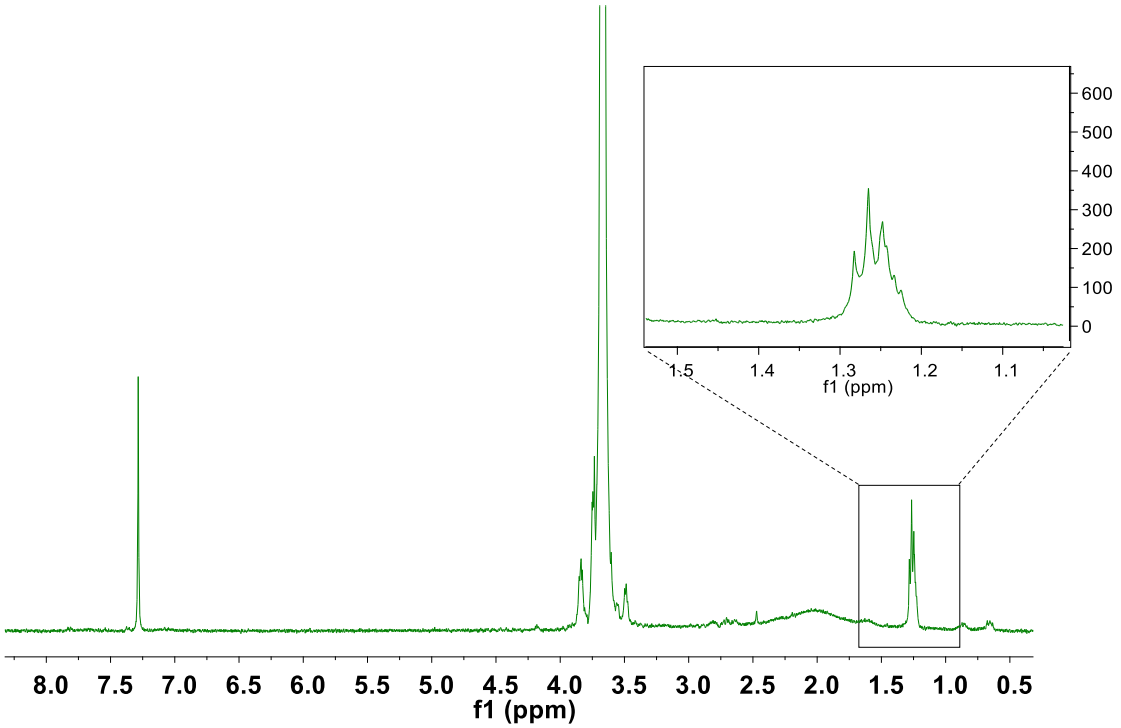

Figure A.31 – ^{1}H NMR (400 MHz) spectra of PEG1 (green), with expansion.